MDC E0731
NAS9-13091
DRL T-818
DRD MA 293T

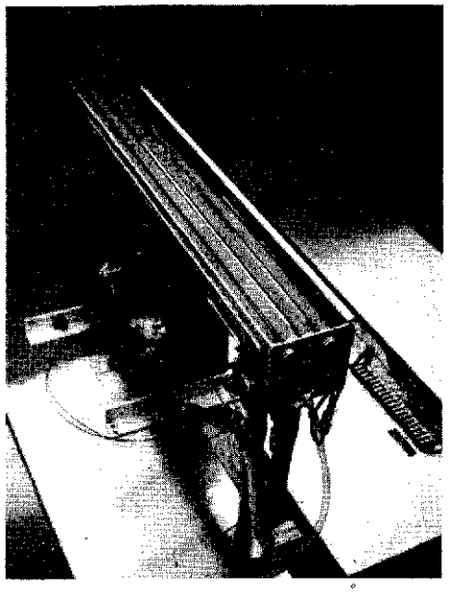

DESIGN AND FABRICATION OF A HIGH TEMPERATURE LEADING EDGE HEATING ARRAY

PHASE I FINAL REPORT

5 DECEMBER 1972

MCDONNELL DOUGLAS ASTRONAUTICS COMPANY - EAST

MCDONNELL DOUGLAS CORPORATION

(NASA-CR-141713) DESIGN AND FABRICATION OF A HIGH TEMPERATURE LEADING EDGE HEATING ARRAY, PHASE 1 Final Report, 29 Jun. - 5 Dec. 1972 (McDonnell-Douglas Astronautics Co.) 115 p HC $5.25

N75-19332

CSCL 22B G3/18

Unclas
14318

COPY NO. 19

DESIGN AND FABRICATION OF A HIGH TEMPERATURE LEADING EDGE HEATING ARRAY - PHASE I

5 DECEMBER 1972

MDC E0731

FINAL REPORT

29 JUNE 1972 TO 5 DECEMBER 1972

SUBMITTED TO NASA/MSC UNDER
CONTRACT NAS 9-13091
DRL T-818
DRD MA 293T

Approved by

B. G. Cox
Deputy

H.E. Christensen
Program Manager

R. H. Lilienkamp
Sr. Group Engineer, Laboratory

D.L. Kummer
Manager Materials and Processes

MCDONNELL DOUGLAS ASTRONAUTICS COMPANY - EAST
Saint Louis, Missouri 63166 (314) 232-0232

MCDONNELL DOUGLAS CORPORATION

FOREWORD

This Final Report was prepared by McDonnell Douglas Astronautics Company - East (MDAC-EAST) for NASA-MSC Contract NAS 9-13091, Design and Fabrication of a High Temperature Leading Edge Heating Array - Phase I. It covers the period 29 June 1972 to 5 December 1972. This effort was performed for the National Aeronautics and Space Administration, Manned Spacecraft Center, under the direction of the Structural Test Branch of the Structures and Mechanics Division with Mr. W. D. Sherborne as the Technical Monitor (STM). Mr. H. E. Christensen was the Program Manager for MDAC-EAST.

ABSTRACT

This report describes the progress made by MDAC-EAST during a Phase I program to design a high temperature heating array for environmentally testing full-scale Shuttle leading edges (30 inch span, 6 to 15 inch radius) at flight heating rates and pressures. Heat transfer analyses of the heating array, individual modules and the Shuttle leading edge were performed, which influenced the array design, and the design, fabrication and testing of a prototype heater module.

A modular heating array was evolved to produce the flight temperature distribution around the Shuttle leading edge. Heater modules utilizing graphite elements were used to produce the high temperatures (up to 3500°F) in the stagnation region and absorber modules are used as necessary to produce the high chordwise thermal gradients. The array is designed to operate in an inert nitrogen atmosphere at near vacuum conditions as well as at sea level pressure. Design features incorporated into the heater module include tapered peg electrodes, a lever arm expansion end assembly, compact bus plates, structural water manifolds, enclosing reflectors, gas spray bars and nesting modules so that even larger specimens can be tested. The newly designed expansion end assembly increases heating uniformity for arrays butted end to end and allows flexibility in orientation of the module. Reflector coating tests were performed which demonstrated a significant increase in the heating efficiency of the system using a gold coating on the reflectors instead of chrome plating. This gold coating is very important because for a given specimen temperature the element temperature is lower thereby reducing the input power, the cooling requirements, and the potential for arcing.

Performance and heat flux uniformity calculations were correlated with full scale testing of the newly fabricated heater module.

Tests were also performed using a heat flux sensor and a specimen-mounted thermocouple as a feedback signal in a successful demonstration of heater module control.

A preliminary design of the full scale heating array was completed and estimates for fabricating and acceptance testing have been forwarded to NASA.

TABLE OF CONTENT

TABLE OF CONTENT (Continued)

DISTRIBUTION LIST

George C. Marshall - Space Flight Center, Huntsville, Ala. 35812

O. K. Goetz S & E ASTN-T Bldg. 4666

J. Loose S & E ASTN - PTC

NASA Manned Spacecraft Center, Houston, Texas 77058

F. S. Coe, ES3

D. H. Greenshields, ES

J. E. Pavlosky, ES3

W. D. Sherborne, ES63

G. Strouhal, ES3

F. R. Tabor, BC76

D. Tillian, ES3

C. M. Grant, JM2

(Documentation Management Office)

List of Pages

1.0 INTRODUCTION

The concept of a reusable Space Shuttle has generated new types of Thermal Protection Systems (TPS) and consequently placed additional requirements on entry heating simulation facilities. One of the key elements of the TPS is the leading edges which must withstand severe entry heating at low pressures of entry for multiple flights. A heating facility is needed to test the performance of this TPS. The heating facility (or array) must be capable of imposing heating which varies in intensity around the leading edge from 3200°F at the stagnation point to 875°F on the trailing surface. Furthermore, such heating must be imposed at flight pressures ranging from 0.5 to 760 torr. Also these conditions must be repeatedly imposed on various sizes of leading edges up to 10 feet in length at a reasonable cost per mission cycle.

This report describes a five month effort (Phase I) in which the TPS test requirements were incorporated into the design of a full scale heating array which is to be fabricated in Phase II. The goal of Phase I was to solve development problems for a 3500°F heating array by analyzing the heat exchange between the test article and the heating array, by fabricating and testing a prototype heater module, and by performing a preliminary design of the full scale heating array including interfaces and auxiliary equipment.

The array employs the graphite heater technology previously developed by McDonnell Douglas Corporation (MDC) to overcome several problems that exist with quartz lamps. Quartz lamps have a relatively short life, are expensive to replace, arc-over at low pressure (1 to 18 torr), and require high density installation to achieve a high heat flux. This high density, in turn, causes over-temperature of the quartz envelope surrounding the tungsten filaments. Alternatively, the graphite heater system has low cost elements which have long life and are simple to replace and operate at low pressures as well as at atmospheric pressure. Graphite heaters achieve a higher heat flux density than quartz lamps because of the higher view factor inherent in the design and the higher emissivity of the graphite when compared to the tungsten filament. MDC and NASA have successfully used the graphite heaters (up to a 30 x 39 inch size) to test flat TPS panels at temperatures up to 2300°F. One of the goals of this program, to increase the test temperature to 3500°F, requires 4.2 times the energy required for the 2300°F testing. In order to accomplish this goal, many design innovations were incorporated into the heater module and into the heating array. These also accomplished other goals of the progra to increase heat flux uniformity and flexibility of the array.

Analyses were performed to determine the size and number of modules comprising the unit to achieve the desired heating pattern on a Shuttle leading edge (6 to 15 inch radius x 30 inch long) bathed in a gaseous nitrogen environment. A unit was designed to fit easily into a vacuum chamber at NASA-MSC and to be compatible with the NASA cooling system. This graphite heater unit is to operate off conventional ignitron or SCR power controllers (such as used for quartz lamps) using an intermediate step-down transformer. The configuration selected for the array (shown in Figure 1-1) employs standard size modules that fit around the leading edge. An individual heater module for this array was successfully designed, analyzed, fabricated and tested during Phase I.

The following sections present the details of the analyses, preliminary designs, fabrication techniques, and test activities performed to design a heating array for testing various size leading edges.

During the course of Phase I, many meetings were held with Mr. W. D. Sherborne (CTM) and other NASA personnel to ensure that the heating array design would meet NASA's needs.

The authors wish to also acknowledge the contributions of the following personnel toward the successful completion of this program:

Thermodynamics	- T. W. Parkinson, J. M. Buchanan
Design and Testing	- F. W. Brodbeck, D. Q. Durant, R. D. Taylor, R. Lenze
Testing	- K. Hoffman
Manufacturing	- H. Stevenson, R. Callier
Physics Laboratory	- R. M. F. Linford, R. J. Schmitt, K. E. Steube
Chemistry Laboratory	- W. Dinger

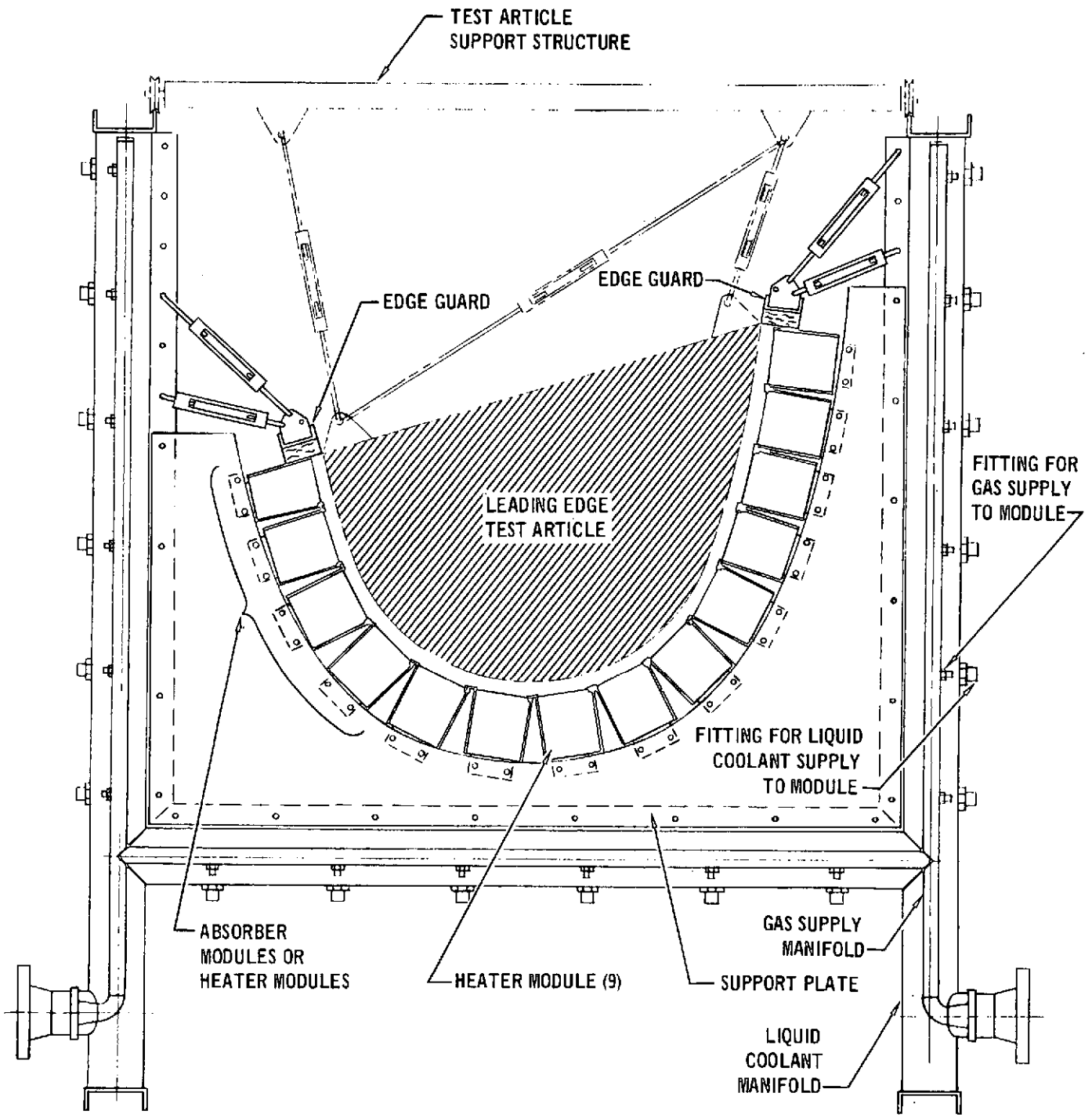

(SECTION B–B)

END VIEW OF HEATING ARRAY

457-3385

FIGURE 1-1

NOTE (PAGE 4 IS BLANK)

2.0 SUMMARY

Following are the principal accomplishments which were made in the design of the high temperature leading edge heating array.

- Temperature and net heat flux calculations for each module in the heating array were performed for 3200°F and 3500°F maximum temperatures and associated distributions around the leading edges.
- Standard size heater and absorber modules were incorporated into the array to achieve the desired environments around the leading edge.
- Design studies and heater tests demonstrated the importance of highly reflective reflectors within the heater module. It was shown that gold coated reflectors were far superior to the polished chrome reflectors previously used, and significantly increased the heater operating efficiency. This greater efficiency reduced the power requirements thereby reducing the arcing potential and the cooling water requirements. For example, at the same power setting, specimen temperature increased from 2725°F to 3239°F using gold in place of chrome plated reflectors.
- Detailed thermal analysis of an existing development heater was used to predict the performance of the new leading edge prototype heater module.
- The heater module and full scale array were designed to meet the system requirement yet incorporate sufficient flexibility to allow for additional tests not encompassed by the design requirements.
- A prototype heater module (5 x 39 inch) was fabricated and tested.
- The design features incorporated into the heater module include tapered peg electrodes, a lever arm expansion end assembly, compact bus plates, structural water manifolds, enclosing reflectors, gas spray bars, and a nesting module design so that even larger specimens can be tested.
- A carbon-carbon specimen from a Shuttle leading edge instrumented with tungsten-rhenium thermocouples and heat flux sensors was positioned over the prototype module and tested in a 10 torr nitrogen environment to determine the performance and heat flux uniformity of the module.
- Detailed thermal modelling of prototype heater module was used to calculate heat flux uniformity and correlate test results.

- Performance and uniformity tests were conducted. A 3010°F specimen temperature was obtained without any problems at a power setting below the design maximum using chrome plated reflectors. Much higher temperatures at the same power settings are possible by using gold coated reflectors.
- Demonstration runs were conducted on the prototype module using thermocouples and heat flux sensors as the feedback signals for controlling the unit.
- A preliminary design of the full scale heating array was completed which includes configuration studies, complete mechanical design, power requirements, control techniques, temperature measurement techniques, interface definition and auxiliary equipment definition. This heating array satisfies all the design requirements and is designed for testing a variety of Thermal Protection Systems (TPS) ranging from a flat panel to a 6 to 15-inch radius leading edge. Some of the types of materials/systems that can be tested are:
  - Carbon-Carbon
  - Ablators
  - Metallics
  - Ceramic Reusable Surface Insulations
  - Antenna Materials
  - Orbital Thermal Control Coatings
- The maximum electrical power required for testing the 8-inch radius prototype leading edge specimen was estimated to be 600 Kilowatts.
- Technical information and cost estimates were forwarded to NASA for fabrication and testing of the full-scale heating array.

3.0 DESIGN GOALS

The objective of Phase I was to study and design a full-scale high temperature leading edge heating array system by developing various design concepts and selecting the best approach from the evaluation of a prototype. The heating array was to be flexible and capable of testing various size leading edges. Figure 3-1 shows a section of the test article to be tested by the array. The design goals for the heating array are summarized from Reference 1 as follows:

Operating Pressure Range: 0.5 to 760 torr in an inert environment (nitrogen)

Array Size: A size which will allow testing of a leading edge of at least 30-inch span with adjustment provided to allow the leading edge radius to vary from 6-inches to 15-inches. Figure 3-2 depicts the test specimen configuration limits.

Maximum Temperature: Referring to Figure 3-1, consistent with the aforementioned leading edge radius adjustment, Area I will be heated to a maximum temperature of 3500°F while Area II and IIA will be heated to a maximum temperature of 2500°F. The adjustment feature will allow Area I to be varied from 19 to 38 inch arc length and radii from 6 to 15 inches. Area II and IIA will be located tangent to the end of the Area I arc.

Heating Rate: 600°F/min. between 80°F and 2800°F.

Cooling Rate: 80°F/min. between 2800°F and 2000°F.

Chordwise Temperature Distribution: Shown in Figure 3-3.

Spanwise Uniformity: Minimum heat flux along the span of any given heating zone to be 90% of the maximum incident heat flux in the same zone during steady state heating at maximum temperature conditions.

The array is to be designed for installation at NASA's Manned Spacecraft Center Test Facility.

The array will have sufficient waste heat removal capacity to prevent heating of uncooled vacuum chamber walls. Coolant temperatures and flow rates of the heater array will be compatible with the MSC closed loop cooling system. Further, the array is to be designed to use and be compatible with 12 or fewer ignitron controllers (440 volt, 400 amp), "Data-Trak" programmers, and "Thermac" temperature controllers furnished by MSC.

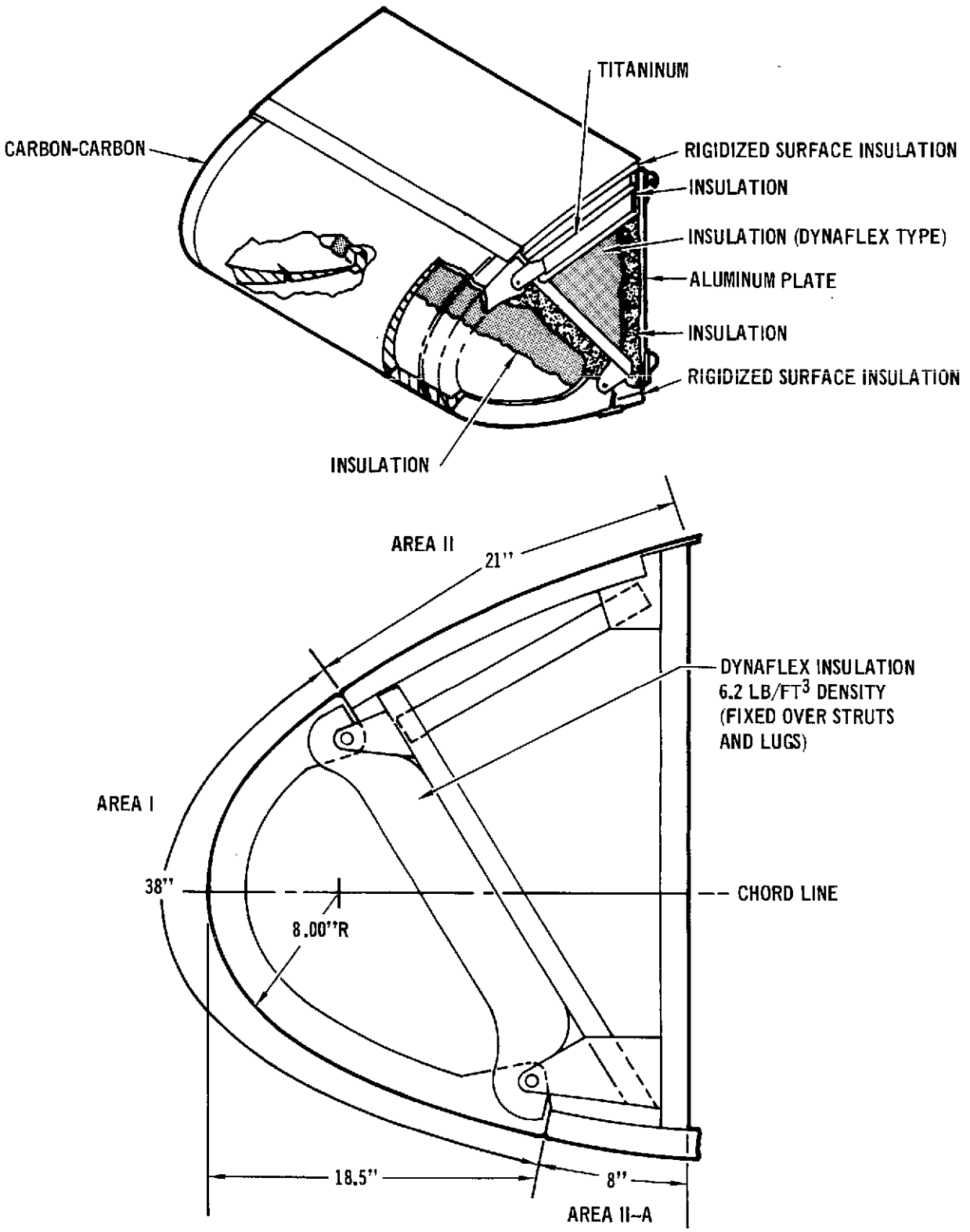

TEST SPECIMEN CONFIGURATION

FIGURE 3-1

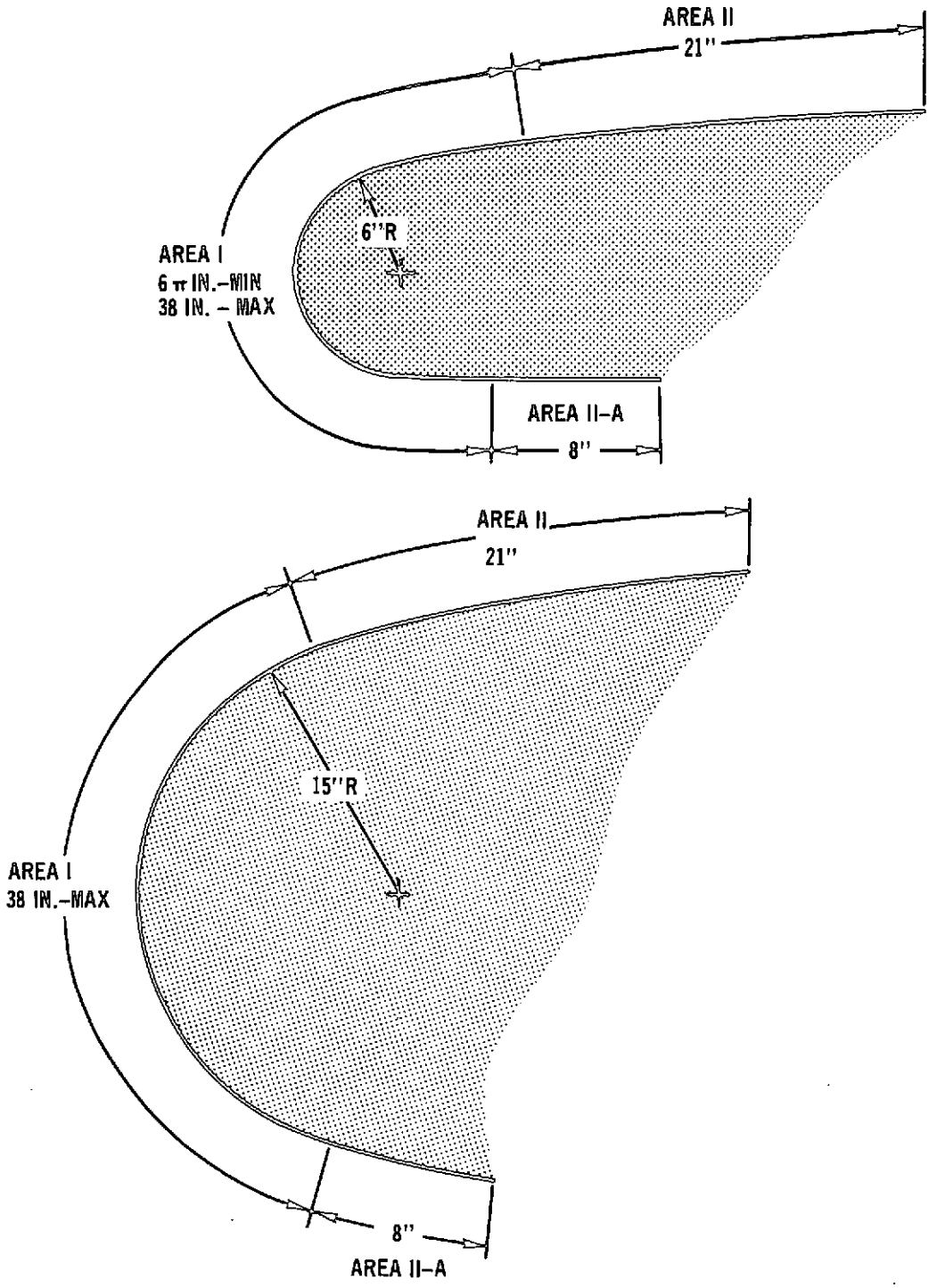

TEST SPECIMEN CONFIGURATION LIMITS

457–2411

FIGURE 3–2

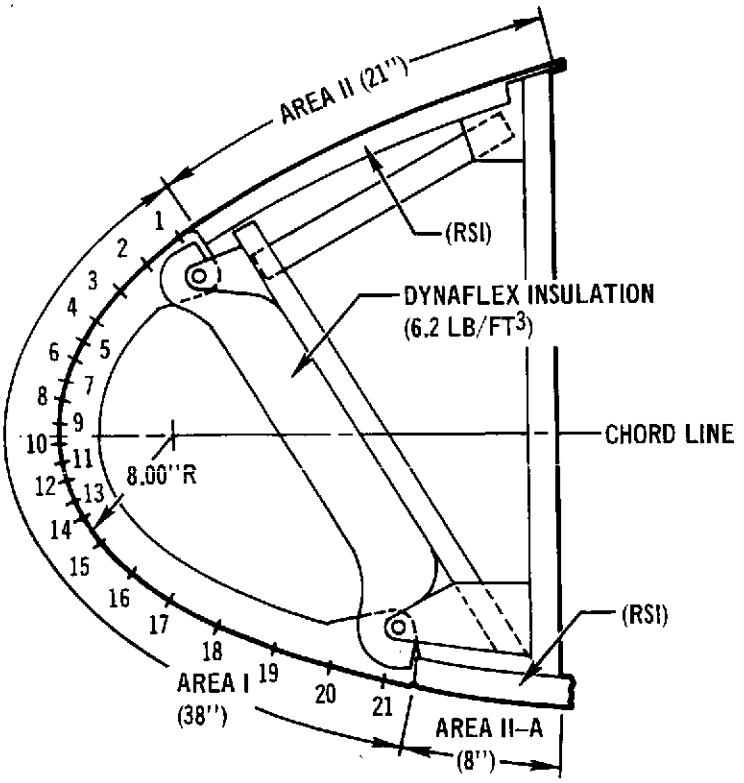

	TEMPERATURE °F	
NODAL POINT	DESIGN CONDITION	OVERSHOOT CONDITION
1	653	874
2	895	1164
3	1767	2210
4	1958	2439
5	2005	2495
6	2139	2656
7	2332	2888
8	2457	3037
9	2510	3107
10	2542	3139
11	2565	3167
12	2592	3200
13	2564	3166
14	2534	3130
15	2504	3094
16	2480	3065
17	2397	2966
18	2329	2884
19	2269	2812
20	2145	2663
21	1998	2487

SURFACE TEMPERATURES FOR NODAL POINTS ON LEADING EDGE
DESIGN AND OVERSHOOT CONDITIONS

457-2419

FIGURE 3-3

4.0 HEAT TRANSFER ANALYSIS OF ARRAY AND FULL SIZE TEST ARTICLE

Heat transfer analyses were performed on the array and test article to guide the design of the heating array and to provide performance information such as power and module temperature.

Heat transfer analyses were performed using multinode thermal models of the entire heating array and the leading edge, heat storage, view factor calculations, and a radiosity network solution for handling radiant energy reflections. After several array configurations had been analyzed, it was concluded that heat absorber modules, as well as heater modules, were required to achieve the desired temperature distributions. The following paragraphs describe, in detail, the models used and the results of the studies.

4.1 SIMULATION OF A LEADING EDGE TEMPERATURE DISTRIBUTION WITH A RADIANT HEATING ARRAY.

A thermal analysis was performed to determine the requirements of a high temperature heating array which would provide a specified leading edge temperature distribution. A large computer model, consisting of 131 nodes (70 thermal nodes and 61 radiosity nodes), was used to perform the thermal analysis. The thermal nodes (shown in Figure 4-1) included 42 carbon-carbon nodes, 8 RSI nodes, 8 fibrous insulation nodes, and 12 heater module control zone nodes. The radiosity nodes were used to describe the radiation transfer (including reflections) between surface nodes. Conduction in the carbon-carbon leading edge was included in both the parallel and perpendicular directions, as well as internal radiation between the carbon-carbon nodes which view each other.

The thermal analysis consisted of specifying temperatures at various points around the leading edge (one temperature across from each heater module) and solving for the heater module temperature and the net power required to maintain that temperature. Figure 4-2 shows the temperature distribution in the carbon-carbon leading edge that was used in the analysis. The aft portion of the leading edge consisted of Reusable Surface Insulation (RSI) whose surface temperatures are characterized by Nodes 22 and 26. Node 22 was controlled to 2300°F and Node 26 was controlled initially to 700°F. Two heater array configurations were analyzed. The first configuration was a 10 heater module array consisting of Nodes 36 through 45 as shown in Figure 4-1. The second configuration was the same as the first except that Nodes 36 and 37 were water cooled absorbers/reflectors rather than heater modules.

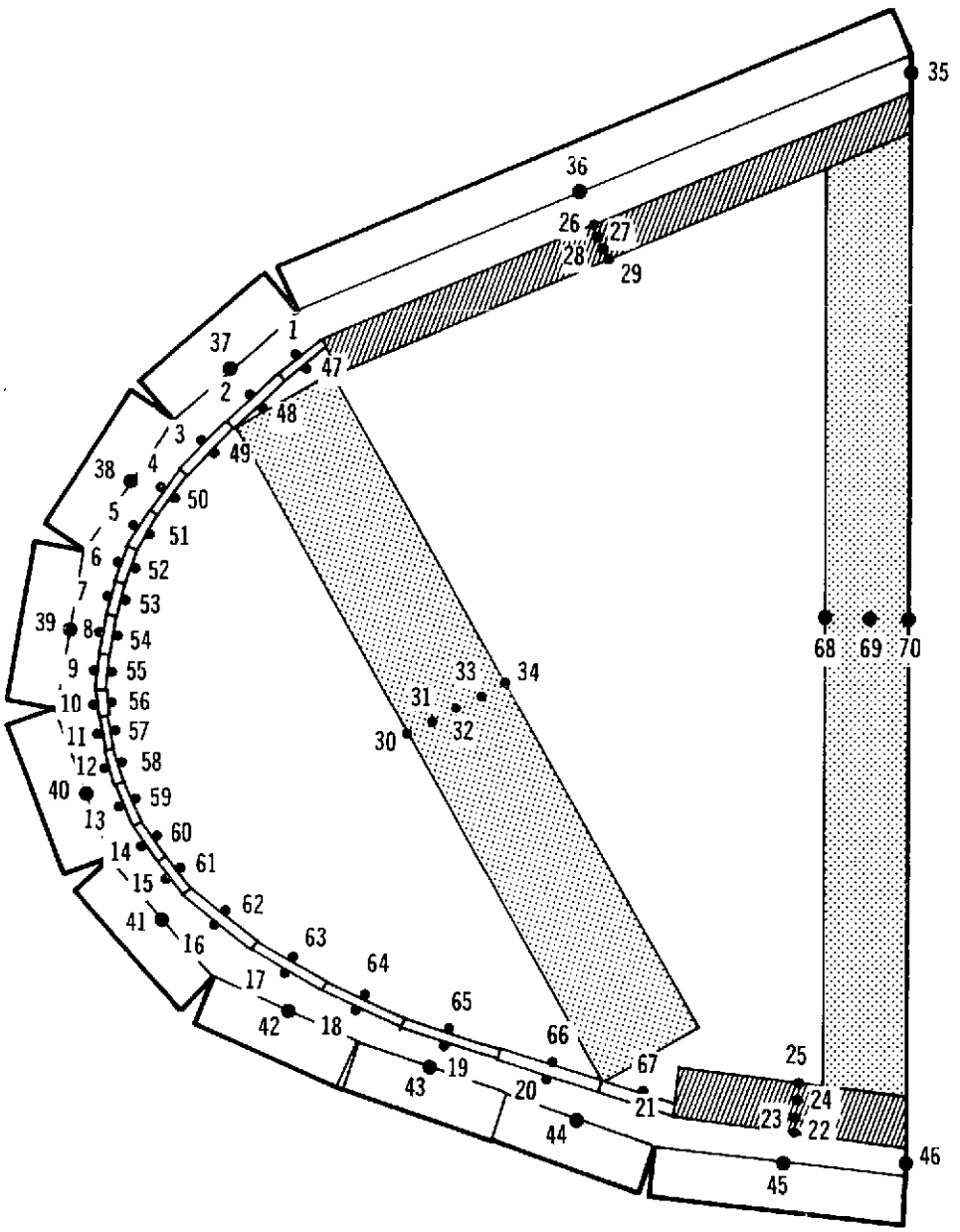

- NODES 1 THRU 21, AND 47 AND 67 ARE CACBON/CARBON
- NODES 22 THRU 29 ARE RSI.
- NODES 30 THRU 34, AND 68 THRU 70 ARE FIBROUS INSULATION
- NODES 35 AND 46 ARE GUARD REFLECTORS
- NODES 36 THRU 45 ARE HEATER MODULES.

COMPUTER MODEL OF LEADING EDGE AND HEATING ARRAY

FIGURE 4–1

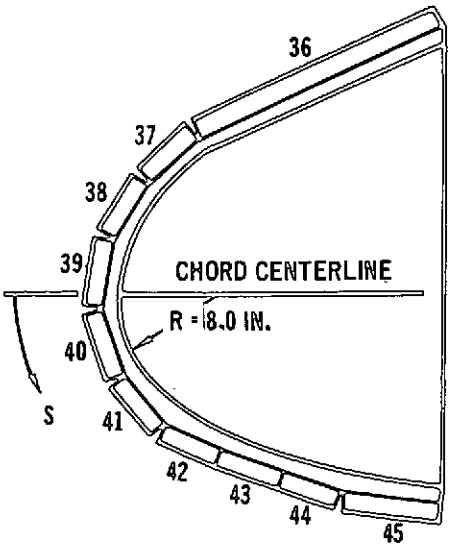

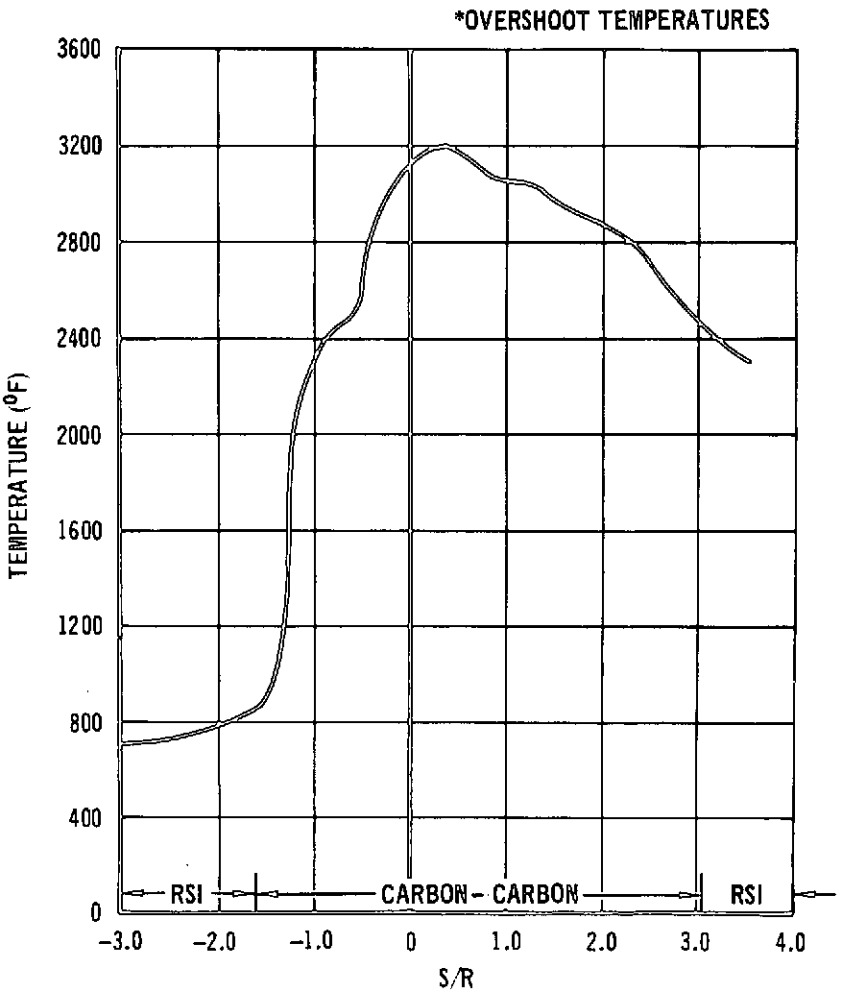

DESIRED LEADING EDGE TEMPERATURE DISTRIBUTION

FIGURE 4–2

4.1.1 Ten Heater Module Configuration. The results of this analysis are shown in Figure 4-3. The solid symbols are the control nodes; the solid line is the desired temperature distribution, and the dashed line is the predicted temperature distribution. The computer solution gives realistic heater module temperatures for all modules except Node 37. An impossible temperature, below 0°R, was calculated for Node 37 in order to achieve a drop from 2210°F to 874°F in 4-inches along the carbon-carbon at the top of the leading edge. This condition resulted from an abundant supply of energy to Nodes 1 and 2 by direct radiation, reflected radiation and conduction from sources other than Node 37.

It is apparent from this thermal analysis that Nodes 1 and 2 must be isolated from radiation emanating from the high temperature areas in order to produce the desired temperature distribution around the carbon-carbon leading edge. This can be achieved by changing the configuration of the heater modules so that the modules essentially come in contact with the carbon-carbon between Nodes 2 and 3. This seemed impractical and would have required a redesign of the modules (Section 6). Another approach would be to provide a curtain that would extend from the Nodes 37-38 intersection to the Nodes 2-3 intersection. The curtain temperature could be controlled through the use of surface coatings. Both of these approaches require further analysis to give greater confidence in controlling to the desired temperature distribution.

Another approach was to examine the heating distribution around the leading edge and to determine alternate temperatures at Nodes 1 and 2. It is felt that the temperature in this area is unusually low for the flight conditions that would produce a 3200°F stagnation point on the leading edge. This conclusion was arrived at by studying Shuttle designs and by discussions with NASA personnel. A thermal analysis was performed with Nodes 38 through 45 as heater modules and Nodes 36 and 37 functioning as water cooled absorbers. The purpose of this analysis was to determine the temperature which could be achieved at Nodes 1 and 2 without changing the configuration shown in Figure 4-1.

4.1.2 Eight Heater Module/Two Absorber Configuration. This analysis was the same as the ten heater module analysis except that Nodes 36 and 37 were held at 100°F and Nodes 1 and 2 in the carbon-carbon were allowed to find their own temperature as determined by the energy balance. Two cases were run to determine the effect of the emittance of Nodes 36 and 37. The results of this analysis are shown in Figure 4-4. The solid symbols are the control nodes and the solid

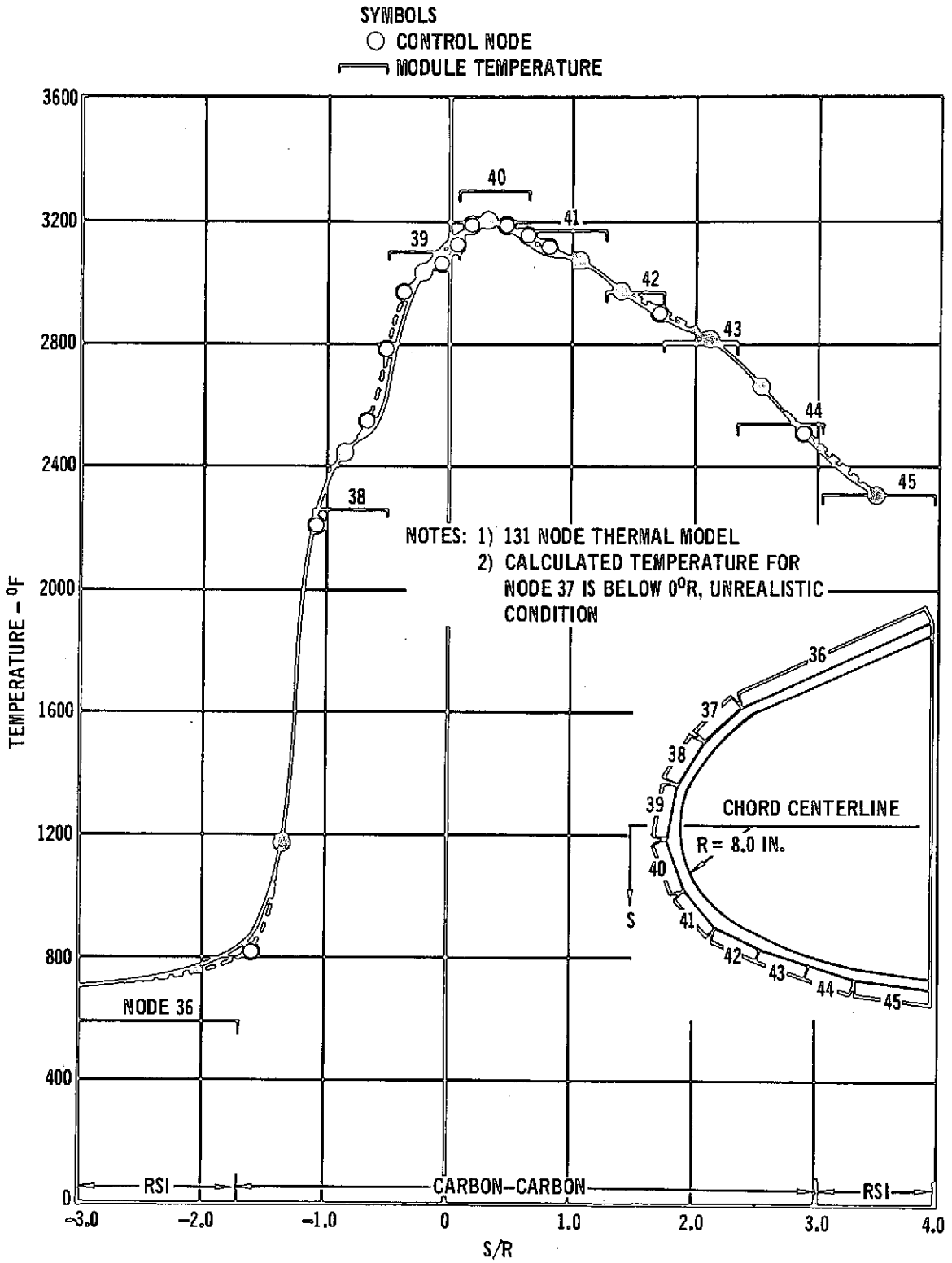

LEADING EDGE AND HEATER MODULE TEMPERATURES FOR THE TEN HEATER MODULE CONFIGURATION

FIGURE 4–3

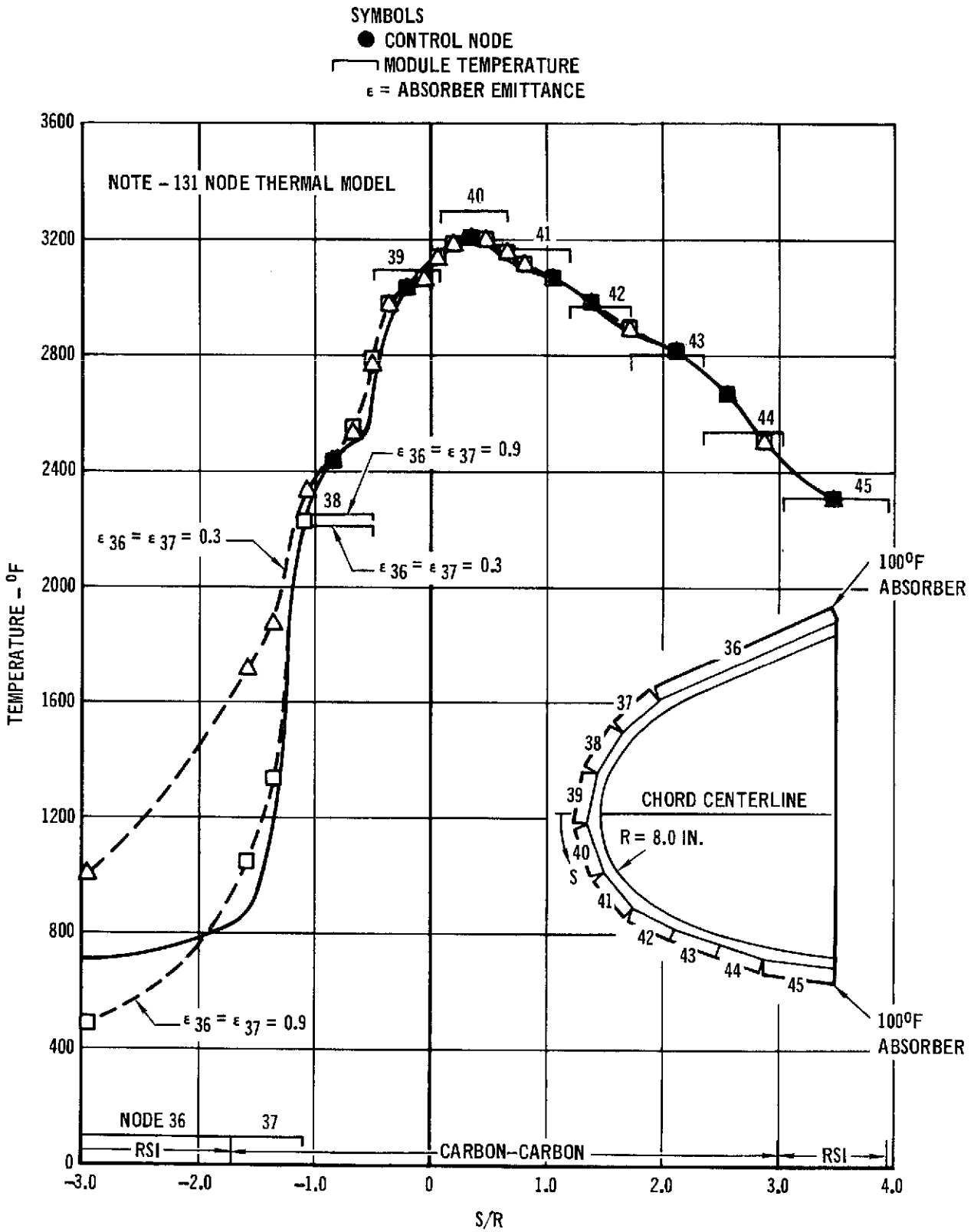

LEADING EDGE AND HEATER MODULE TEMPERATURES FOR THE EIGHT HEATER MODULE TWO ABSORBER MODULE CONFIGURATION

FIGURE 4-4

line is the desired temperature distribution. Two predicted temperature distributions are shown for an emittance of 0.9 and 0.3 for Nodes 36 and 37. It can be seen that if Nodes 36 and 37 are water cooled absorbers, (ε = 0.9), a reasonable temperature distribution in the carbon-carbon leading edge can be achieved. If Nodes 36 and 37 are water cooled reflectors (ε = 0.3), much higher temperatures are obtained at Nodes 1 and 2 illustrating the importance of reflected radiant energy in determining temperatures in this area. Figure 4-5 is a summary of the heating array temperatures and heat fluxes required to maintain those temperatures for the eight heater module configuration. These are steady state results for the leading edge temperature distribution shown in Figure 4-4. The maximum net heat flux generated by a heater module is 11.22 Btu/ft^2-sec (for Node 40 operating at 3300°F). It should be noted that the net heat flux does not include the heat losses within the individual heater modules. The heat losses within a module are discussed in Sections 5 and 6.

4.2 SIMULATION OF A 3500°F LEADING EDGE TEMPERATURE DISTRIBUTION USING THE HEATER ARRAY. The heater array is intended to be capable of heating a carbon-carbon leading edge to 3500°F surface temperature. A thermal analysis was performed in order to establish the heater configuration and power requirements for this condition. The same thermal model and analysis procedure described in Section 4.1 was employed utilizing the eight heater module/two absorber array configuration. The 3500°F (3960°R) temperature distribution (Figure 4-6) to be achieved on the leading edge was calculated by scaling the 3200°F (3660°R) temperature distribution using a factor of 1.082 (1.082 = 3960/3660).

The computed temperatures are shown in Figure 4-7. The solid symbols are control nodes on the leading edge, the solid curve is the desired temperature distribution, and the dashed line is the predicted temperature distribution. Also shown are the heater module temperatures required to produce the leading edge temperatures. This analysis indicates that a reasonable temperature distribution on the leading edge can be achieved with the eight heater module configuration. Figure 4-8 is a summary of the temperatures and net heat fluxes required to maintain those temperatures for steady state conditions. The net heat flux does not include the heat losses experienced within the individual heater modules. The maximum net heat flux required for a heater module is 14.09 Btu/ft^2-sec for Node 40 operating at 3596°F.

A) Water Cooled Absorbers ($\epsilon_{36} = \epsilon_{37} = 0.9$)

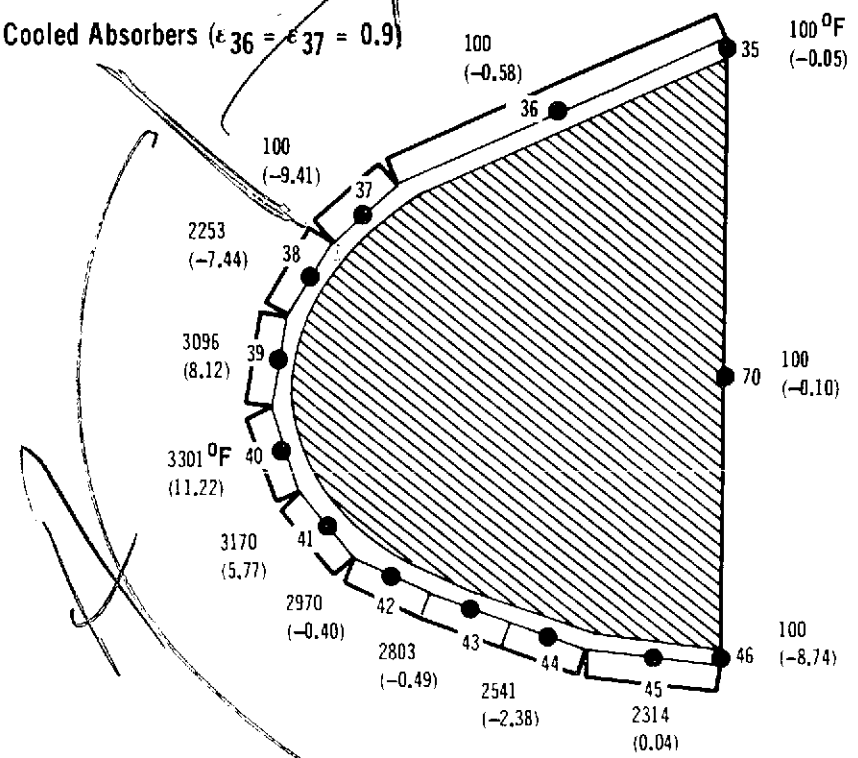

B) Water Cooled Reflectors ($\epsilon_{36} = \epsilon_{37} = 0.3$)

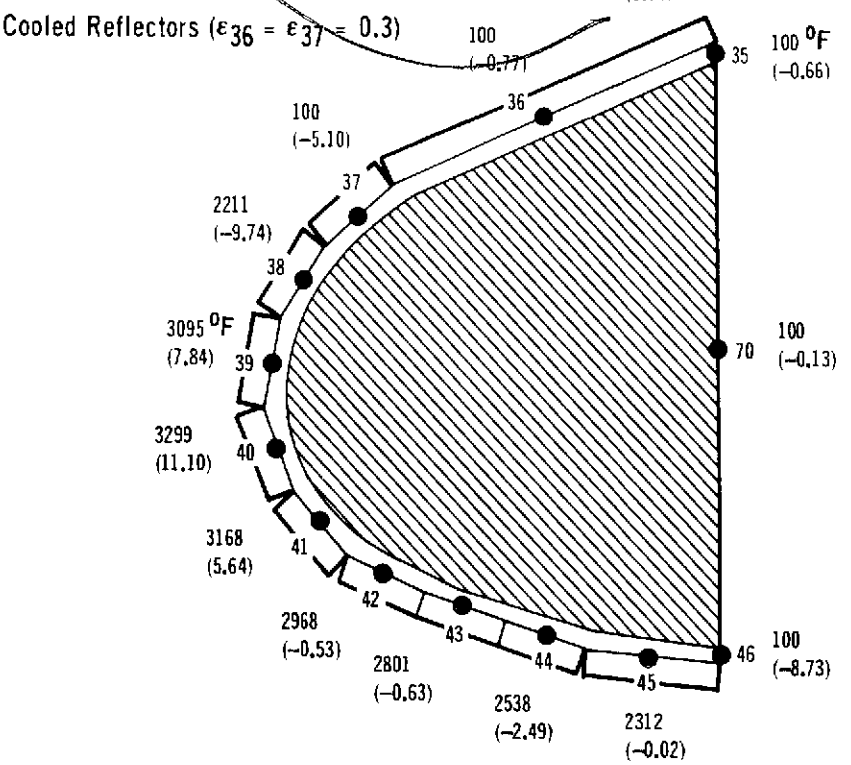

- 3200°F MAXIMUM LEADING EDGE TEMPERATURE
- STEADY STATE ANALYSIS
- XXX – TEMPERATURE (°F)
- (YYY) – HEAT FLUX (BTU/FT^2-SEC)

PREDICTED LEADING EDGE HEATING ARRAY TEMPERATURE AND HEAT FLUX DISTRIBUTIONS FOR THE EIGHT HEATER MODULE CONFIGURATION

FIGURE 4–5

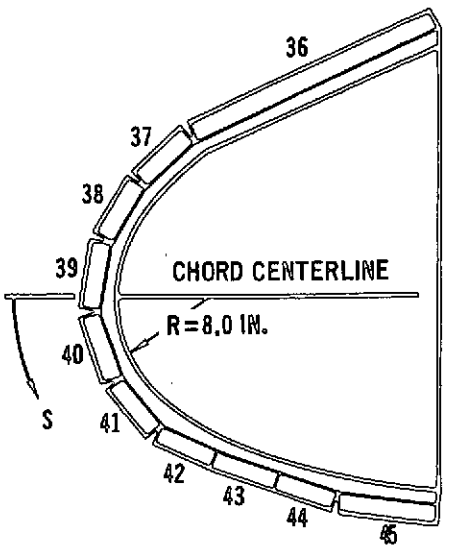

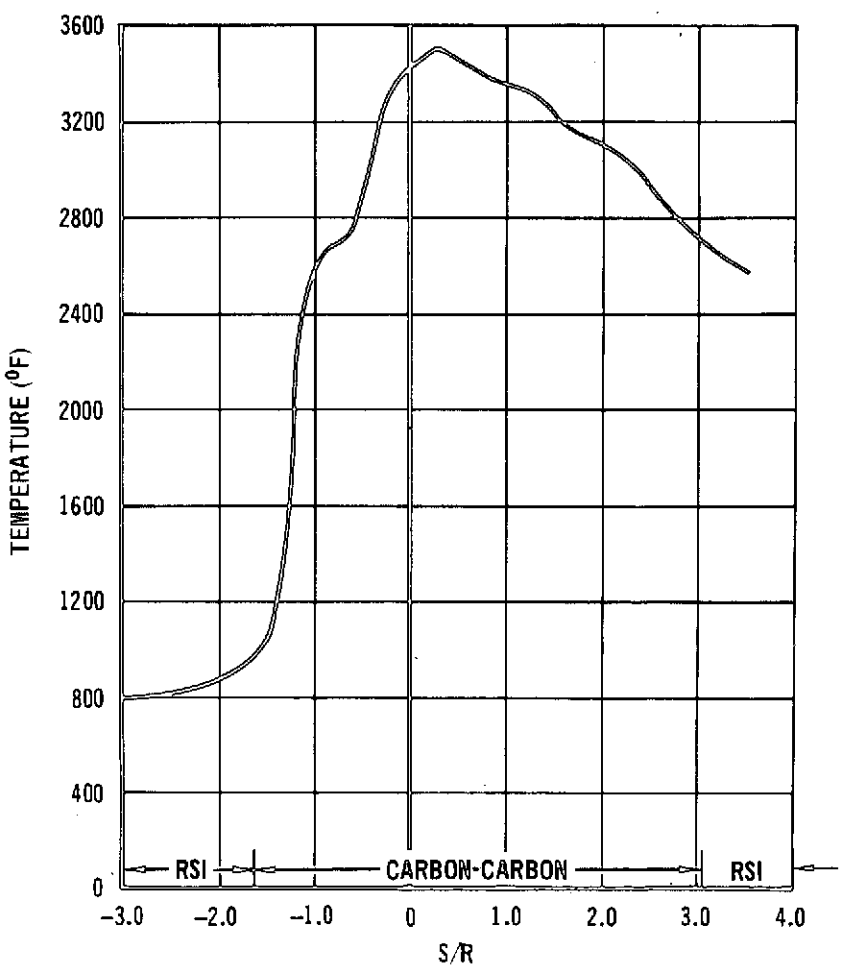

3500°F LEADING EDGE TEMPERATURE DISTRIBUTION

FIGURE 4-6

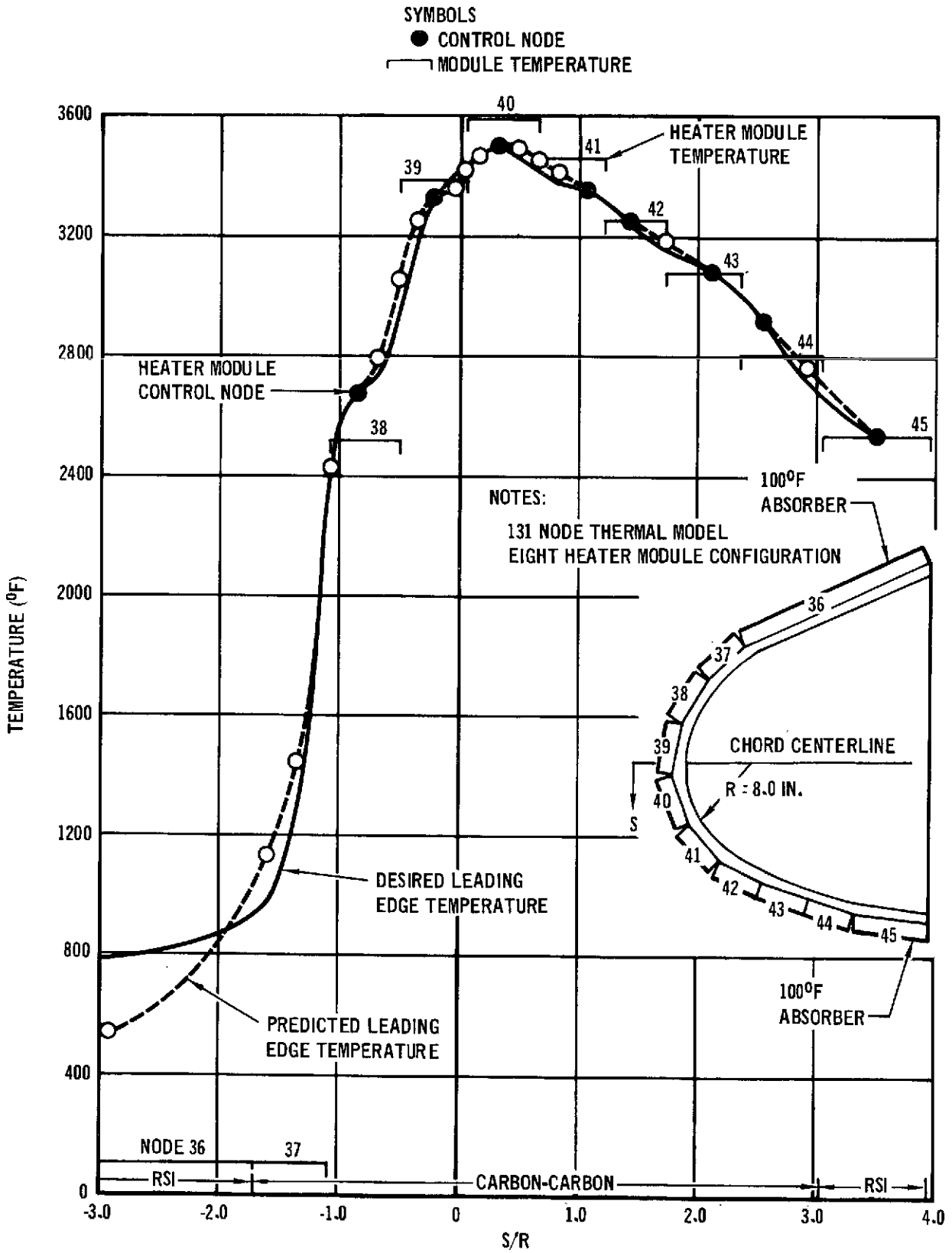

LEADING EDGE AND HEATER MODULE TEMPERATURES
FOR A PEAK CARBON–CARBON TEMPERATURE OF 3500° F

FIGURE 4–7

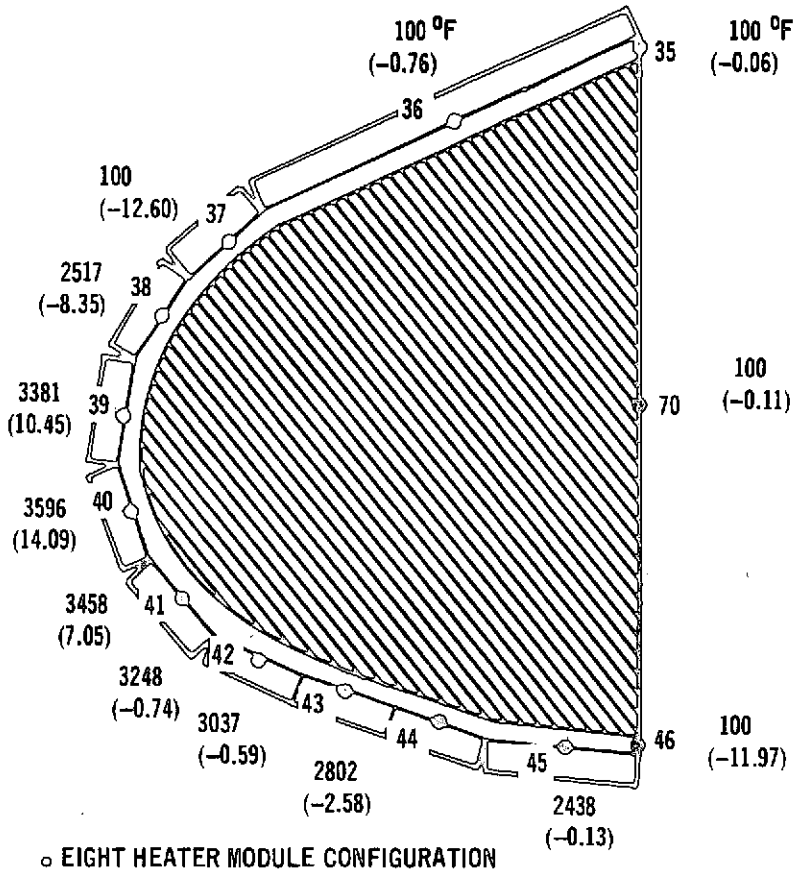

- EIGHT HEATER MODULE CONFIGURATION
- STEADY STATE ANALYSIS
- MODULES 36 AND 37 ARE WATER COOLED ABSORBERS
- TEMPERATURES ARE SHOWN IN DEGREES FAHRENHEIT
- HEAT FLUX (IN PARENTHESES) IS SHOWN IN BTU/FT^2-SEC

PREDICTED LEADING EDGE HEATING ARRAY TEMPERATURE AND HEAT FLUX DISTRIBUTIONS FOR A 3500°F PEAK LEADING EDGE TEMPERATURE

FIGURE 4-8

In all thermal analyses that have been performed, the emittance of the graphite elements was assumed to be 0.9. Figure 4-9 shows the emittance of the graphite element material (Speer Carbon grade 890S) is well below 0.9 at expected operating temperatures. A comparative thermal analysis was performed using the graphite emittance shown in Figure 4-9 to determine the effect on required element temperatures. The results show a rather small change in element temperatures. Several of the elements had a temperature change of less than one degree Fahrenheit. The largest temperature increase required was for Node 40 where the element temperature was 29°F higher (3625°F compared to 3596°F) than when the emittance was assumed to be 0.9.

REFERENCE: NASA CR-111841

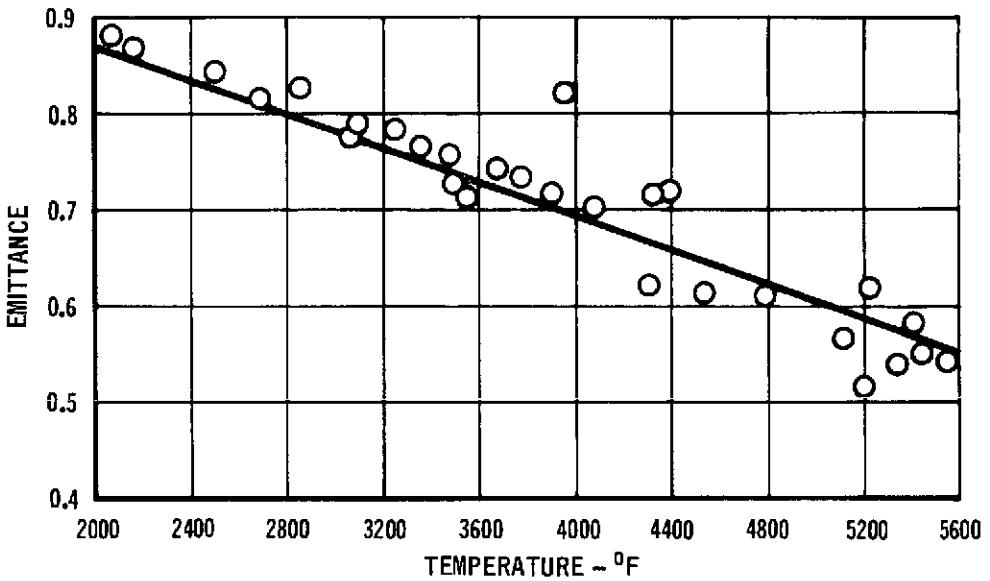

TOTAL NORMAL EMITTANCE – 890S GRAPHITE

FIGURE 4-9

A reasonable temperature distribution around the leading edge can be achieved using eight heater modules and two large absorbers. The absorber modules can be composed of smaller, standard size modules and achieve the same temperature distribution. Heat transfer analyses were also performed to correlate preliminary testing and testing of the prototype heater module.

5.0 PRELIMINARY EXPERIMENTAL EVALUATION

Early in the program, preliminary arcing studies were conducted using an existing development graphite heater of similar geometry to the leading edge heater module (described in Section 6). This testing led to an investigation of instrumentation techniques pertaining to operation and development of high temperature heaters. A study was performed to improve the performance of graphite heaters by evaluating various coatings for the reflector.

5.1 ARC INVESTIGATION TEST.

5.1.1 Objective. The arc investigation test was initiated early in the program; its objective was to observe for arcing the heating of a representative test specimen to 3500°F using a representative heater operated at 100-115 volts and 0.5 to 10 torr. These tests were very valuable in understanding heater operation at high temperature, identifying the required instrumentation and facilitating expeditious testing of the prototype module (described later).

5.1.2 Test Setup. The arc test setup, shown in Figure 5-1, consisted of an existing development graphite heater module, (Figure 5-2), a test article, an ignitron power controller, a 4:1 stepdown transformer, and a vacuum chamber. The heater had geometry similar to the leading edge heater (described in Section 6) and was used for the arc investigations at 2500°F peak temperature on Contract NAS9-12570. The test article consisted of a 0.25-inch thick graphite plate backed by three 0.25-inch layers of graphite felt. A water-cooled plate behind the felt absorbed all transmitted energy. Because of the relatively straightforward objective of the test, only rudimentary instrumentation was installed initially.

5.1.3 Results. In spite of the apparent simplicity of the proposed test, the first run was practically a catastrophe because the 80 KW being dissipated heated the test specimen apparently to only slightly over 3000°F and an arc was experienced at 10 torr which damaged the setup. Along with this, two independent methods of measuring the specimen temperature yielded remarkably different results, about 300°F difference. The heater assembly was repaired and additional instrumentation was installed in an attempt to determine the system heat balance; however, because of the rudimentary nature of the test, the heat balance was not achieved, the specimen temperature could not be accurately determined, and persistent arcing continued to mask post-test analyses. At this point testing was stopped. The obvious problems along with some possible reasons for their existence were categorized and are listed as follows:

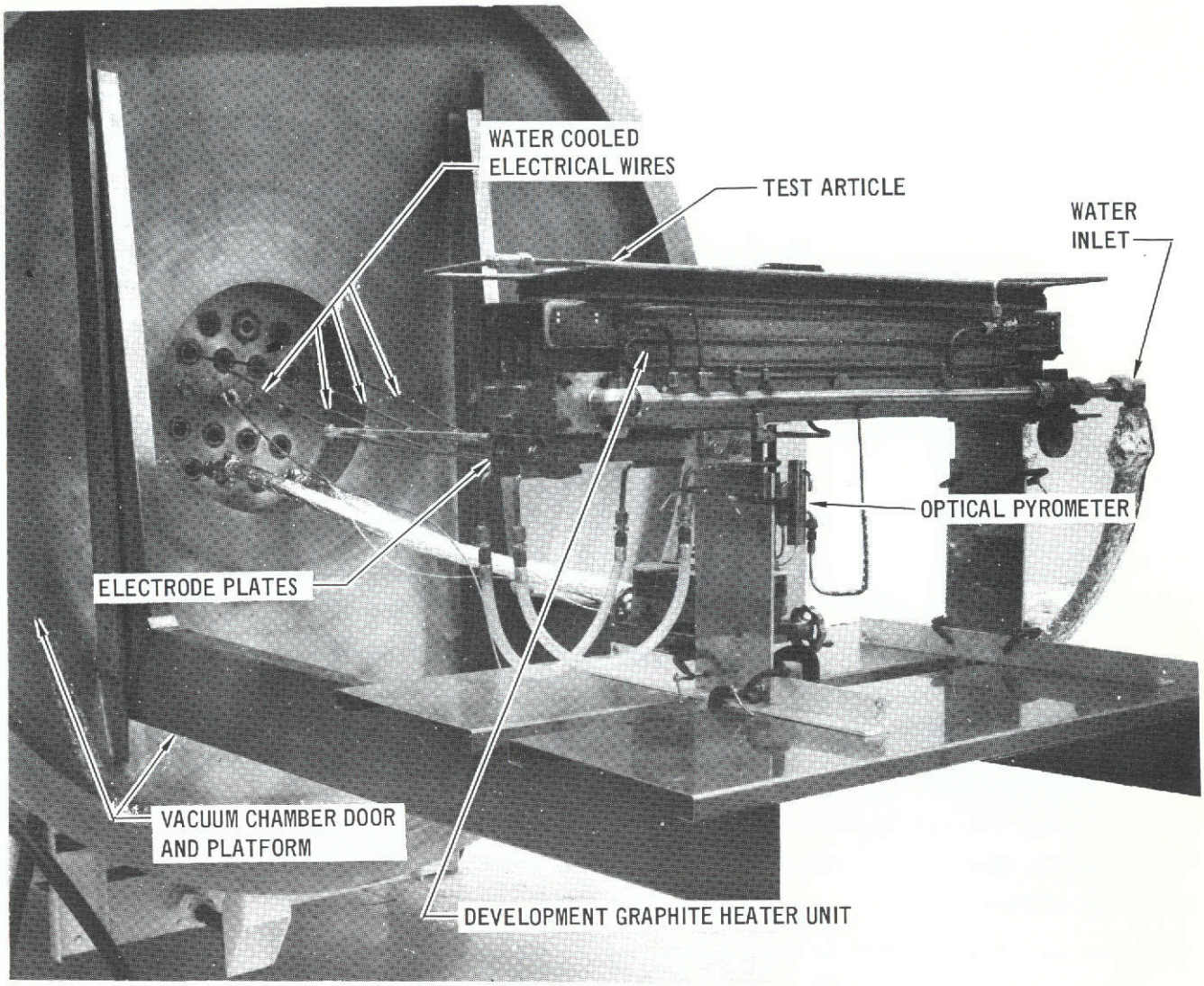

PRELIMINARY EVALUATION TEST SETUP
(Development Heater Unit)

FIGURE 5-1

(1) Specimen temperature achieved at a given power setting lower than anticipated.

- o Inaccuracy in temperature measurement
- o Inaccuracy of power measurement
- o Power lost to things other than the specimen
- o Lack of precision in input power calculations
- o Specimen power absorption larger than anticipated.

(2) Heat balance not achieved

- o Inaccuracy of power measurment
- o Inaccuracy of water temperature change measurement

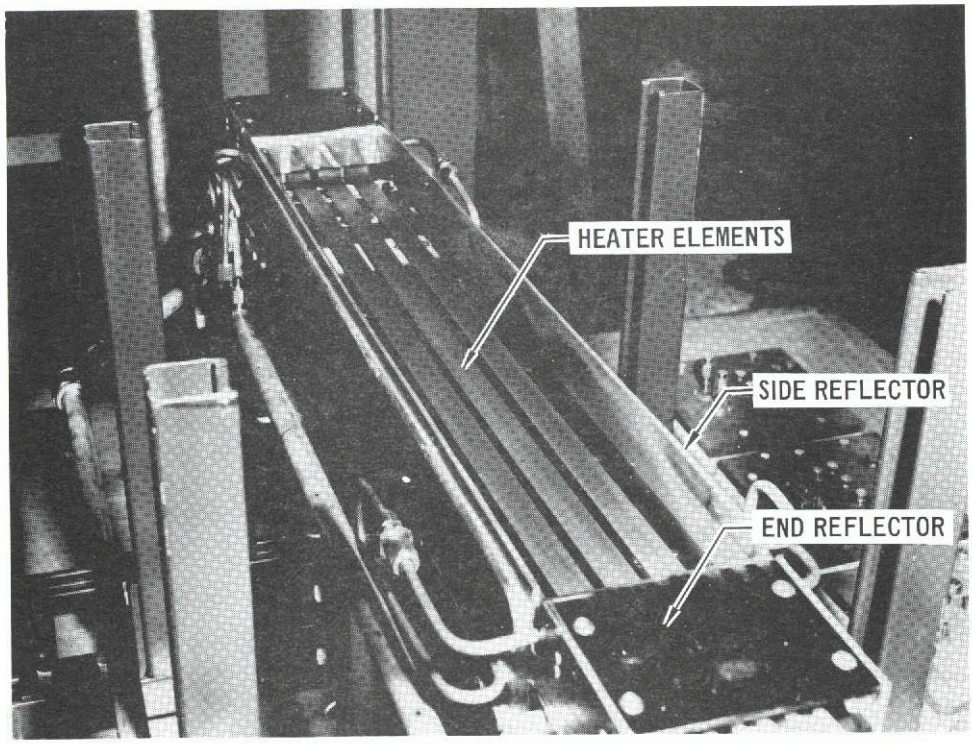

DEVELOPMENT HEATER MODULE UNIT

FIGURE 5-2

- o Inaccuracy of water flow measurement
- o Electrical losses not accounted for
- o Unaccounted for heat leaks.

(3) Arcing

- o High element temperature causing smoke and arcing
- o Low pressure coupled with high element temperature
- o Degraded setup, i.e., water leaks, carbon tracks, arc marks, etc.

From the above results it was clear that to successfully operate the leading edge heater and to determine its performance at temperatures up to 3500°F, it would be necessary to have a carefully assembled and instrumented test setup. This was done with the development heater module while the leading edge prototype heater was being fabricated (Section 6.0). The upgraded instrumentation is described in the next section.

5.2 INSTRUMENTATION TECHNIQUES.

5.2.1 Objectives. In view of the results achieved in the arc investigation tests, the primary objective of this testing was to develop instrumentation and techniques capable of measuring the parameters of interest with sufficient

accuracy and repeatability to obtain generally consistent results. Specifically, it was desired to achieve a heat balance, consistent specimen and element temperatures, and a test capability for trouble-free evaluation of the leading edge prototype heater performance.

5.2.2 Test Setup. The basic test setup was the same as for the arc investigation tests, shown in Figures 5-1 and 5-2, except that the heater assembly was carefully refurbished to eliminate the sources of spurious arcing. The o-ring seals in the heater assembly were replaced to stop water seepage. All electrical contact surfaces along the current path were cleaned to reduce extraneous power losses. The heater reflectors were cleaned and all rough edges were smoothed to eliminate sharp protrusions which might promote arcing. All evidence of previous arcing, such as carbon deposits and arc "tracks", was carefully removed with abrasive cloth and solvents. In addition, it was decided to operate the heater at less than its maximum possible power to further minimize the possibility of arcing. The test article was modified to minimize the heat leak by adding more insulation, reducing the edge conduction, and isolating the mounting from the cooled heat sink. To eliminate unaccounted for electrical losses from the input power determination, the voltage tap was installed directly on the heater terminals and the secondary current was measured. True RMS meters indicating the voltage and current were used to eliminate any effects caused by the ignitron. Water flowmeters replaced the prerun flow calibration used previously and water temperature rise was measured using sheathed differential thermocouples mounted in direct contact with the water, which increased ΔT accuracy. A pair of optical pyrometers of different design were employed with the capability of viewing either the specimen or the elements through a hole in the bottom reflector via a mirror and a window in the vacuum chamber. Further, a tungsten-rhenium thermocouple was installed in the test article by drilling a hole into the edge of the carbon plate.

5.2.3 Results. After the setup and instrumentation was completed, testing was resumed and the power level was stepped up gradually until a specimen temperature of about 3000°F was achieved with the power level at about 47 KW. No arcs were experienced during any of the runs, which were made at a chamber pressure of 50 torr, and utilized a maximum voltage of 80 volts. Although the optics and various other phenomena caused an uncertainty in the pyrometer measurements of up to 100°F, the two pyrometers produced identical temperatures which were repeated on succeeding runs. The power absorbed by the cooling water matched the input electrical power within 2%.

It was concluded after this series of tests that the test setup was ready for performance evaluation of the prototype heater module.

5.3 REFLECTOR EVALUATION. As part of the preliminary evaluation the effects of various different reflector coatings were examined to determine if the performance of the heater could be increased. Commercial chrome plating of reflectors has been used on all MDC graphite heaters up to this time because of the economics of application, the durability, and the ease of cleaning. To achieve the highest possible element and specimen temperature for a given power setting, a reflector coating with a high reflectance in the wavelength band of the element emission is desirable. Several metals and nonmetallic diffuse coatings have spectral reflectances higher than chrome in the near infrared. To evaluate the possible improved performance of a higher reflectance coating, two readily available and easily applied materials were considered for comparison with the chrome. These were: Eastman 6080 white reflective paint and gold coated tape (Y91-84A, gold film deposited on 1 mil Kapton with 2 mils acrylic adhesive).

5.3.1 Reflector Test Results. The reflectors of the development module were coated with these materials and a series of heater runs was performed. Figure 5-3 is a summary of the element and specimen temperatures at several power levels with the chrome, painted, and gold tape reflector coatings. It can be seen that the white reflective paint exhibits poorer performance than the chrome until the highest power point. This is not considered unusual since this paint has extremely high reflectance in the visible and near infrared but becomes nearly a total absorber at wavelengths beyond 2.4 microns. The gold tape, on the other hand, demonstrated vastly superior performance when compared to the chrome as shown by the 60 volt level where the specimen temperature with the gold was 3102°F and with the chrome was 2515°F. At the 70 volt condition a specimen temperature of 3239°F was obtained before the gold tape deteriorated and the test had to be terminated. This deterioration was expected because of the relatively low thermal conductivity of the Kapton film and the 450°F limit on the acrylic adhesive causing the tape to overheat and to bubble and summarily perish. This condition can be rectified by plating the gold directly onto the cooled reflector. Not only does the gold coating increase specimen temperature, but less power is required and hence less cooling water for a given test program. Candidate methods for applying gold to the reflector are discussed in Section 5.3.3. As a result of this investigation we feel strongly that the heater modules in the full heating array should have gold coated reflectors. The reflectors for the prototype module (discussed in Section 6.0) had already been

REFLECTOR COATING	ELEMENT POTENTIAL (VOLTS)	ELEMENT POWER (BTU/SEC)	REFLECTOR COOLING WATER FLOW RATE (LB/SEC)	REFLECTOR COOLING WATER DELTA TEMP (^{0}F)	HEAT ABSORBED BY REFLECTORS (BTU/SEC)	ELEMENT TEMPERATURE (^{0}F)	SPECIMEN TEMPERATURE (^{0}F)
CHROME	50	18.8	1.12	16	17.9	2485	2265
	60	25.9	1.10	23	25.3	2710	2515
	70	35.7	1.12	31	34.8	2946	2725
	80	44.5	1.13	39	44.0	3130	2907
EASTMAN 6080 REFLECTIVE PAINT	50	17.8	1.12	16.5	18.5	2334	2080
	60	24.8	1.13	22	24.8	2630	2380
	70	32.6	1.15	28	32.2	2895	2665
	80	41.6	1.13	36	40.6	3141	2907
GOLD COATED TAPE (Y91-84A)	50	15.8	–	–	–	2907	2830
	60	21.75	–	–	–	3170	3102
	70	26.7	–	–	–	–	3239

(1) DEVELOPMENT HEATER MODULE

REFLECTOR TEST RESULTS

FIGURE 5-3

chrome plated at this point in the program and schedules did not permit recoating.

5.3.2 Analytical Studies of Reflectance on Heater Performance. A thermal analysis was performed to predict heater element and test specimen temperatures for the 4.5 inch x 26 inch development heater used in the preliminary evaluation tests. The results of the analysis emphasize the importance of the reflectance of the reflectors on heater power requirements. When the heater modules are operated at high temperatures, outgassing products from the elements and/or test article form deposits on the reflective surfaces of the heater. This, in turn, may affect the reflectance of that surface and consequently the required power. The analytical predictions were used in conjunction with the test results (Figure 5-3) to estimate the effective reflectance of the three reflector coatings during heater operation.

The thermal analysis utilized a three-dimensional thermal model (designated model B) consisting of 9 reflector nodes, a single heater element node, 1 test specimen node, and 12 radiosity nodes. The reflector surfaces form five sides of a box 26 in. long, 4.5 in. wide, and 3 in. high. The test specimen is represented by a surface 4.5 in. x 26 in. which forms the sixth side of the box. The heater elements are represented by a surface inside the box located 2 in. from and parallel to the test specimen. The assumption was made that the test specimen was adiabatic and that the reflectors absorbed all the heater element power. Examina-

tion of the heater power dissipated and heat absorbed by the reflectors during the reflector evaluation tests (Figure 5-3) substantiates this assumption. The reflectors were held to 100°F and power was input to the node representing the heater elements. The heater element and test specimen temperatures were then computed for steady state conditions.

Figures 5-4 and 5-5 present the calculated test specimen and element temperatures, respectively, as a function of heater element power and reflector reflectance for the 4.5 in. x 26 in. development heater. It can be seen that significantly more power is required to produce a given test specimen or element temperature as the reflector reflectance decreases. Figures 5-6 and 5-7 present the analytical results in a format which allows the effective reflectance of the three reflector coatings to be estimated from the test results. The effective reflectance of the chrome and reflective paint ranges between 0.60 and 0.70 based upon the reflector test results. It can be seen that the reflective paint becomes a better reflector as the temperature increases. The gold had a high effective reflectance (0.86) which was the reason the higher specimen temperatures were obtained using gold coated reflectors.

The effective reflectance of the reflectors used to calculate test specimen and element temperatures presented in Figures 5-4 through 5-7 for the 4.5 inch x 26 inch development heater, were also applied to the new prototype being assembled. Therefore, the estimated power requirement for the new prototype heater was based upon its configuration and the effective reflectance values presented here.

The effective reflectances thus obtained are a correlation between the measured data for the development heater and a particular computer model, which had single nodes and heater elements, and the test article. A different effective reflectance was obtained (Section 6.3) for the prototype module using a more sophisticated uniformity thermal model.

5.3.3 Gold Coating - Methods and Reflectance Measurements. Since testing and analytical studies have shown that gold coated reflectors can markedly improve the performance of a graphite radiant heater, the methods of applying a gold coating were investigated along with the measurement of the spectral reflectance of the coated specimens.

The most obvious way to gold coat a reflector is, of course, electroplating, but, because of the reflector size (up to 40 inches long), only a few electroplating firms are suitably equipped to gold plate reflectors. The quality and reflectance

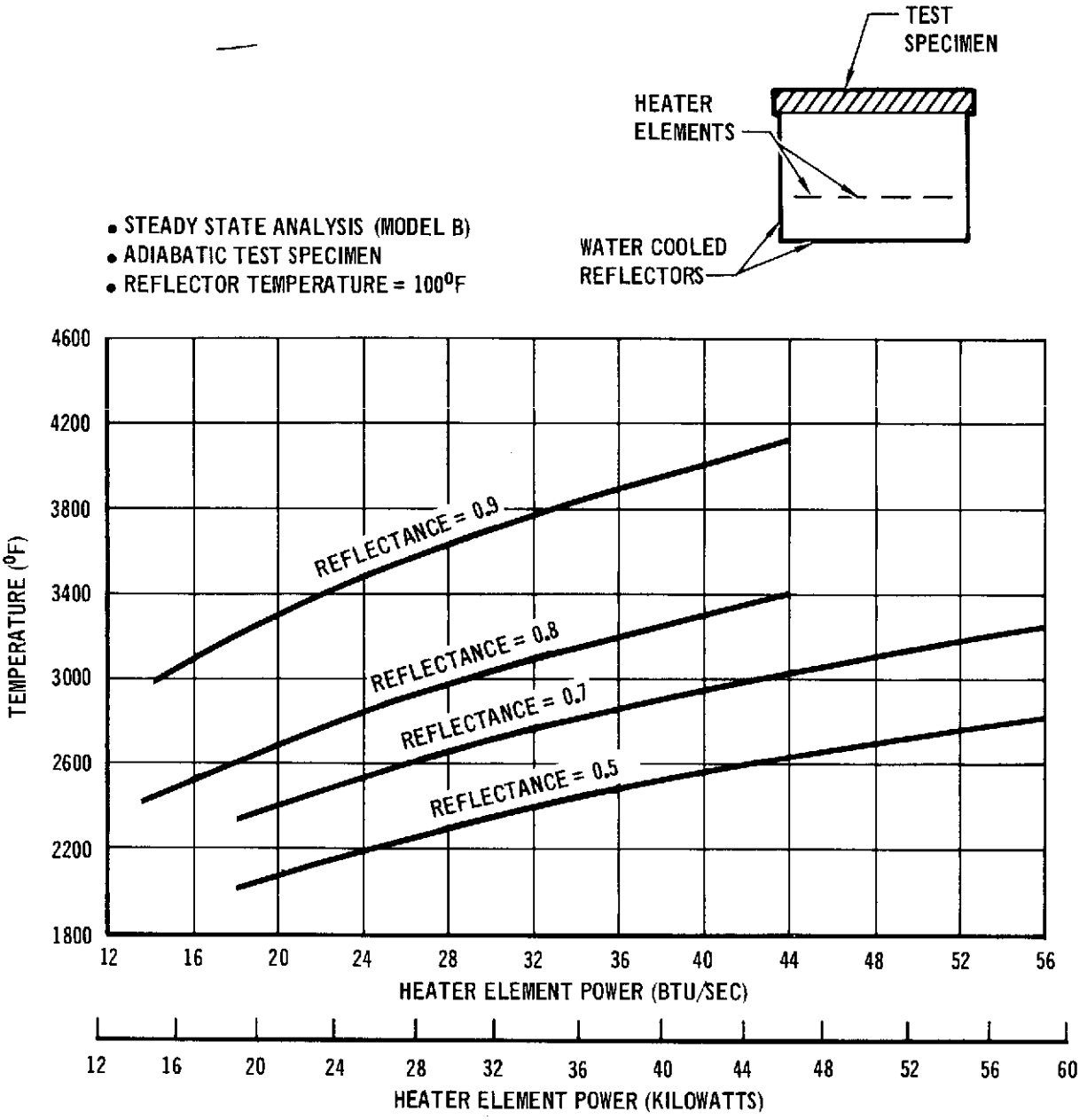

PREDICTED TEST SPECIMEN TEMPERATURES FOR 4.5" x 26" DEVELOPMENT HEATER

FIGURE 5-4

of the electrolytic gold is dependent on application technique and polishing of a suitable substrate on the copper reflectors.

Another popular method of gold coating is by vacuum deposition using an electron beam source. This is a standard bell-jar procedure which can be performed in the McDonnell Douglas Corporation (MDC) Laboratories, and the coating can be applied directly over the chrome plated polished reflectors. However, the size of

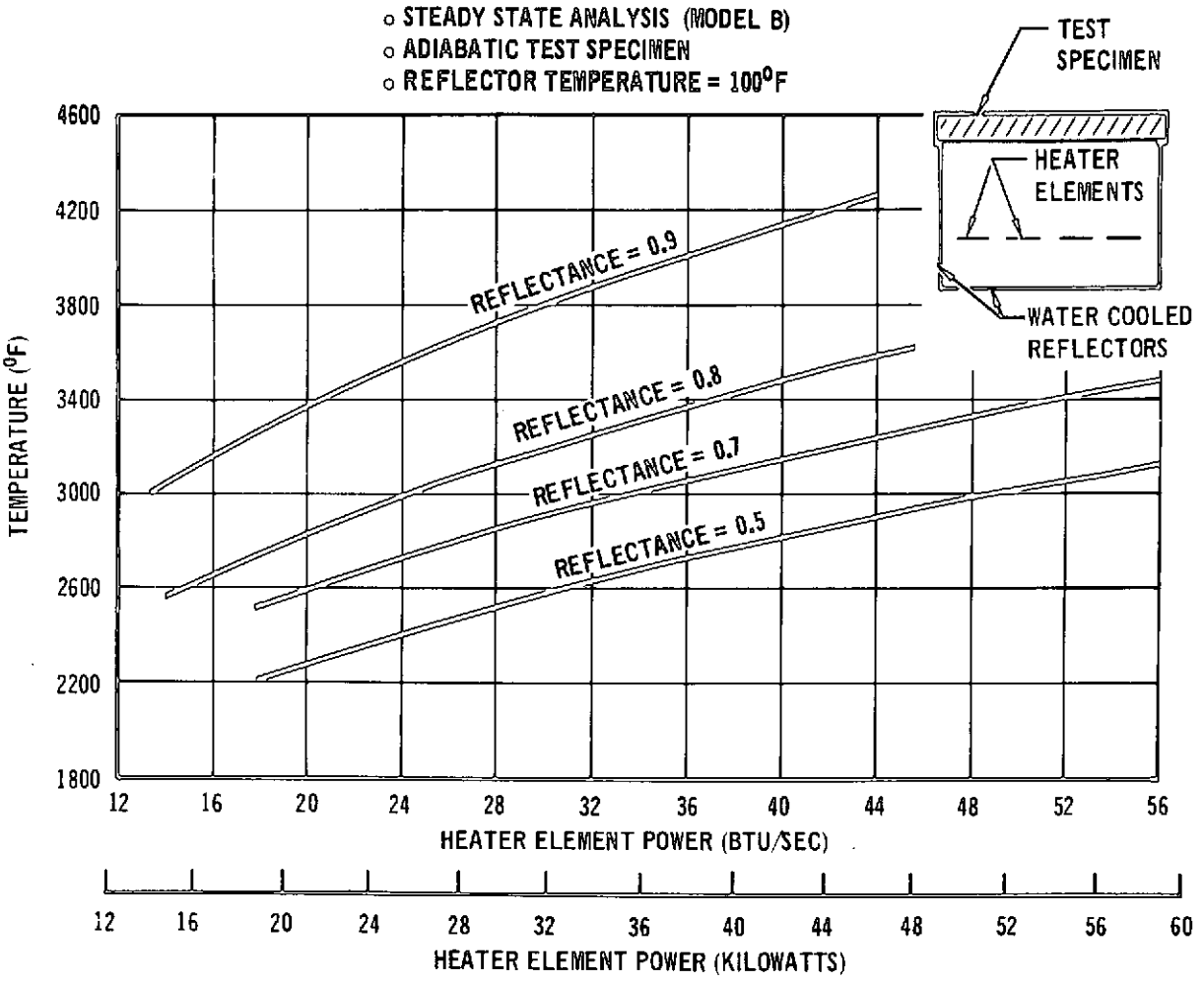

PREDICTED HEATER ELEMENT TEMPERATURES FOR 4.5" x 26" DEVELOPMENT HEATER

FIGURE 5-5

the reflectors requires the use of a larger vacuum chamber and either a traversing source or a multi-source arrangement not available in MDC Laboratories. Further, because the vacuum deposited gold coating is so thin (0.15 μm) and soft, an over-coating of a dielectric material such as silicon dioxide or magnesium fluoride must be deposited to protect the gold form physical damage during cleaning operation in service.

Heat conversion gold is another method of applying a gold coating which involves painting the surface with a solution of gold salt and then heating the piece to reduce the salts and leave the gold. This method requires three applications to achieve a high reflectance as substantiated by reflectance measurements. The 950°F bake required by this method causes another potential problem. The method

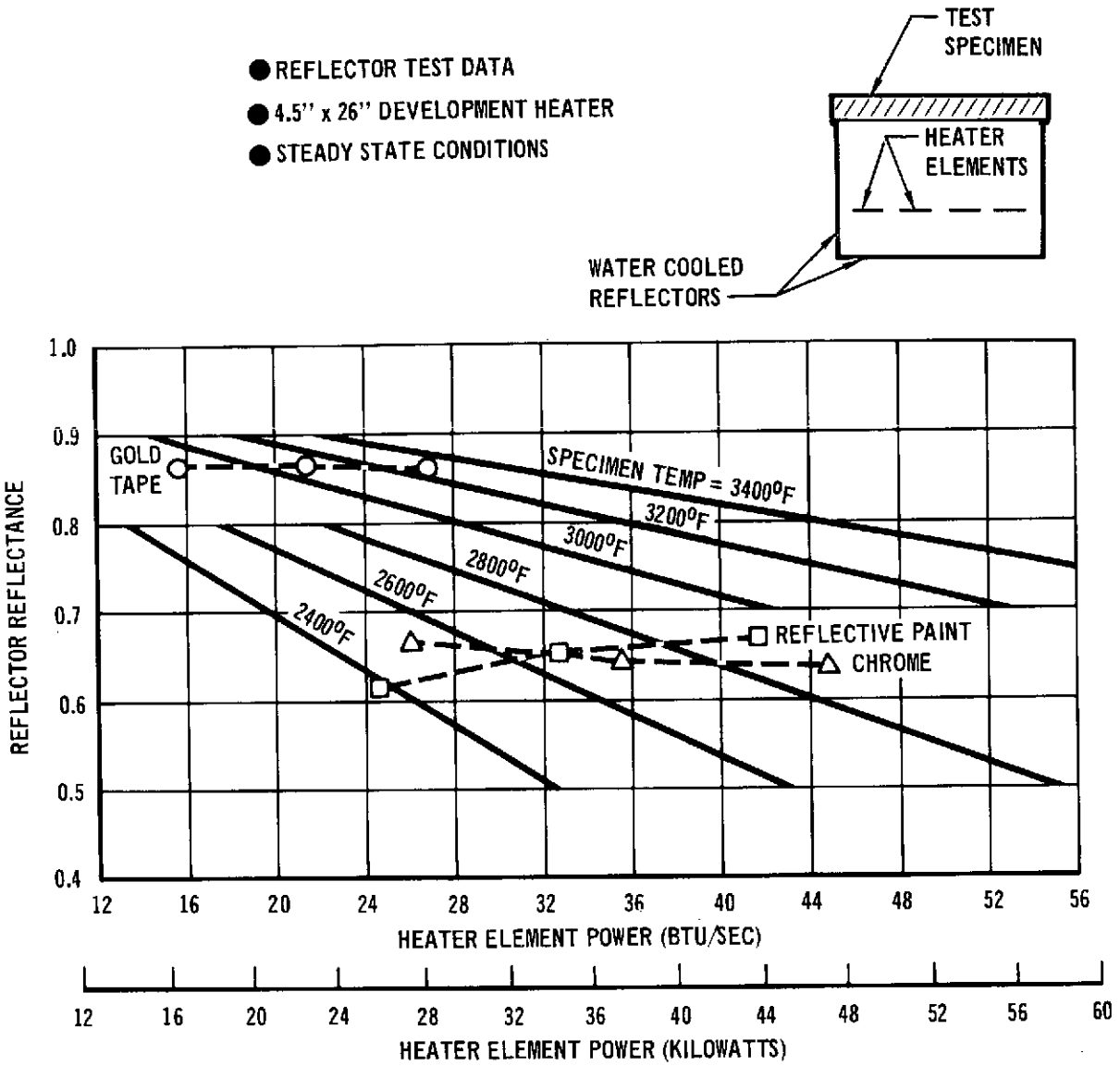

EFFECTIVE REFLECTANCE FROM MEASURED TEST SPECIMEN TEMPERATURES

FIGURE 5-6

developed in MDC Laboratories for attaching the cooling tubes to the chrome plated reflectors employs an oven soldering after plating the reflector to avoid damage to the tubing during the plating and polishing operation. It is not known if the gold plating by any method would be affected by this procedure. For electroplating and vacuum depositing, the coating could be applied before or after soldering whereas the conversion gold plating would have to be applied before the soldering operation due to the lower temperature solder used.

Three reflector specimens were prepared for spectral reflectance measurements, one by vacuum depositing gold onto a polished chrome plated coupon with a magnesium

- ○ REFLECTOR TEST DATA
- ○ 4.5" x 26" PROTOTYPE HEATER
- ○ STEADY STATE CONDITIONS (MODEL B)

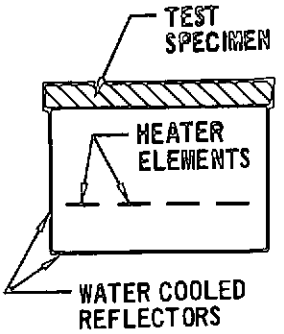

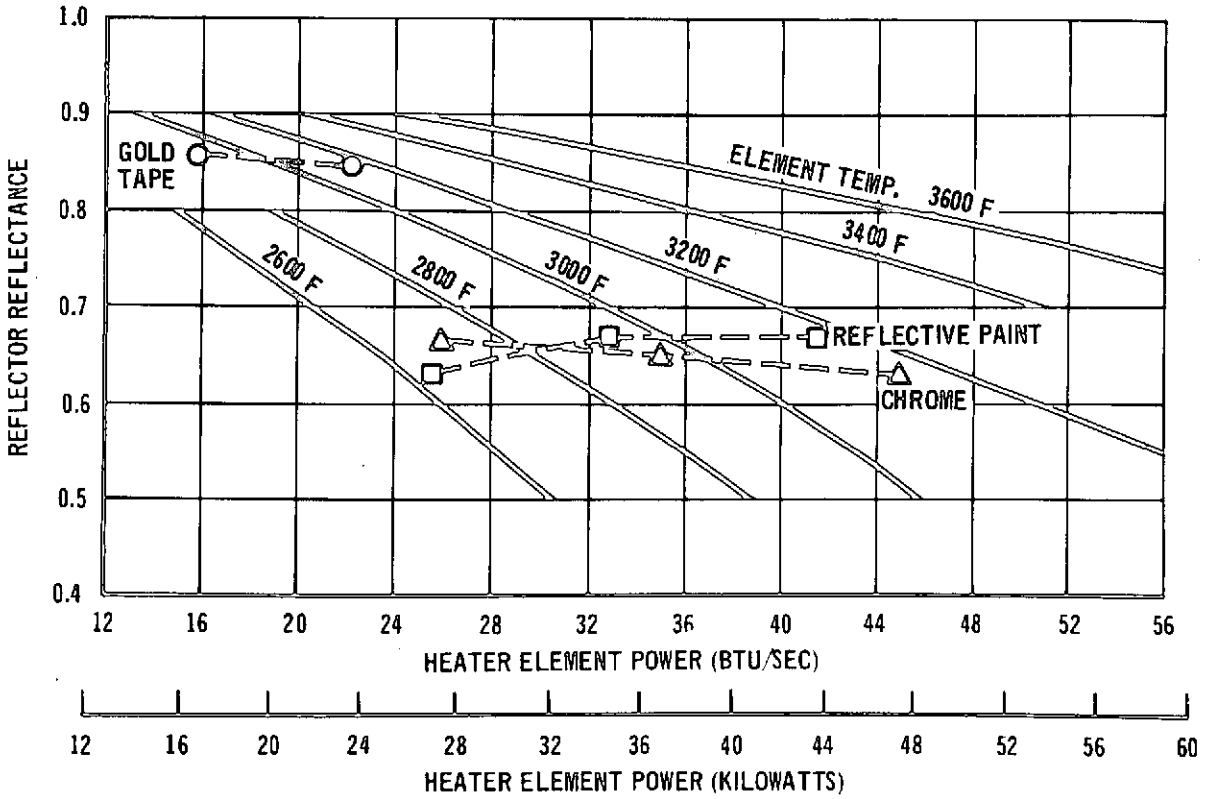

EFFECTIVE REFLECTANCE FROM MEASURED HEATER ELEMENT TEMPERATURES

FIGURE 5-7

fluoride overcoat, a second with the three coats of heat conversion gold onto a polished chrome plated coupon, and the third a standard polished chrome plated coupon. The spectral reflectance measurements were made using a Beckman DK-2 Spectrophotometer and the results are presented in Figure 5-8 along with a normalized 3500°F black-body curve for reference purposes. This data clearly substantiates the test and analytical results showing that gold coated reflectors are better than chrome plated from a performance standpoint. The chromium has a reflectance of 0.65, heat conversion gold has 0.86, and the vacuum deposited gold

achieves 0.96 reflectance for the peak radiant intensity of 1.3 μm at 3500°F. Further investigations in techniques for achieving a gold coated reflector are necessary before the full size heating array is assembled.

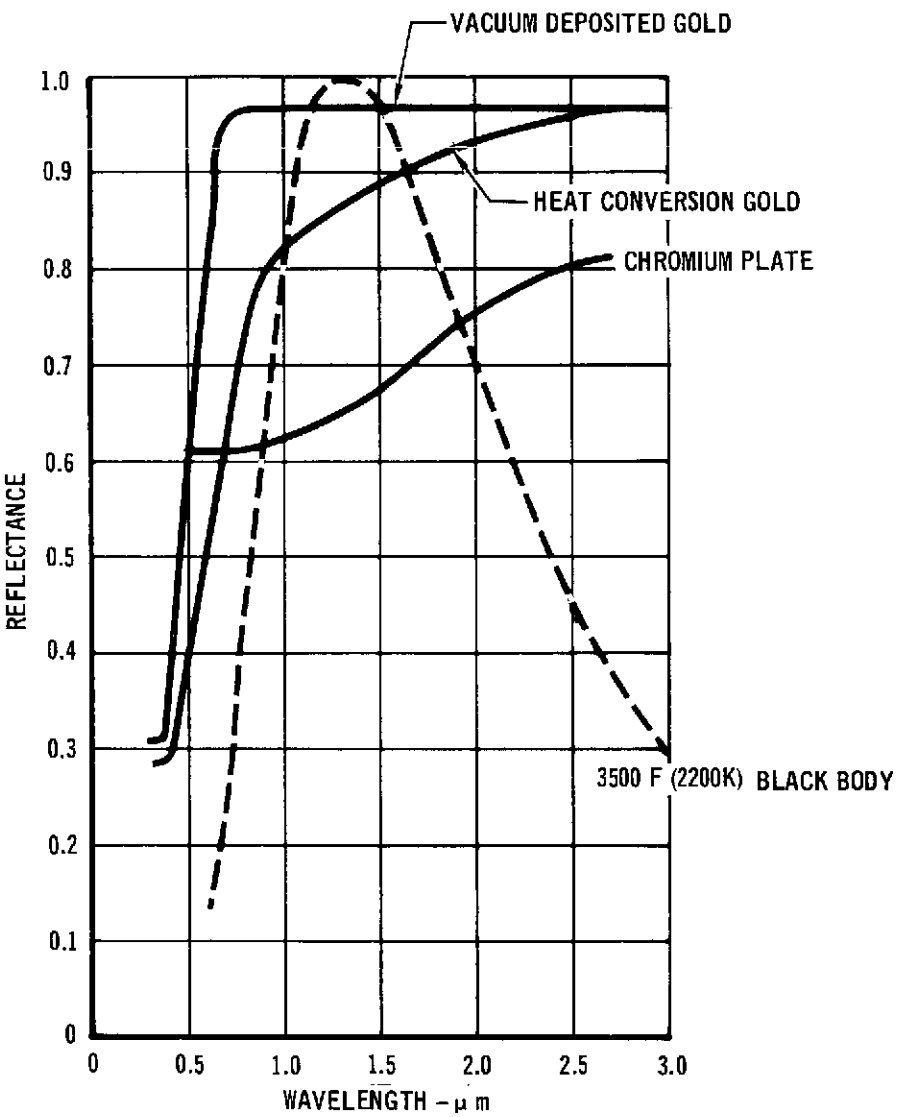

SPECTRAL REFLECTANCE OF CANDIDATE REFLECTORS FOR GRAPHITE HEATERS

FIGURE 5-8

6.0 DESIGN AND FABRICATION OF PROTOTYPE HEATER MODULE

To meet the design goals and to verify heater performance a prototype heater model that will constitute the basic building block of the heating array was designed and built.

6.1 DESIGN OF PROTOTYPE MODULE. The prototype heater needed to be of sufficient size to demonstrate the properties of the full size array, and to have all the features of the full size array which might affect its performance. The basic design was evolved from our knowledge of graphite heater design and the potential trouble areas investigated in previous graphite heater development programs. The succeeding paragraphs describe the approach taken to meet the design goals and the design features incorporated in the prototype module.

6.1.1 Prototype Size. The width of the prototype evolved from two criteria: (1) maintaining element strip width and spacing the same as proven designs in previous development programs, and (2) including enough strips to utilize one power control channel. The prototype contained four strips .80 inches wide, with .25 inch spacing between strips, and 0.25 inch spacing between the elements and side reflectors. This resulted in a 4.45 inch inside dimension for the module. The over-all width of the module was determined by other criteria discussed shortly.

Because of time restrictions of Phase I and the lead time required to obtain new elements from the vendor, a "best quess" element length of 36 inches was chosen. This length enabled evaluation of element fragility and tension requirements to minimize sag, while at the same time providing the basis for mapping spanwise heat flux uniformity. The basic module configuration is 5 x 39 inch as shown pictorially in Figure 6-1.

6.1.2 Heater Elements. The heater module employs two serpentine, two-pass graphite heater elements similar to those used in our in-house heaters and in heaters delivered to NASA-Langley and NASA-MSC. The elements were fabricated from Airco Speer Grade 390S graphite. Electrical connection to the elements was made by fitting tapered holes in the thickened ends of the graphite elements to water-cooled copper tapered pegs brazed to the electrode end assembly (described in the next section). The tapered connection system minimized unheated areas in the module and does not depend on module orientation for element retention. Both ends of the element were thickened relative to the thin heated length to facilitate power input at the electrode end and turn-around at the expansion end.

The element thickness was determined by scaling known power requirements from the development unit described in Section 5.0 to the new module sizes and adding

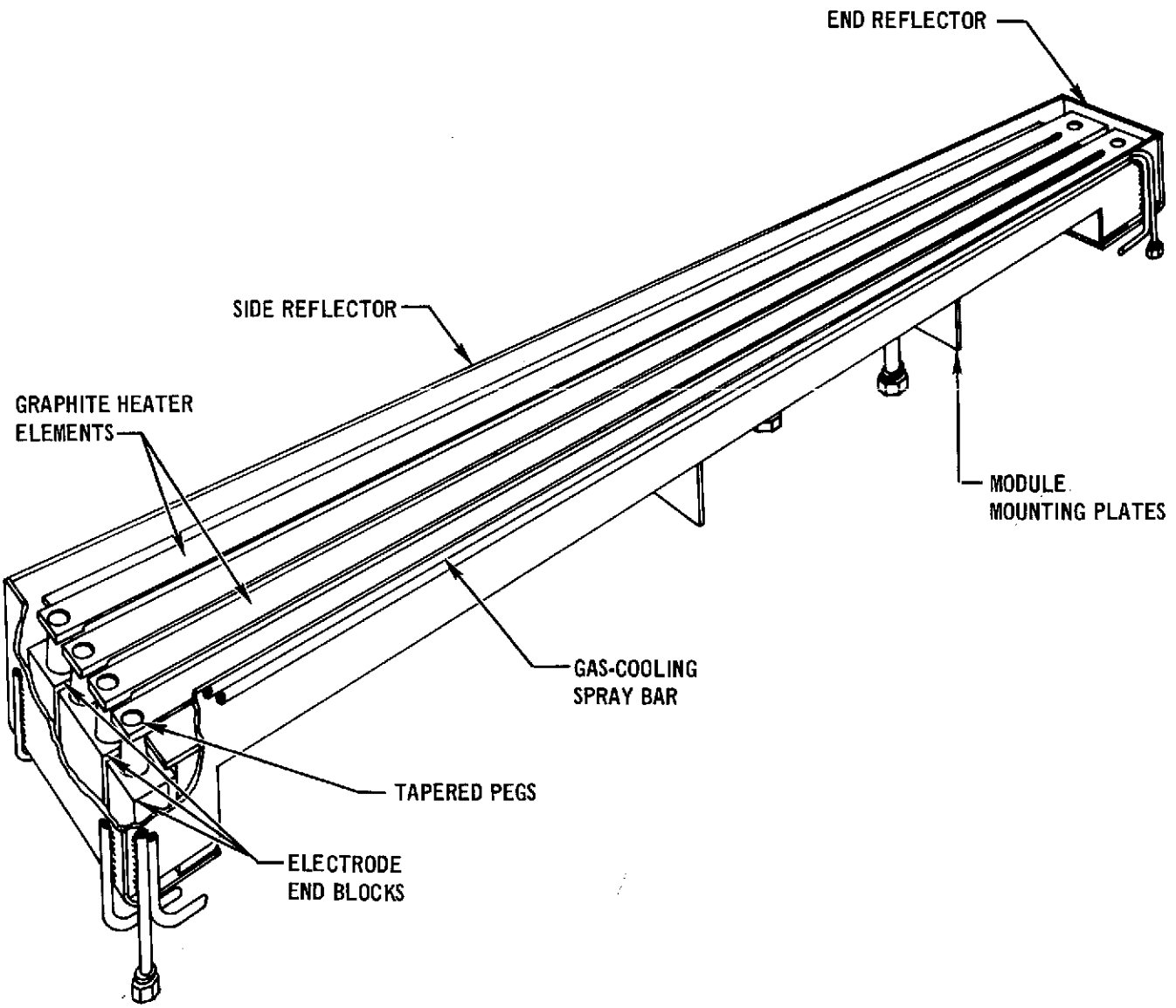

PICTORIAL VIEW - PROTOTYPE HEATER

FIGURE 6-1

a safety factor for contingencies. The power used for calculations was 100 KW per module (or 25 KW per element pass). The elements are connected in parallel with a maximum voltage of 100 volts/element delivered by 4:1 stepdown transformers. This arrangement results in 50 volts/pass and a current requirement of 500 amperes for a pass resistance of 0.1 ohm. Then utilizing the formula

$$R = \frac{\rho L}{Wt}$$

where, R = pass resistance

ρ = resistivity of graphite

L = heated length

W = pass width, and

t = element thickness,

an element thickness of 0.125 inches was determined. The shape of the heater element can be seen in Figure 6-2.

6.1.3 Electrode End Design. Minimizing the unheated area at both ends of the heater was of primary concern. The design goal was to expand the heater array eventually to accept a 10 foot test article with a minimum of heat flux nonuniformity This requirement prompted a new end block design which was essentially a turned-under version of the ones on the heater delivered previously to NASA, MSC. This makes the unit more compact. Figure 6-2 shows this arrangement and Figure 6-3 contains the design details of electrode end assembly.

Brazed atop the end block is the water-cooled copper tapered peg which retains one end of the heater element and transmits the power to the element. Since the elements were connected in parallel, the center end block is siamese, with two tapered pegs making a common connection between the two elements.

Brass rods .50 inches in diameter are soldered into sockets in each end block. These rods pass through the brass end manifolds, and copper bus plates are clamped to the ends. The end blocks and rods are electrically insulated from the heater structure by ceramic spacers and phenolic sleeves. O-rings fitted in grooves sealed the water passages between the components. A constant clamping force is exerted on the O-ring seals by a wave spring washer held in place with a snap retaining ring.

Figure 6-3 and 6-4 show the bus plate detail. The bus plates are positioned beneath the modules which increases its compactness. Two copper bus plates connect the heater elements in parallel and supply the two connecting points for water-cooled power leads. A phenolic spacer bolted to the bus plates maintains mechanical separation for electrical reasons and adds rigidity to the assembly.

6.1.4 Expansion End Design. A method was needed to apply a tensile load to the elements to prevent excessive sagging and also to take up the thermal expansion of the elements as they heat up. The first design attempt is shown in Figure 6-5. This sliding block arrangement was an adaptation of the tension system used in previous graphite heaters. The turned-under end block, however, prevented the

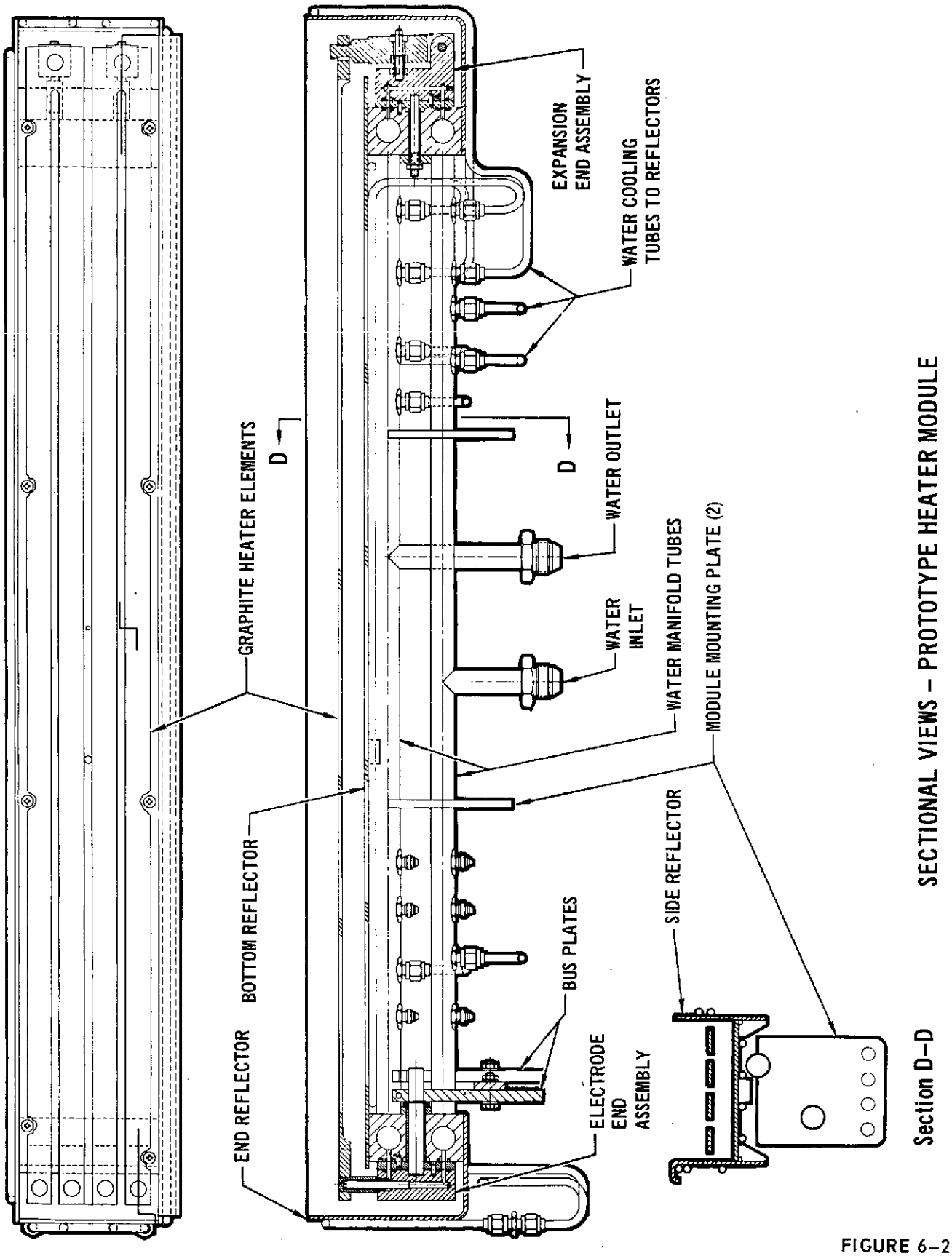
EXPANSION END ASSEMBLY
WATER COOLING TUBES TO REFLECTORS
GRAPHITE HEATER ELEMENTS
D
D
WATER OUTLET
WATER INLET
WATER MANIFOLD TUBES
MODULE MOUNTING PLATE (2)
BOTTOM REFLECTOR
SIDE REFLECTOR
BUS PLATES
END REFLECTOR
ELECTRODE END ASSEMBLY
SECTIONAL VIEWS – PROTOTYPE HEATER MODULE
Section D–D

FIGURE 6–2

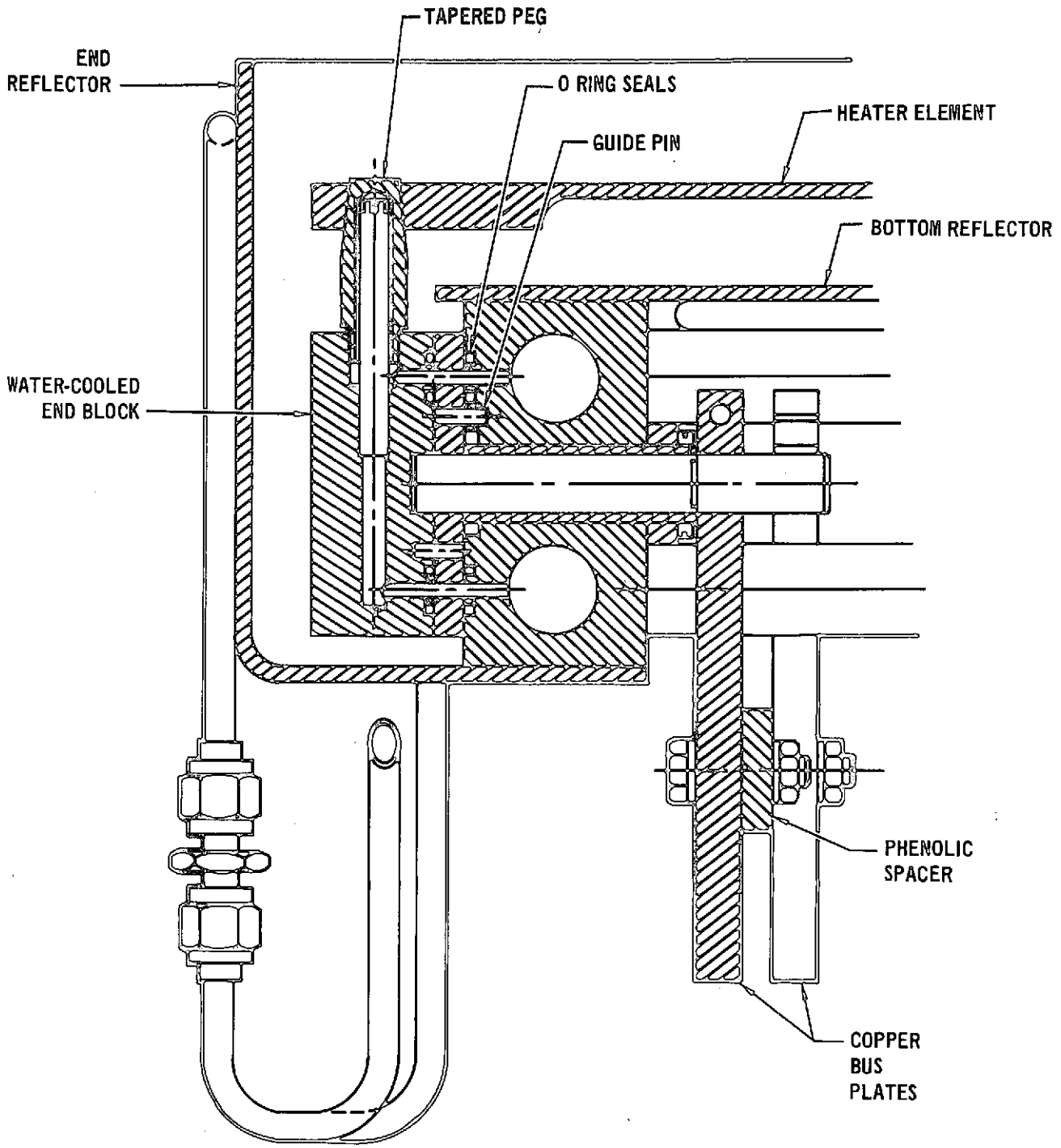

ELECTRODE END DESIGN DETAILS

FIGURE 6-3

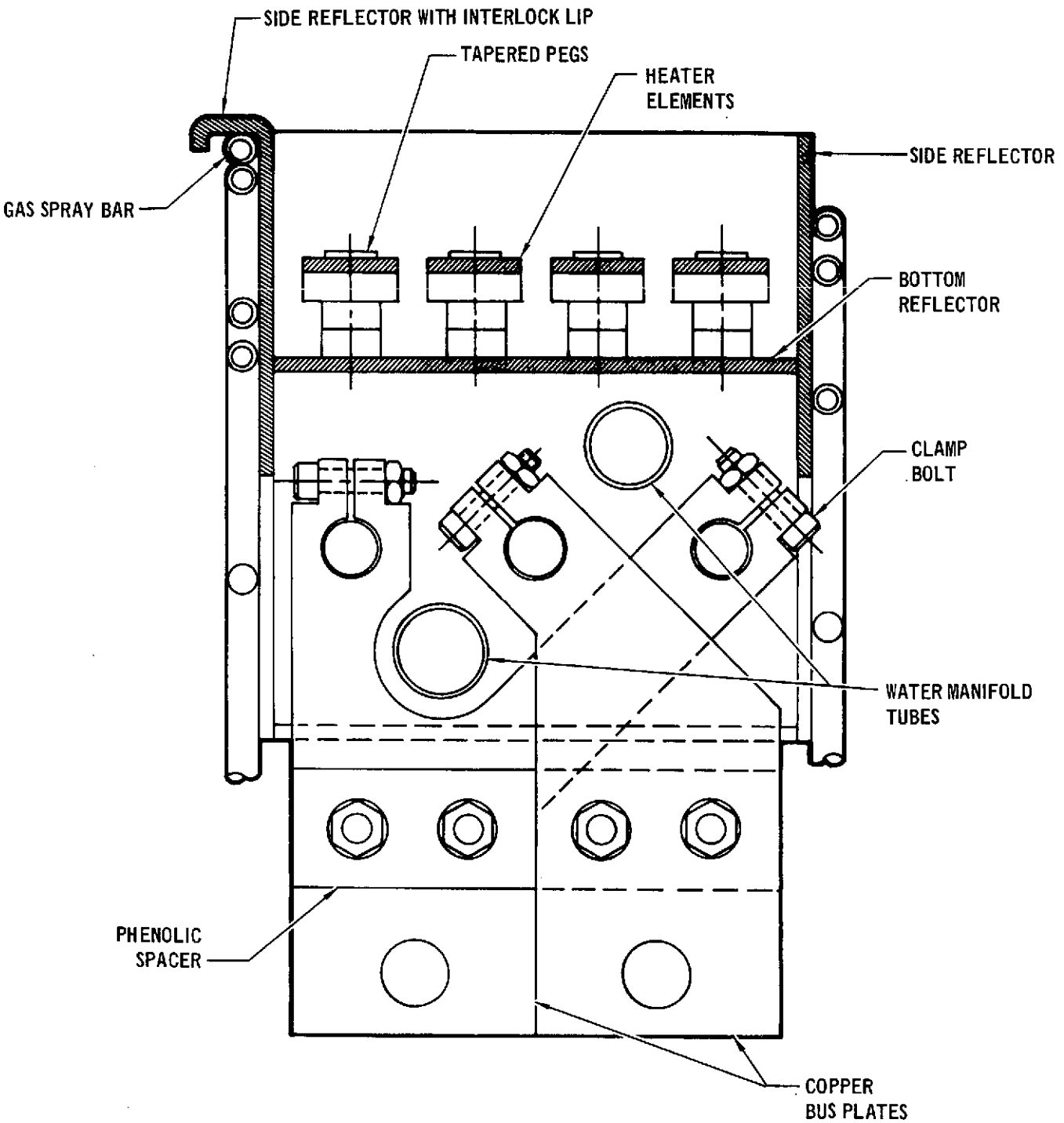

BUS PLATE DETAIL

FIGURE 6–4

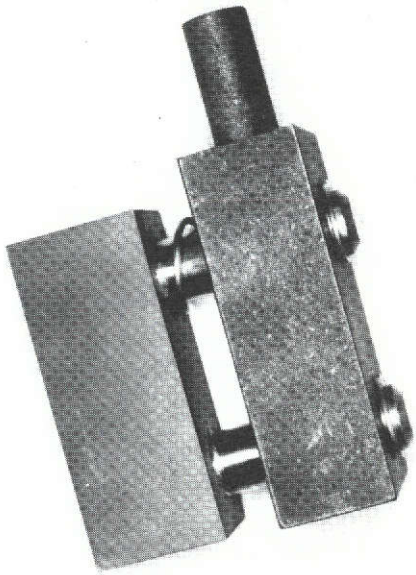

NOTE:
NONUNIFORM
COMPRESSION
OF MODEL
PREVENTS
SLIDING OF
ASSEMBLY.

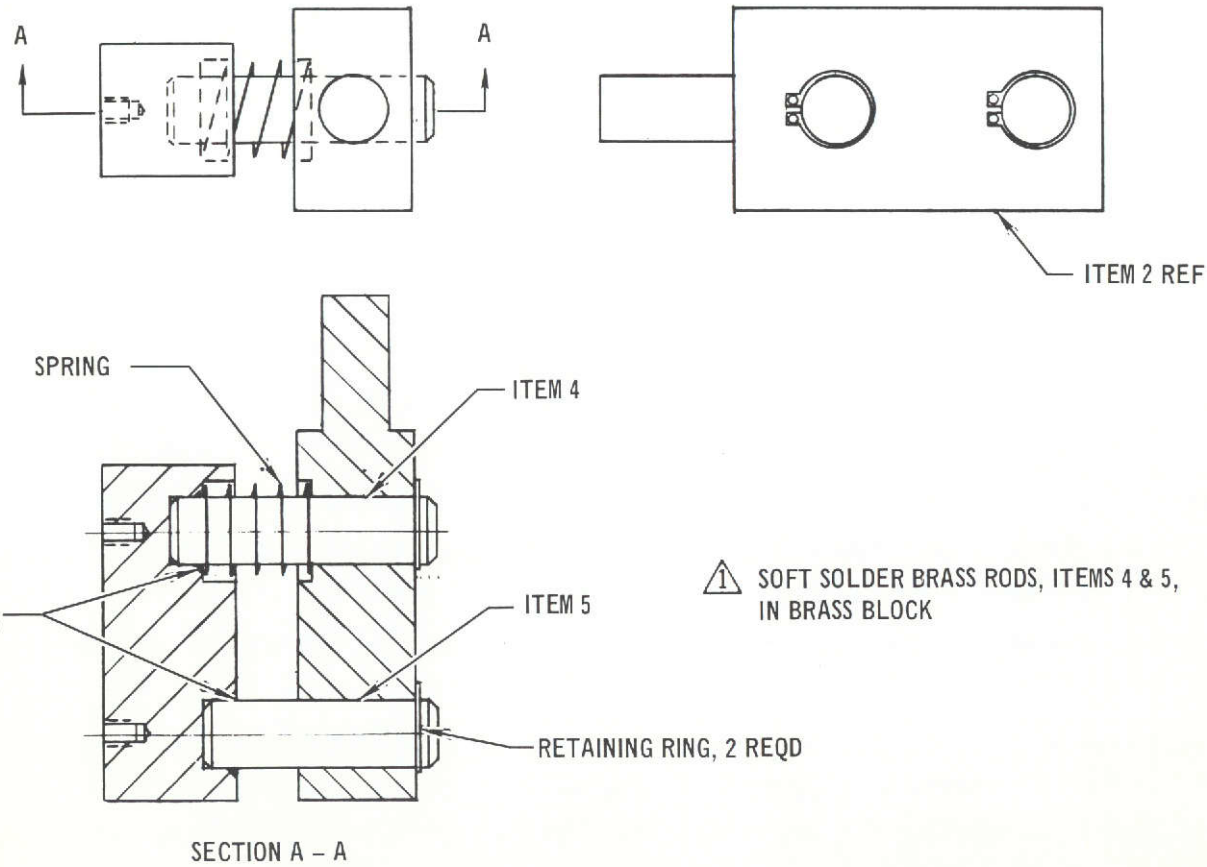

PARALLEL SLIDING DEMONSTRATION MODEL FOR EXPANSION END ASSEMBLY

FIGURE 6–5

applied and reactive forces from being coaxial. This resulted in binding in the demonstration model and, eventually, to discarding this design.

The successful design is shown in Figure 6-6. This design consists of a graphite lever pinned at the bottom to the water-cooled brass end block through a protruding ear. The tension force is supplied by a compression spring between the lever and end block. A guide rod and snap ring kept the assembly in place.

As on the electrode end, electrical insulation was provided by a ceramic insulator between the end block and the water manifold and a phenolic sleeve and washer around the clamping stud. A nut on the clamping stud was used to clamp the O-rings sealing the water passages between the components.

The top of the graphite lever has a lip to retain the element and keep it properly located.

6.1.5 Water Manifolding System. The water manifolding system supplies water to the entire module through one inlet and one outlet connection. Figure 6-2 shows the manifolding system. The two manifold tubes served a dual purpose. They fed water to the end water manifolds and all the reflectors while also providing the structural backbone of the module. The module mounting plates were welded to these tubes.

The reflectors are supplied cooling water from the manifold tubes by individual connections welded to the tubes for each reflector plate. The end-block manifolds were brazed to the tube ends and provided a rigid structure for fastening the reflectors.

6.1.6 Reflectors. Chrome plated reflectors were used to contain the radiated energy and reflect it back to the test article. All the reflectors were mounted to the brass end-block manifolds and formed a box with only the area above the elements open for radiating to the test article. The shape of the enclosure thus formed can be seen in Figure 6-2. This box arrangement offers an additional advantage for the full size array which is discussed in Section 8.8.

A gas spray bar was incorporated in one of the side reflectors to provide a means of impinging cold gas on the test article surface to cool it. The spray bar was located beneath a lip provided on one side reflector to interlock with the adjacent heater module in the full-size array. Interlocking prevents escape of radiated energy between adjacent modules. The spray bar and interlock can be seen in Figure 6-4.

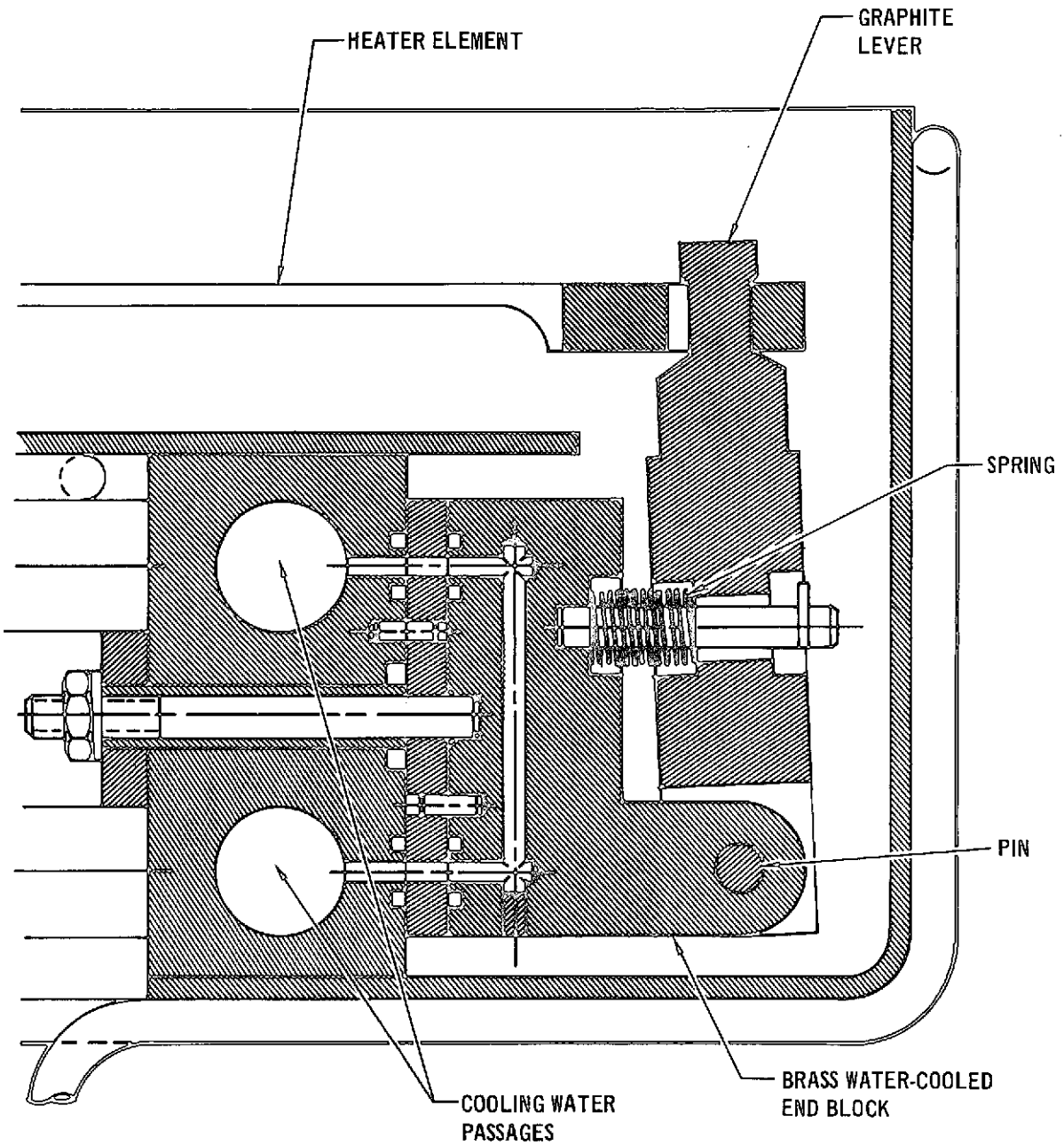

FINALIZED EXPANSION END DESIGN DETAILS

FIGURE 6-(

Water cooling tubes were soldered to the outside of the reflectors to remove the energy absorbed by the reflectors. These tubes were arranged so that they nested with the cooling tubes on the adjacent module. This reduced the width of the unheated streps between modules. This nesting feature was used not only on the side reflectors but also on the ends, so that entire heating arrays could be nested

end-to-end. Although only one prototype module was built, the tubes were arranged properly to test the cooling capability of the nesting configuration.

6.2 FABRICATION OF PROTOTYPE MODULE. The majority of the prototype fabrication was done in the MDC Electro-Mechanical Development Laboratory. Figures 6-7 to 6-9 show the module components and assemblies during various stages of fabrication.

EXPANSION END ASSEMBLY

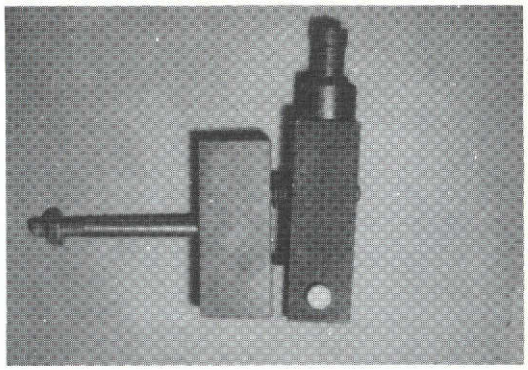

ELECTRODE BLOCK ASSEMBLIES

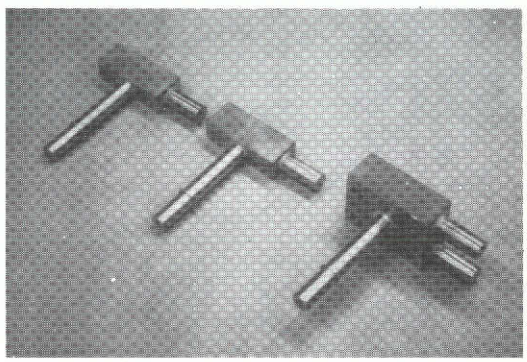

TERMINAL PLATES

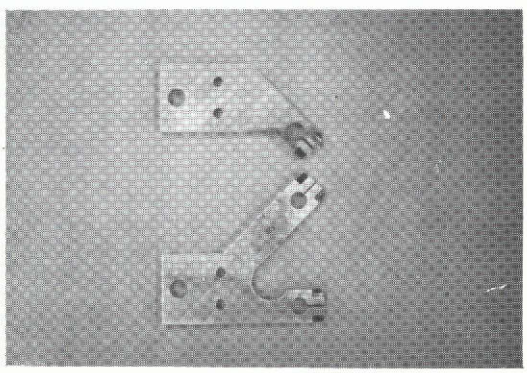

EXPANSION END, ELECTRODE BLOCKS AND BUS PLATES FOR PROTOTYPE HEATER MODULE

FIGURE 6-7

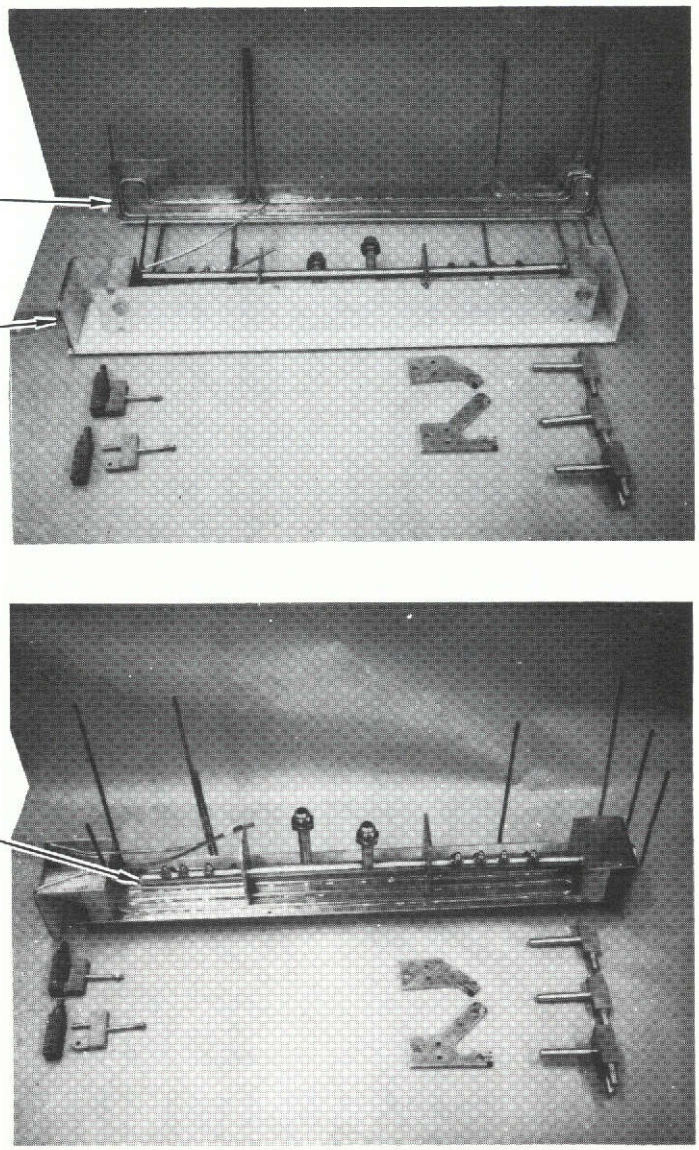

VIEWS OF THE PROTOTYPE HEATER MODULE
DURING FABRICATION

FIGURE 6–8

As the heater was assembled, provisions were made for part of the instrumentation to be used during prototype evaluation testing. A hole was cut in the bottom reflector to provide an optical path for optical pyrometer temperature measurements. The hole was located so that both elements and test article surfaces could be seen. Also, mounts for two types of heat flux sensors were attached to the bottom reflector.

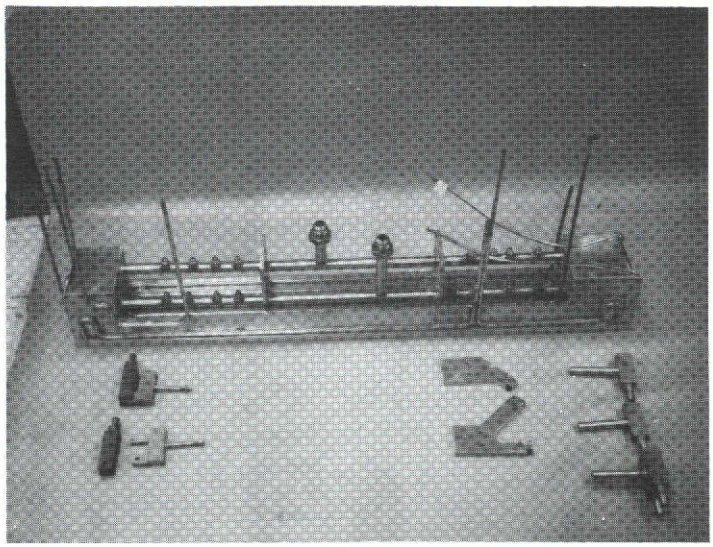

SIDE REFLECTORS AND BOTTOM REFLECTORS
ASSEMBLY AS SEEN DURING MODULE FABRICATION

FIGURE 6-9

No problems arose during heater fabrication, and standard fabrication techniques were used. The vendor who supplies the heater elements per our design did experience some tooling problems and element breakage during the initial phases of fabrication. These problems were solved and the only effect was a delay in receiving the first shipment.

6.3 PREDICTED PERFORMANCE OF THE PROTOTYPE HEATER MODULE. A thermal analysis was performed to predict heater element and test specimen temperatures for the 5-in x 39-in prototype heater module. Temperatures were calculated for both gold and chrome reflectors on the prototype module. An effective reflectance of 0.86 for gold reflectors was used as determined from tests. Similarly, a reflectance of 0.65 was used for the chrome reflectors.

The thermal analysis of the prototype module utilized a three-dimensional thermal model consisting of 9 reflector nodes, 1 heater element node, 1 test specimen node, and 12 radiosity nodes. The reflector surfaces form five sides of a box 37.75 inches long, 4.5 inches wide, and 2.125 inches deep. The test specimen is represented by a surface 4.5 x 37.75 inches which forms the sixth side of the box. The heater elements are represented by a surface inside the box located 1.25 inch from and parallel to the test specimen. The assumption was made that the test specimen was adiabatic and that the reflectors absorbed all the heater element power. The reflectors were held to 100°F and power was input to the node represen-

ting the heater elements. The dimensions and view factors of the prototype module were incorporated into Thermal Model "B" for the prediction. The heater element and test specimen temperatures were then computed as a function of heater element power for steady state conditions. The results of this analysis are presented in Figure 6-10. A prototype heater with chrome reflectors requires approximately 2.4 times the power of a prototype heater with gold reflectors to achieve a given test specimen temperature in the 3000-3500°F temperature range.

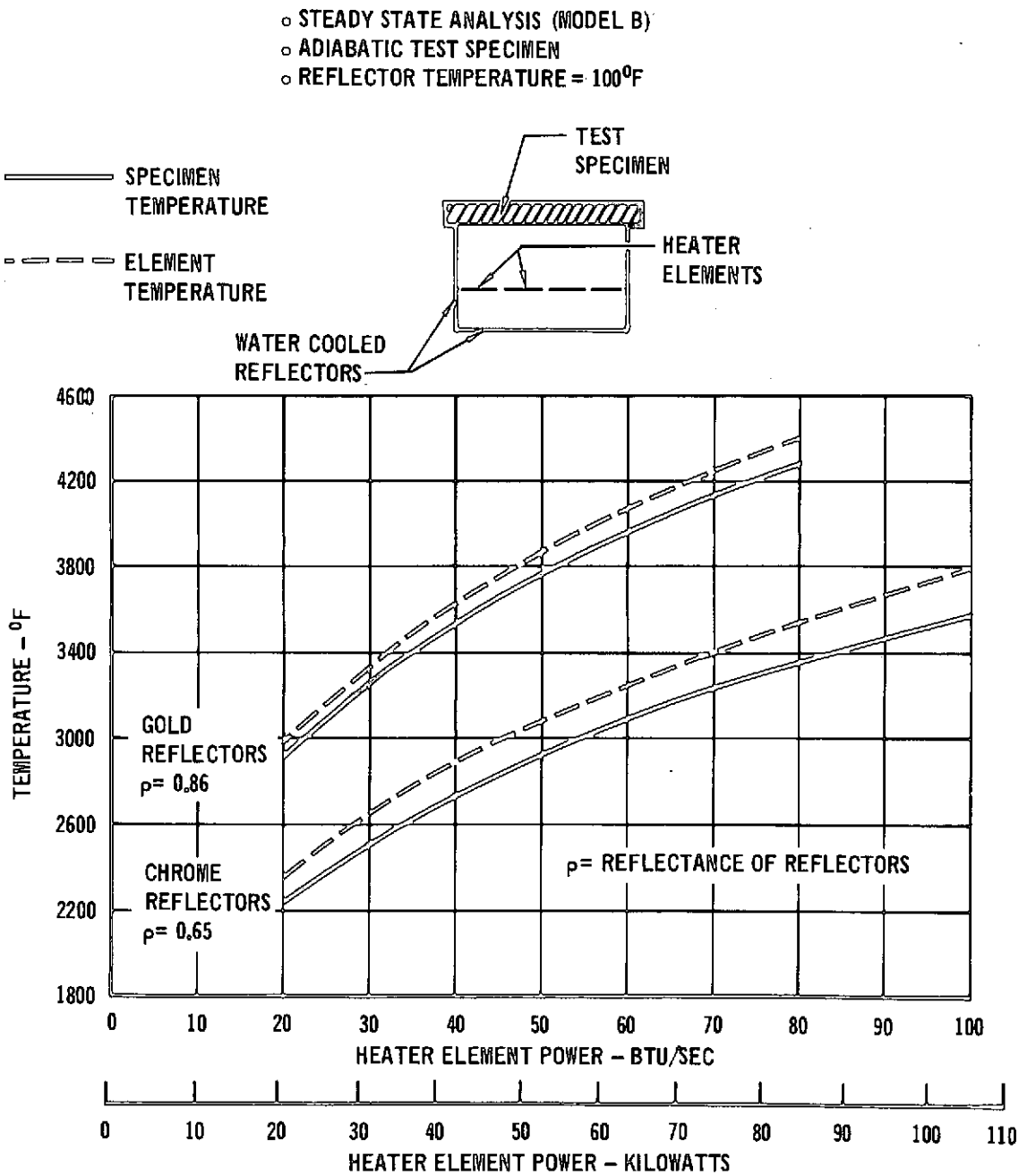

PREDICTED TEMPERATURES FOR 5.0" x 39" PROTOTYPE HEATER MODULE

FIGURE 6-10

NOTE: (PAGE 48 IS BLANK)

7.0 PERFORMANCE TESTING OF PROTOTYPE HEATER MODULE

Only a limited amount of performance testing could be conducted with the prototype heater module because of a delay in element delivery and the short duration (5 months) of the program. This section describes the test article, the test setup and presents a discussion of the test results. The testing consisted largely of determining the performance characteristics of the heater module at a chamber pressure of 10 torr and investigating spanwise uniformity of the heat flux incident upon the test article. The maximum specimen temperature achieved during this testing was 3010°F at a power input of 69.4 KW. This is below the expected capabilities of the module especially for gold coated reflectors; and, early in Phase 2, additional mapping of the performance of the modules should be performed to determine its heating limits.

7.1 TEST ARTICLE. The test article assembly designed to test the prototype heater module is shown schematically in Figure 7-1 and pictorially in Figures 7-2 and 7-3. It consists basically of two sections of ribbed carbon-carbon lay up cut from a MDC prototype leading edge and mounted in a water-cooled support structure. Two ribs of each carbon-carbon section extend through slots cut in the top support plate and are held in place with carbon pegs. The amount of insulation placed between the carbon-carbon and the chrome plated inner surfaces of the water-cooled plates can be varied to effect essentially any desired specimen heat transfer rate.

The instrumentation includes a pair of tungsten-rhenium thermocouples, one of which is against the inside surface of the carbon-carbon and the other in a small recess drilled into the inside surface of the carbon-carbon. Two water-cooled calorimeters mounted to the top support plate and extending down through the carbon-carbon section are used to map the heat flux uniformity in the axial direction. To obtain a value for the total amount of heat absorbed by the test article, the support structure coolant flow rate and temperature rise were measured.

7.2 TEST SETUP. The prototype graphite heater module was set up on the movable door of a 5.5 foot diameter vacuum chamber for the performance tests. Several views of the heater with and without the test article during the setup are shown in Figure 7-4 and the final assembly and overall view of the test and chamber are shown in Figure 7-5.

In addition to the aforementioned instrumentation of the test article, the prototype heater was instrumented to allow measurement of coolant flow and temperature change, voltage and current, and heat flux sensed by calorimeters mounted in

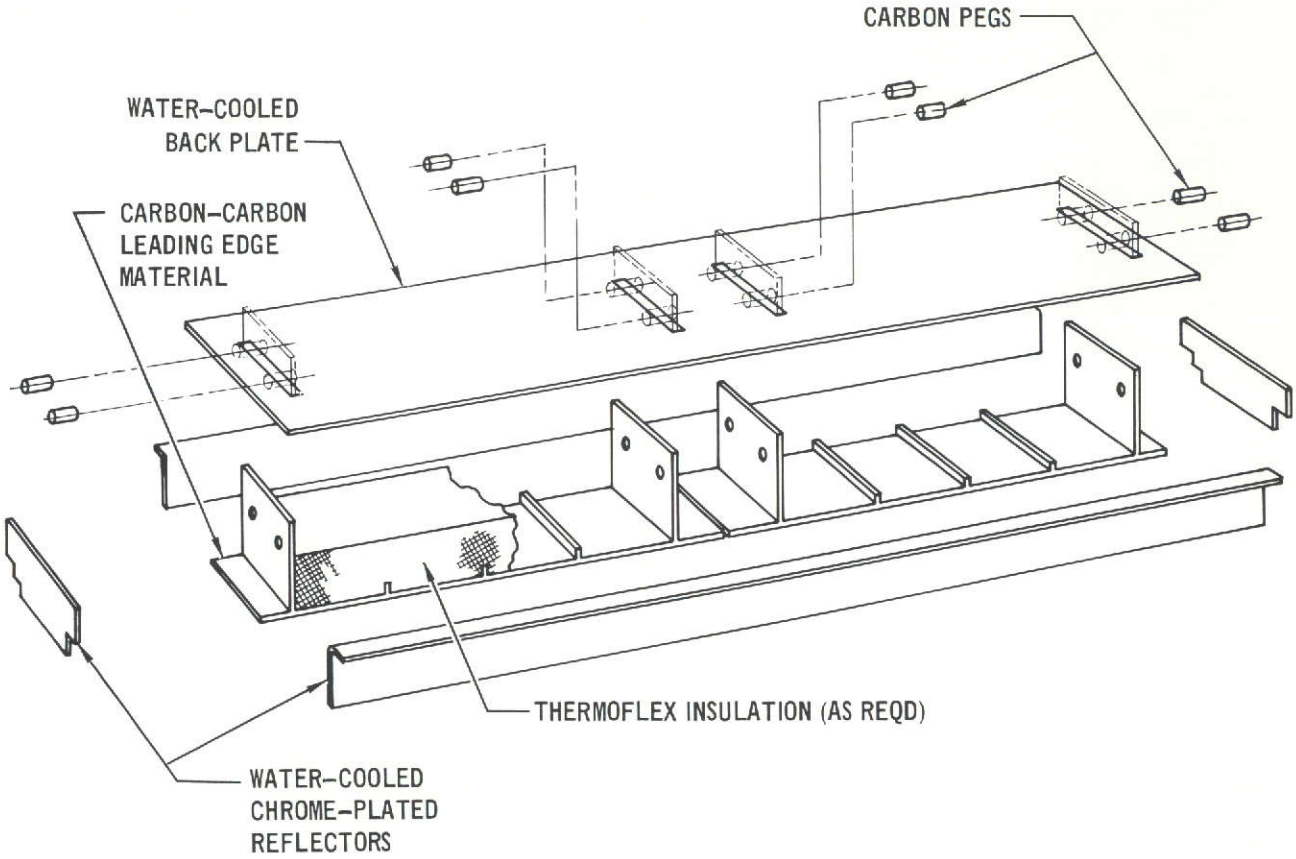

TEST ARTICLE FOR TESTING PROTOTYPE HEATER

FIGURE 7–1

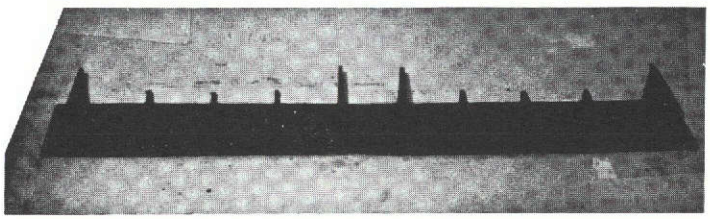

CARBON–CARBON TEST ARTICLE (5 x 40 INCH)
DURING FABRICATION

FIGURE 7–2

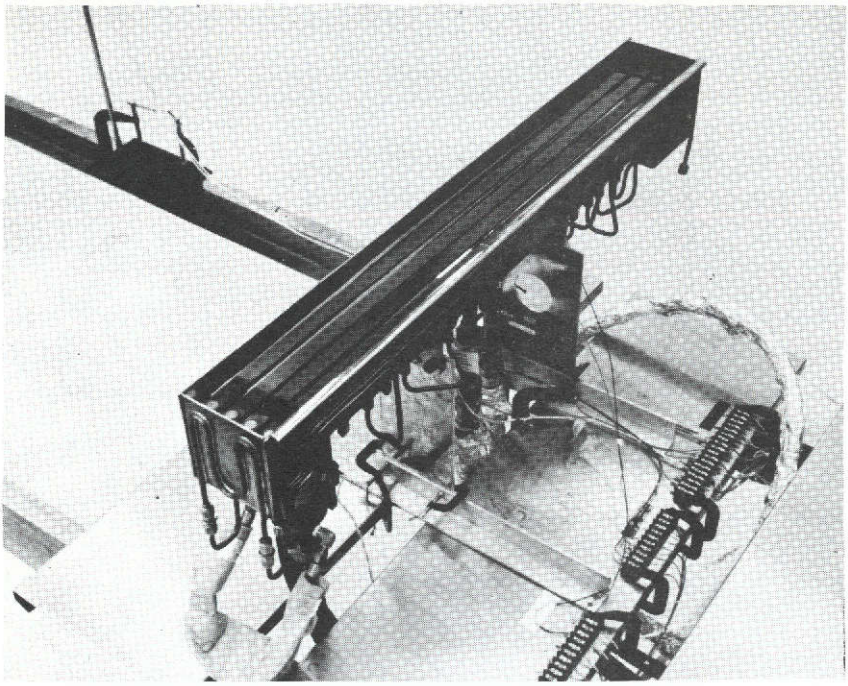

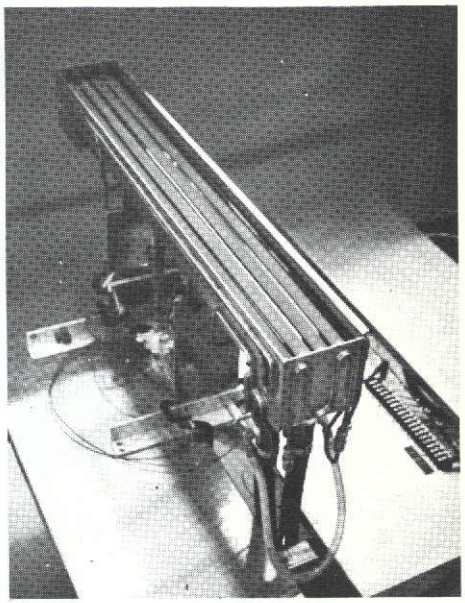

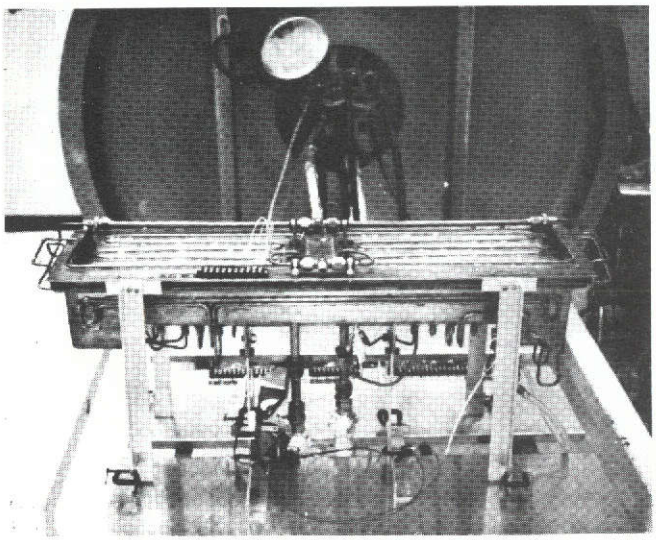

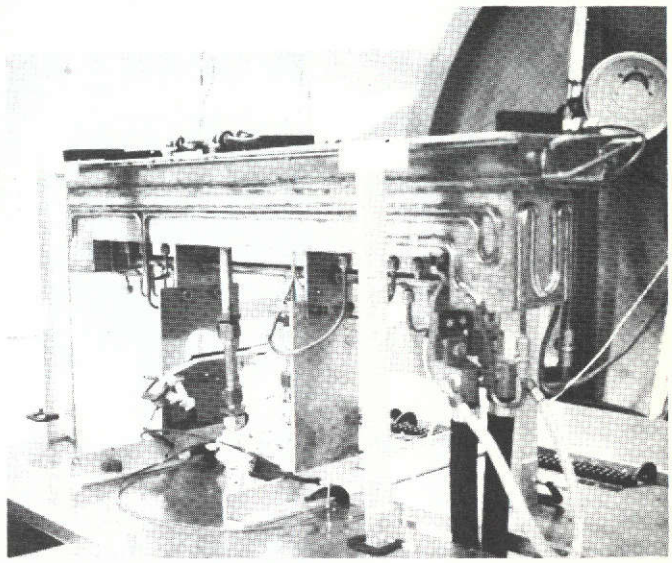

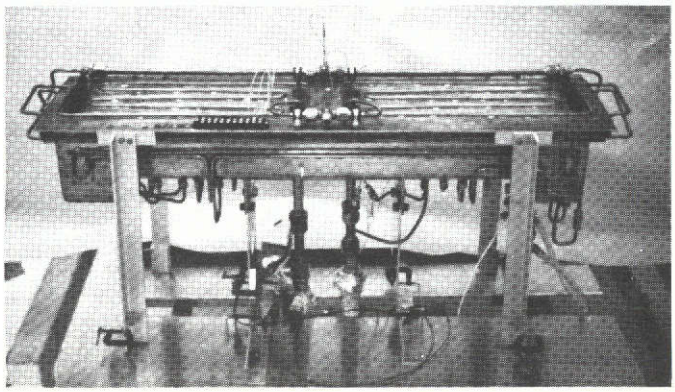

VIEWS OF THE PROTOTYPE LEADING EDGE HEATER MODULE TEST SETUP

FIGURE 7–4

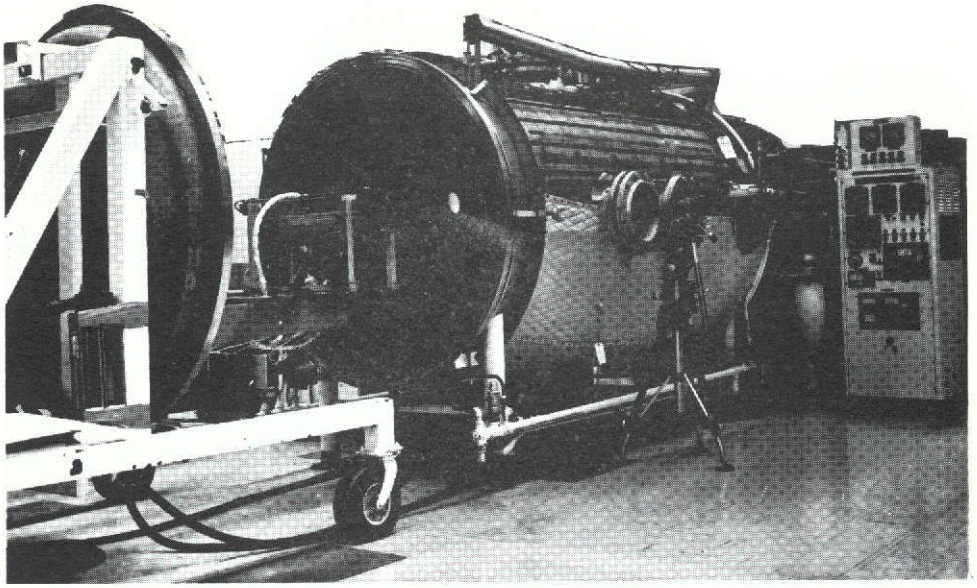

5.5 FOOT VACUUM CHAMBER WITH GRAPHITE HEATER MODULE AND TEST ARTICLE DURING PERFORMANCE TESTING

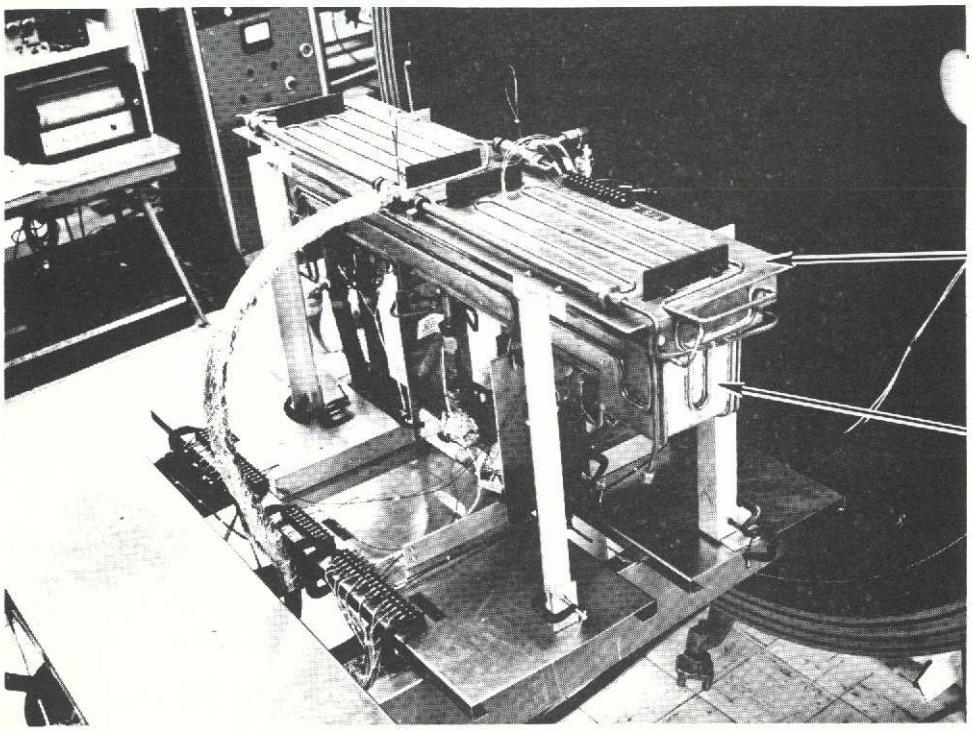

GRAPHITE HEATER MODULES AND TEST ARTICLE MOUNTED ON VACUUM CHAMBER DOOR

FIGURE 7–5

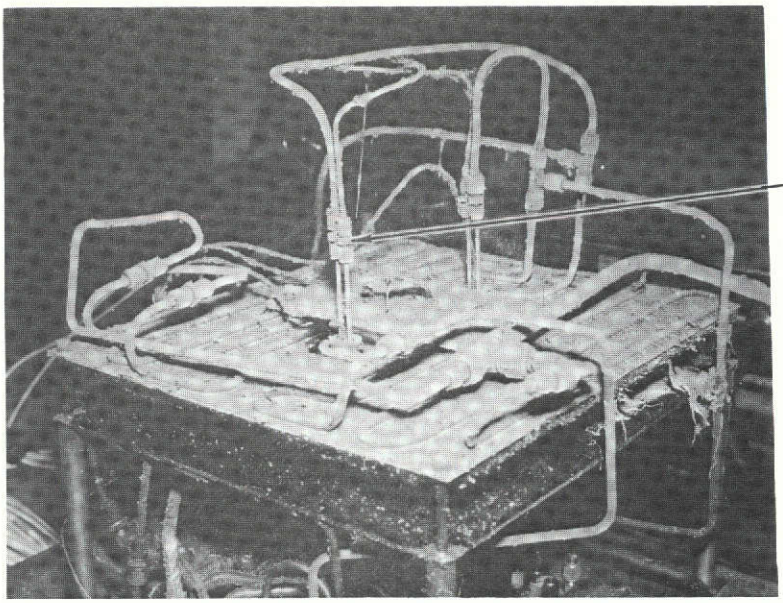

DEPOSITION OF ABLATION PRODUCTS ON
COLD PLATES OF GRAPHITE HEATER TEST SETUP

Figure 8–14

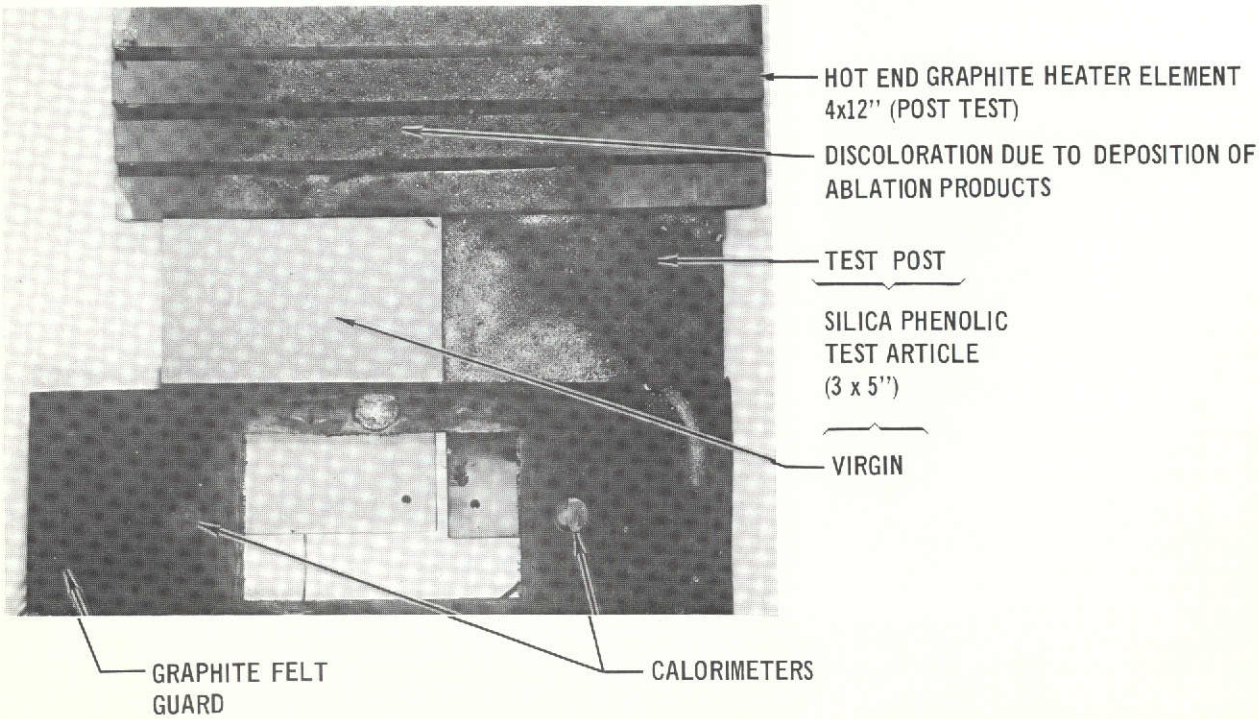

TESTING OF A SILICA PHENOLIC ABLATOR WITH THE GRAPHITE HEATER

Figure 8–15

NOTE: (PAGE 102 IS BLANK)

normal performance during the shake-down tests was that one element ran considerably hotter than the other when the same voltage was applied to each. Examination of the elements showed that although they were dimensionally identical, their resistance was different, possibly due to difference in material densities or grain orientation. The condition was eliminated by selecting elements with matched resistances.

After the initial shake-down runs, a series of tests was conducted to determine the basic performance characteristics of the heater assembly. The voltage was increased in 10 volt steps until 80 volts had been reached at which setting the corrected specimen temperature measured with the optical pyrometer was 3010°F. This was done in two series of runs because of a film that formed on the reflectors caused by outgassing at high temperature of the binder of the test article insulation. Simple cleaning restored the reflectors and no further difficulty was experienced after the insulation had been thoroughly "cooked out." A summary of the reduced data for these test runs is presented in Figure 7-6.

Specimen and element temperatures as a function of input power are shown in Figure 7-7 for both predicted (thermal model "B") and measured data. The information in the figure is for chrome plated reflectors, and constant reflectance (0.65) was used for calculating temperatures at all wavelengths. The measured temperatures have a spread of up to 150°F for some power settings, part of which can be attributed to a 100°F uncertainty in temperature measurement caused by such things as emissivity uncertainties, emittance enhancement, wavelength considerations and optical losses. It can be seen in this figure, that the trend is for the temperature to be higher than predicted at low power settings and lower than predicted at high power settings. This effect is most likely due to modeling and dependence of the reflectance of the chrome surface on wave length. Additional thermal modeling is described in Section 7.4.1.

In addition to these "set point" runs, the prototype heater was operated using the ignitron controller feedback control system to demonstrate the feasibility of this type of control. Two feedback elements were implemented: the heat flux sensor in the bottom reflector of the heater and one of the tungsten-rhenium thermocouples in the test article. Both systems operated satisfactorily, thereby demonstrating that the heater can be controlled using either a heat flux sensor or a thermocouple. For these demonstration runs, ramp type functions (Figures 7-8 and 7-9) were programmed using a "Data-Trak."

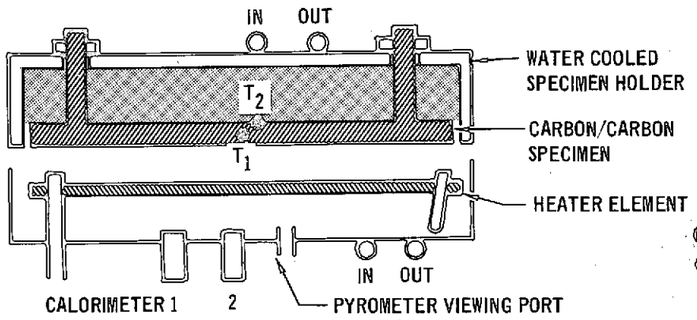

(1) TEMPERATURE CORRECTED FOR EMITTANCE PER NASA CR–111841
(2) TEMPERATURE CORRECTED FOR EMITTANCE OF 0.90
(3) NOT CORRECTED FOR EMITTANCE (ϵ = 0.825) COATING

TEST NO.	TEST PRESSURE (TORR)	HEATER POWER INPUT				HEATER COOLING			SPECIMEN COOLING			TOTAL COOLING	UNACCOUNTED FOR POWER		TEMPERATURES (°F)				CALORIMETERS(3) (BTU/FT²SEC)	
		VOLTS	AMPS	POWER (KW)	POWER (BTU/SEC)	WATER FLOW (LB/SEC)	ΔT (°F)	POWER (BTU/SEC)	WATER FLOW (LB/SEC)	ΔT (°F)	POWER (BTU/SEC)		(BTU/SEC)	%	ELEMENT (PYRO) (1)	SPECIMEN (PYRO) (2)	SPECIMEN BACKSIDE T_2	SPECIMEN RECESS T_1	q_1	q_2
8	10	29.5	390	11.5	10.9	1.45	6.47	9.4	0.433	2.16	0.9	10.3	0.6	5.5	2016		1600	1745	15.4	16.0
9		40.0	503	20.2	19.1	1.47	11.65	17.1	0.433	3.88	1.7	18.8	0.3	1.6	2353	2167	1925	2040	25.4	25.5
11		40	487	19.5	18.5	1.450	11.21	16.3	0.425	3.88	1.65	17.95	0.5	2.8	2353	2176	1975	2055	26.8	26.0
12		40.2	485	19.5	18.5	1.433	11.21	16.1	0.425	4.74	2.01	18.01	0.5	2.8	2419	2252	2043	2125	29.4	28.4
13		50.3	584	29.4	27.9	1.450	17.25	25.0	0.425	5.60	2.38	27.38	0.5	1.8	2647	2469	2270	2350	41.6	40.0
14		60	675	40.5	38.4	1.470	23.70	34.8	0.417	7.32	3.05	37.85	0.5	1.3	2849	2625	2465	2550	52.7	50.5
15		60	678	40.7	38.6	1.470	22.83	33.6	0.417	6.89	2.87	36.47	2.1	5.8	2907	2708	2545	2625	55.5	53.7
16		70	775	54.3	51.5	1.470	31.00	45.5	0.417	9.05	3.77	49.27	2.2	4.5	3082	2872	2710	2790	68.7	66.3
17		80	868	69.4	65.8	1.474	40.10	59.0	0.433	11.21	4.86	63.86	1.9	3.0	3230	3010	2820	2915	82.2	79.4
20		50	595	29.8	28.3	1.467	15.95	23.4	0.500	6.47	3.24	26.64	1.7	6.4	2625	2421	2275	2355		
21		60	691	41.5	39.4	1.467	22.40	32.8	0.500	8.62	4.31	37.11	2.3	6.2	2838	2635	2480	2560		
22		70	785	55.0	52.1	1.467	29.80	43.6	0.483	9.92	4.80	48.40	3.8	7.9	3033	2782	2650	2750		
22		50	597	29.8	28.3	1.432	15.95	22.8	0.466	6.90	3.22	26.02	2.3	8.8	2666	2469	2315	2400		
23		60	687	41.2	39.1	1.418	23.30	33.0	0.466	8.62	4.02	37.02	2.1	5.7	2888	2700	2535	2625		
24		70	782	54.7	51.9	1.450	30.20	43.7	0.483	10.79	5.21	48.91	3.0	6.1	3102	2862	2715	2800		
25		50	591	29.5	28.0	1.432	15.95	22.8	0.483	7.34	3.54	26.34	1.7	6.4	2666	2487	2320	2410		
26		60	687	41.2	39.1	1.418	22.40	31.7	0.466	9.50	4.43	36.13	3.0	8.3	2888	2700	2540	2640		
27		70	780	54.6	51.8	1.432	29.80	42.6	0.466	11.22	5.24	49.84	2.0	4.0	3082	2872	2720	2810		
28		50	589	29.4	27.9	1.400	16.39	22.9	0.466	7.33	3.42	26.32	1.6	6.1	2666	2497	2300	2395		
29		60	680	40.8	38.7	1.400	23.80	33.3	0.449	9.50	4.26	37.56	1.1	2.9	2907	2723	2535	2635		
30		70	772	54.0	51.2	1.432	30.60	43.8	0.466	11.22	5.24	49.04	2.2	4.5	3112	2916	2725	2825		
31		50	587	29.3	27.8	1.432	15.53	22.2	0.466	7.34	3.42	25.62	2.2	8.6	2705	2533	2340	2445		
32		60	682	41.0	38.8	1.432	22.00	31.5	0.466	9.50	4.43	35.93	2.9	8.1	2916	2735	2550	2650		
33	10	70	772	54.0	51.2	1.432	29.80	42.6	0.466	11.22	5.24	47.84	3.4	7.1	3131	2916	2740	2840		

OPERATIONAL DATA FOR 5.0 x 39.0 INCH PROTOTYPE HEATER MODULE

FIGURE 7–6

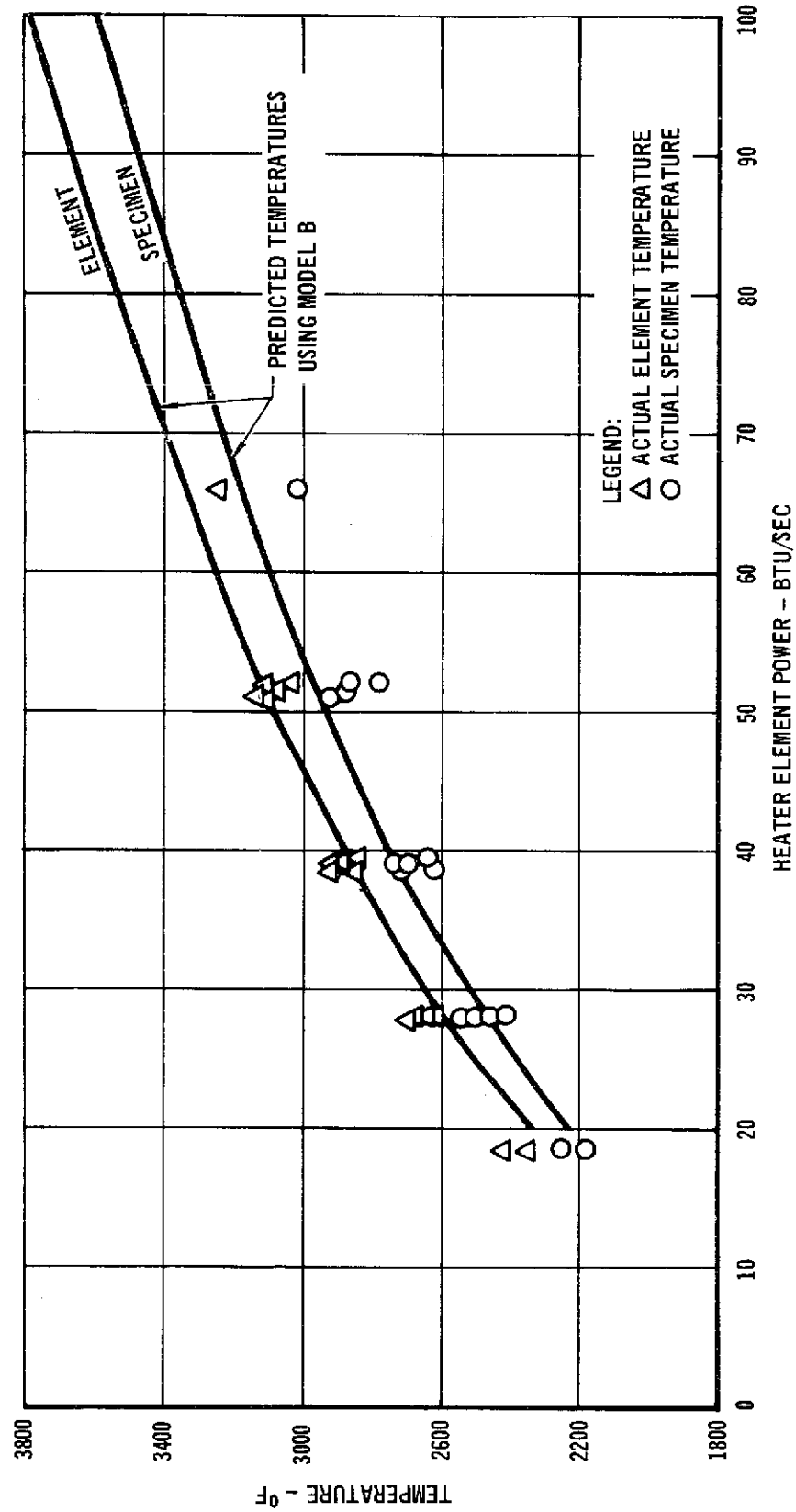

COMPARISON OF PREDICTED AND ACTUAL TEMPERATURES FOR
5.0 x 39.0 IN. PROTOTYPE HEATER MODULE

FIGURE 7–7

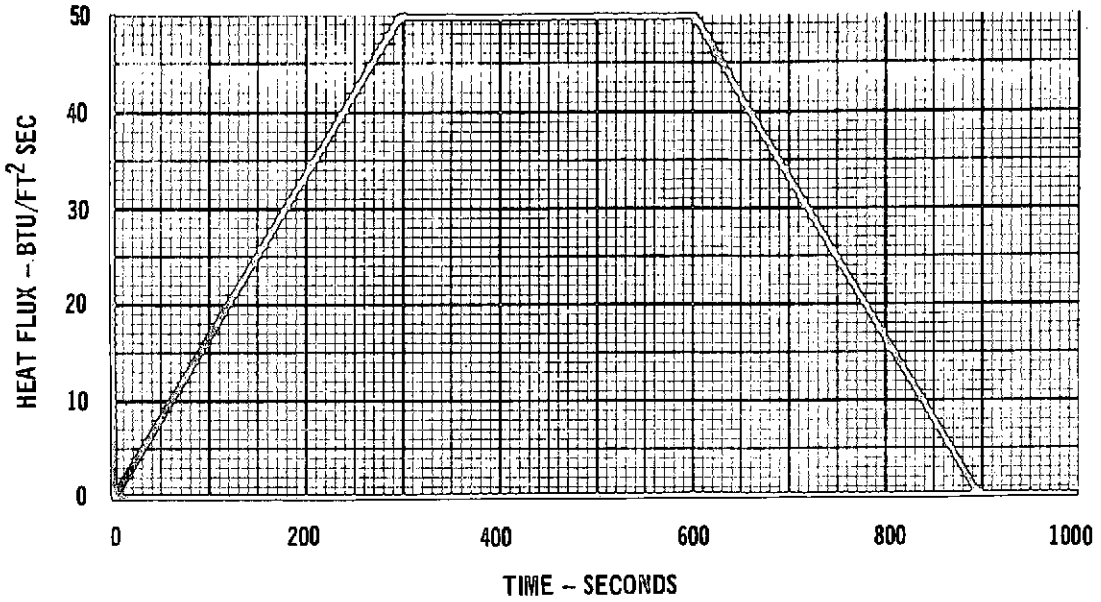

PROGRAMMED HEAT FLUX PROFILE USED TO DEMONSTRATE HEATER CONTROL

FIGURE 7–8

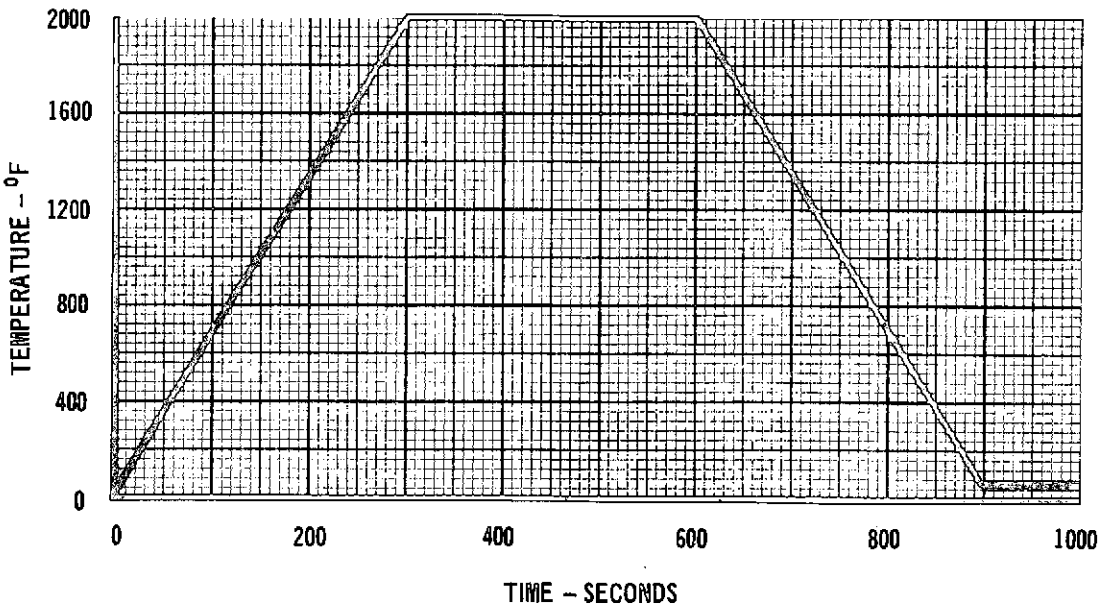

PROGRAMMED TEMPERATURE PROFILE USED TO DEMONSTRATE HEATER CONTROL

FIGURE 7–9

Uniformity of heat flux at the specimen plane in the span direction was investigated in the following manner: the test article with the calorimeters installed was positioned over the heater which was then operated at three stabilized power levels and the calorimeter readings were recorded. By moving the test article relative to the heater module in subsequent sets of runs, it was possible to map heat flux along the length of the module. The results of this investigation are tabulated in Figure 7-10 and compared with the analytical predictions in Section 7.4.2. As seen in this figure, the heat flux becomes more uniform with increasing power. This is because, as the power is increased, conduction down the element to the cooled end block becomes less significant than the radiative heating to the test article.

DISTANCE FROM MODULE ℄ TOWARD ELECTRODE (IN.)	% DEVIATION FROM MAXIMUM HEAT FLUX		
	29 KW	41 KW	54 KW
3	0	0	0
5.2	0	0	0
7.2	0	0	0
11	5.9	5.0	4.9
13	16.6	14.4	12.4
15	43.4	41.0	36.6

VARIATION OF HEAT FLUX UNIFORMITY WITH POWER LEVEL

FIGURE 7-10

Contained in Figure 7-6 is an energy balance for each test run. In the heat flux uniformity runs (20 to 33), there seemed to be an excess of unaccounted for heat with no apparent pattern to explain it, (various from 2.9 to 8.8%). Earlier runs appeared to have a smaller amount of unaccounted for power. This was most likely due to the longer runs used initially and hence steady state heat transfer conditions were more nearly achieved.

7.4 HEAT FLUX UNIFORMITY. Both analytical and experimental heat flux distributions along the span of the prototype module were determined. It would be desirable from the TPS evaluation view point to test with no gradients in heat flux at all. However, due to view factors and the physical close out of a heating unit at its ends, the heat flux drops off. Detailed thermal modeling of the prototype module was performed to predict performance, to correlate measured data and to better understand system characteristics at higher power settings.

7.4.1 Calculated Uniformity. The thermal model (designated Model "C") used to compute temperature and heat flux distribution along the span of the prototype module was much more detailed than the Model "B" (Section 5.3.2). Instead of characterizing the graphite heater elements by a single node, the heater element was divided into 19 nodes (Figure 7-11); and the expansion and electrode end assemblies were modeled. The test article was also subdivided into 15 nodes instead of a single node. Also nodes were spaced closer together near the ends of the test article when gradients were expected. A system of 38 radiosity nodes was employed to describe radiant exchange (including reflection) between the heater elements, test article, and reflectors (bottom, sides and ends). The electrode peg (or pin) through the elements as well as the reflectors, and other water-cooled components were maintained at 100°F. A heat generation term was assigned to each heater element node according to its volume and based on a current in the element and the electrical resistance of the graphite. For the first steady state analyses performed on the General Heat Transfer computer program, the reflectances ($\rho_{CHROME} = 0.65$ and $\rho_{GOLD} = 0.86$) obtained from the Model "B" were used. The computed temperature distributions along elements and specimens are shown in Figure 7-12. As was expected, using the graphite lever arm expansion end design results in more uniform temperatures at that end of the module compared to the electrode end where the element is in direct contact with the water cooled pin. Also, the temperature difference between the element and specimen is smaller for the gold reflector than for the chrome reflector. The computed temperatures at the module center were higher using Model "C" than using Model "B". It was concluded that this was due to the better simulation using Model "C" which has a finer network of nodes. A small study was then performed to determine the appropriate reflectances to use with Model "C". Figure 7-13 shows the influence of reflectance on module center temperatures computed using Model "C". The 25 Btu/sec heating condition was used to reestimate the reflectances for Model "C" to achieve a correlation with Model "B" results. The reflectance for chrome was reduced to 0.55 whereas the reflectance for gold coating was revised downward slightly to 0.83. Figure 7-14 contains the resulting temperature distributions along the span of the module computed using these lower reflectances.

7.4.2 Comparison of Measured and Calculated Heat Flux Uniformity. Incident heat fluxes were measured at six locations along the span of the carbon-carbon test article as described in Section 7.3. Tests were conducted using chrome plated

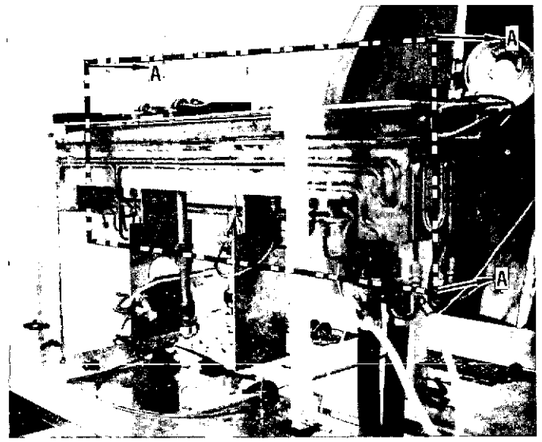

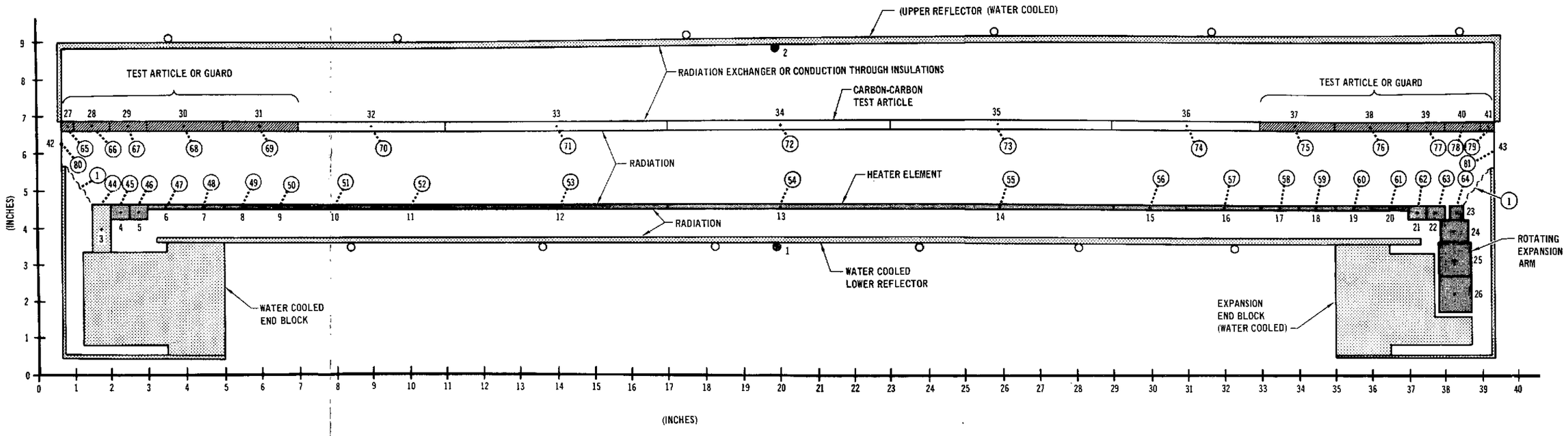

View A–A

- HEAT GENERATED PER UNIT VOLUME OF GRAPHITE
- 3–D RADIATION HEAT TRANSFER
- CONDUCTION
- CALCULATES TEMPERATURE DISTRIBUTIONS IN SPAN-WISE DIRECTION
- CIRCLED NUMBERS ARE RADIOSITY NODES
- CONNECTIONS TO RADIOSITY NODES ARE REPRESENTED BY ⁄ SYMBOL

SPAN-WISE THERMAL MODEL OF PROTOTYPE HEATER MODULE (MODEL C)

FIGURE 7–11

FOLDOUT FRAME 1

FOLDOUT FRAME 2

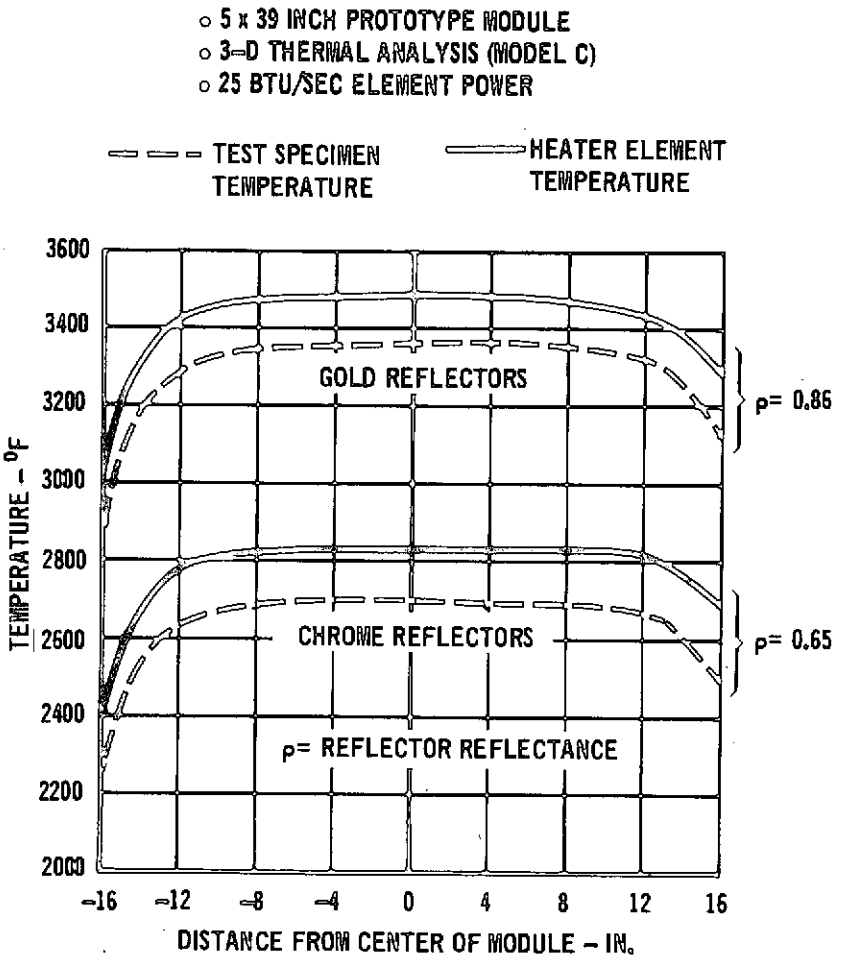

PREDICTED SPECIMEN AND ELEMENT TEMPERATURE REFLECTANCES DISTRIBUTION USING MODEL B

FIGURE 7-12

reflectors and test results were compared with the analytical distribution as shown in Figure 7-15. The measured heat flux remained more uniform over the center of the module and then dropped off more sharply near the end of the module. The calculated and measured heating distributions are in good agreement, except at the end of the unit where additional heat losses may have occurred.

Heat flux distributions along the element were computed (using Model "C") for two power settings and for gold as well as chrome reflectors. Figure 7-16 is an expansion of Figure 7-15 showing the additional calculated heating profiles. The calculated heat flux uniformity increases at higher power settings similar to the measured data. The heat flux uniformity increases still further for the more efficient reflectors.

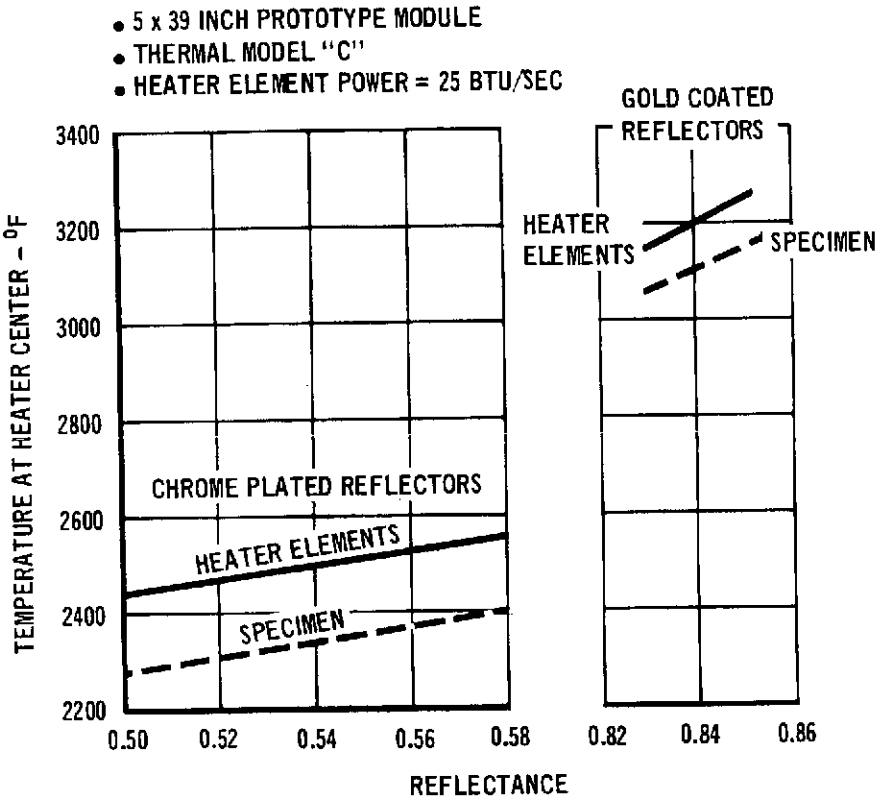

EFFECT OF REFLECTOR EFFICIENCY ON ELEMENT AND SPECIMEN TEMPERATURE

FIGURE 7-13

The uniformity thermal model (Model "C") was then used to recalculate the emperature of the specimen and heater element as a function of heater element power. igure 7-17 contains this information.

The heat flux comparisons described in the preceding paragraphs are at the lectrode end of the module where the water cooled peg reduces flux uniformity more han experienced at the expansion end. The resulting heating distribution is kewed toward the expansion end (See Figure 7-18). The heat generation length of he heater element for the 39-inch prototype module is 34 inches. Also shown on the igure is the heat flux distributions for three and six-inch longer elements. The nformation on Figure 7-18 was used to generate Figure 7-19 which summarizes the xpected heat flux uniformity over various length test specimens. For the prototype odule (L = 34 inches), twenty-six inches of the specimen has greater than 90% heat lux and heat flux drops to 81.7% at the ends of a 30-inch test specimen. As can be een in the figure increasing the element length by six inches to L = 40, results in

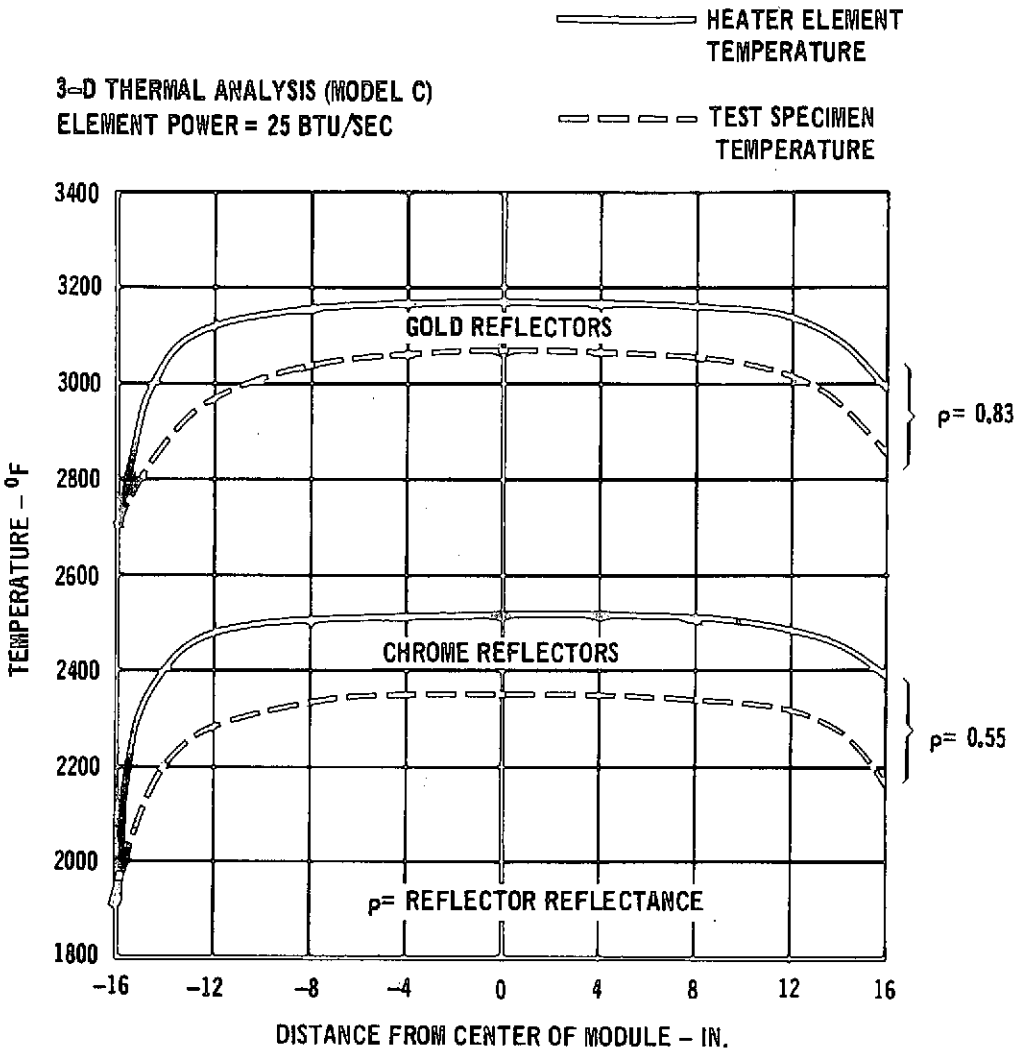

CALCULATED TEST SPECIMEN AND HEATER ELEMENT TEMPERATURE UNIFORMITY FOR PROTOTYPE HEATER MODULE

FIGURE 7-14

a 91% heat flux uniformity on a 30-inch specimen which exceeds the design goal of 90%. Heater elements can be readily machined to the longer length for the full size array and thereby achieve the design goal. On the other hand, if the uniformity goal were reduced to 80% for a thirty-inch specimen, the present prototype unit could be used.

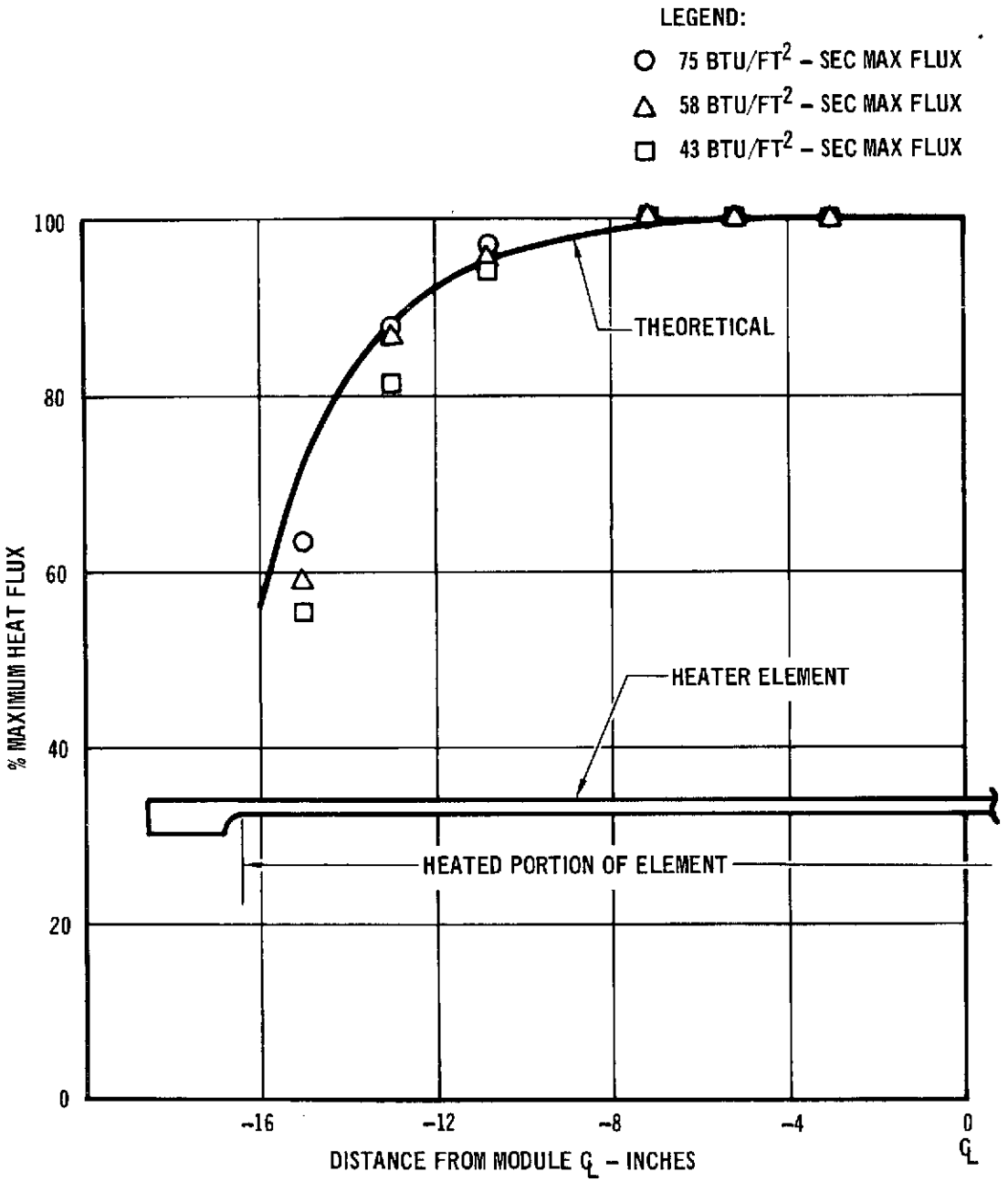

PROTOTYPE MODULE HEAT FLUX UNIFORMITY
(Electrode End of Unit)

FIGURE 7–15

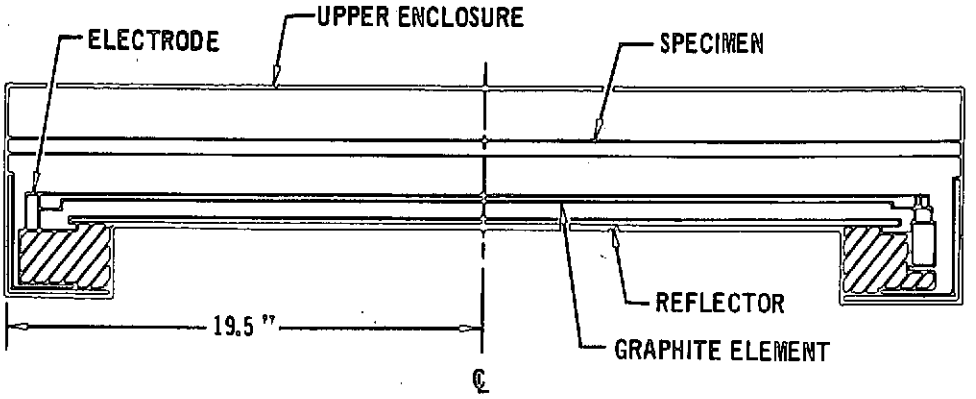

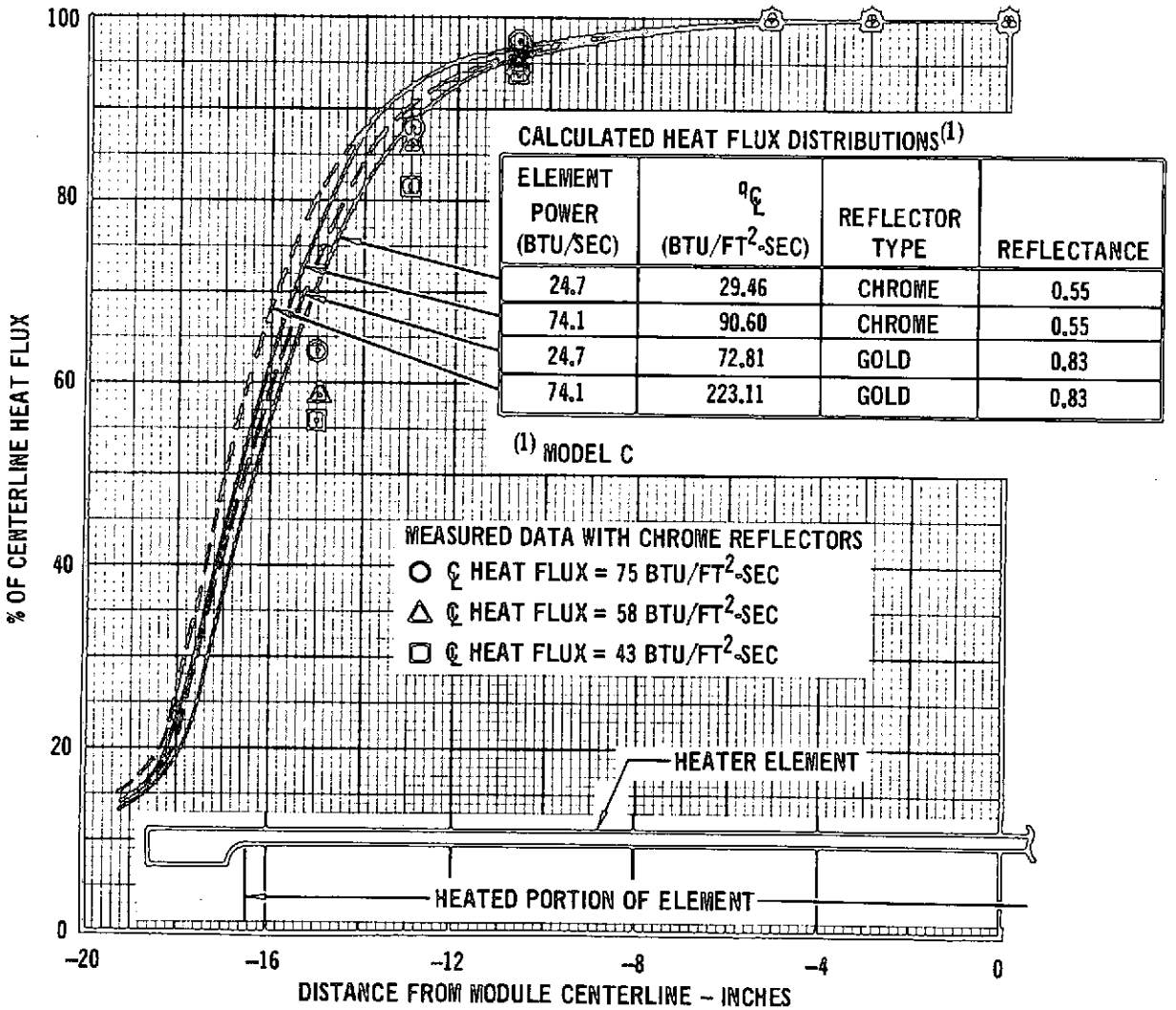

CALCULATED AND MEASURED HEAT FLUX DISTRIBUTIONS, ELECTRODE END OF 5 x 39 IN. PROTOTYPE HEATER MODULE

FIGURE 7–16

- STEADY STATE ANALYSIS (MODEL C)
- ADIABATIC TEST SPECIMEN
- REFLECTOR TEMPERATURE = 100°F

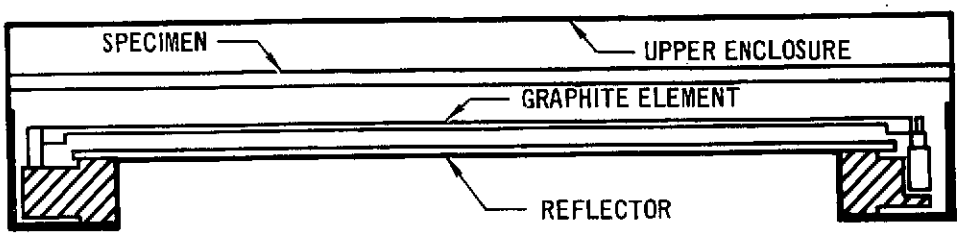

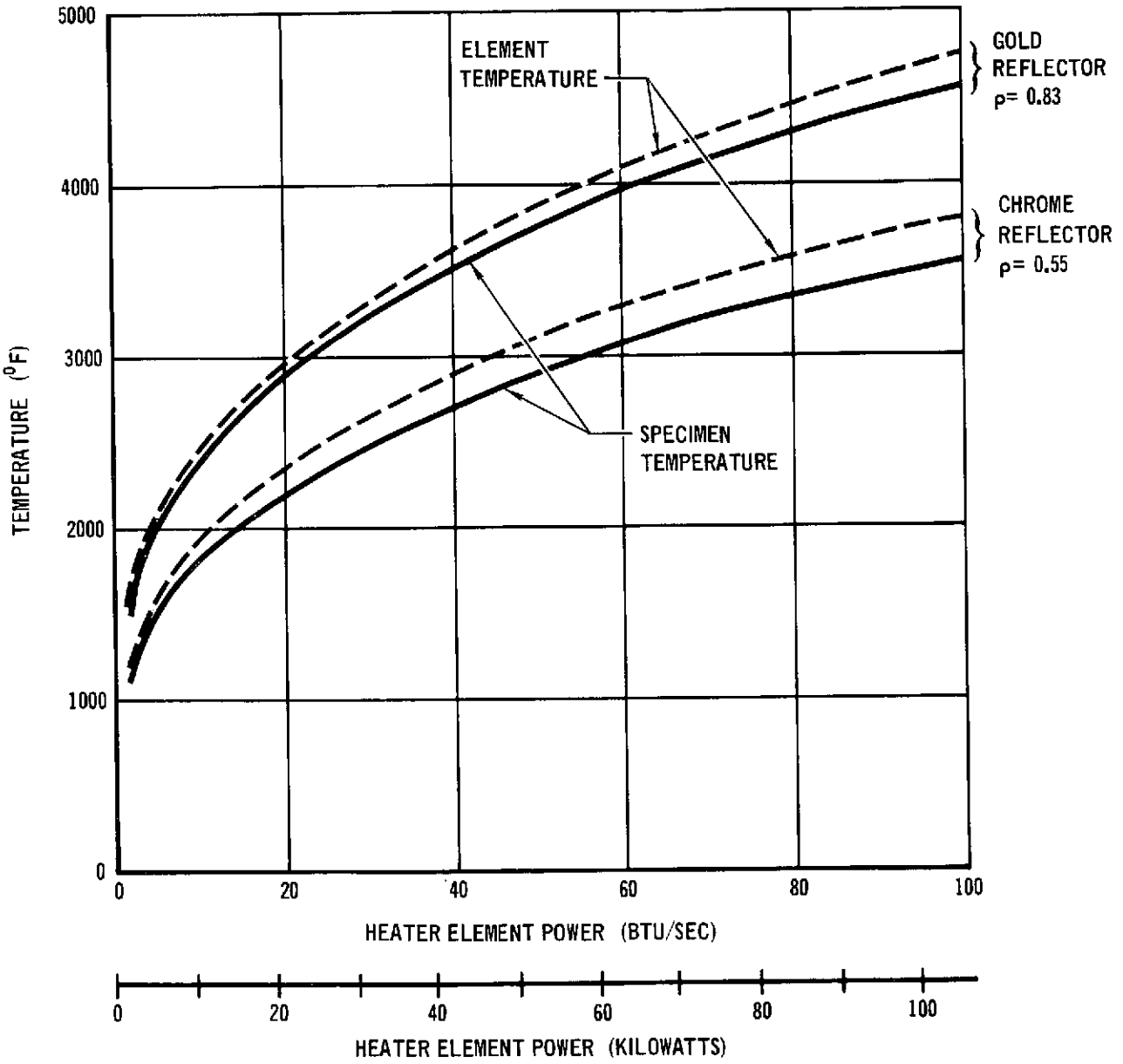

CALCULATED MIDPOINT TEMPERATURES FOR 5 x 39 INCH PROTOTYPE HEATER MODULE

FIGURE 7-17

- GOLD REFLECTORS (ρ= 0.83)
- POWER INPUT OF 24.7 BTU/SEC (25.8 KW)
- MODEL C, 100°F REFLECTORS

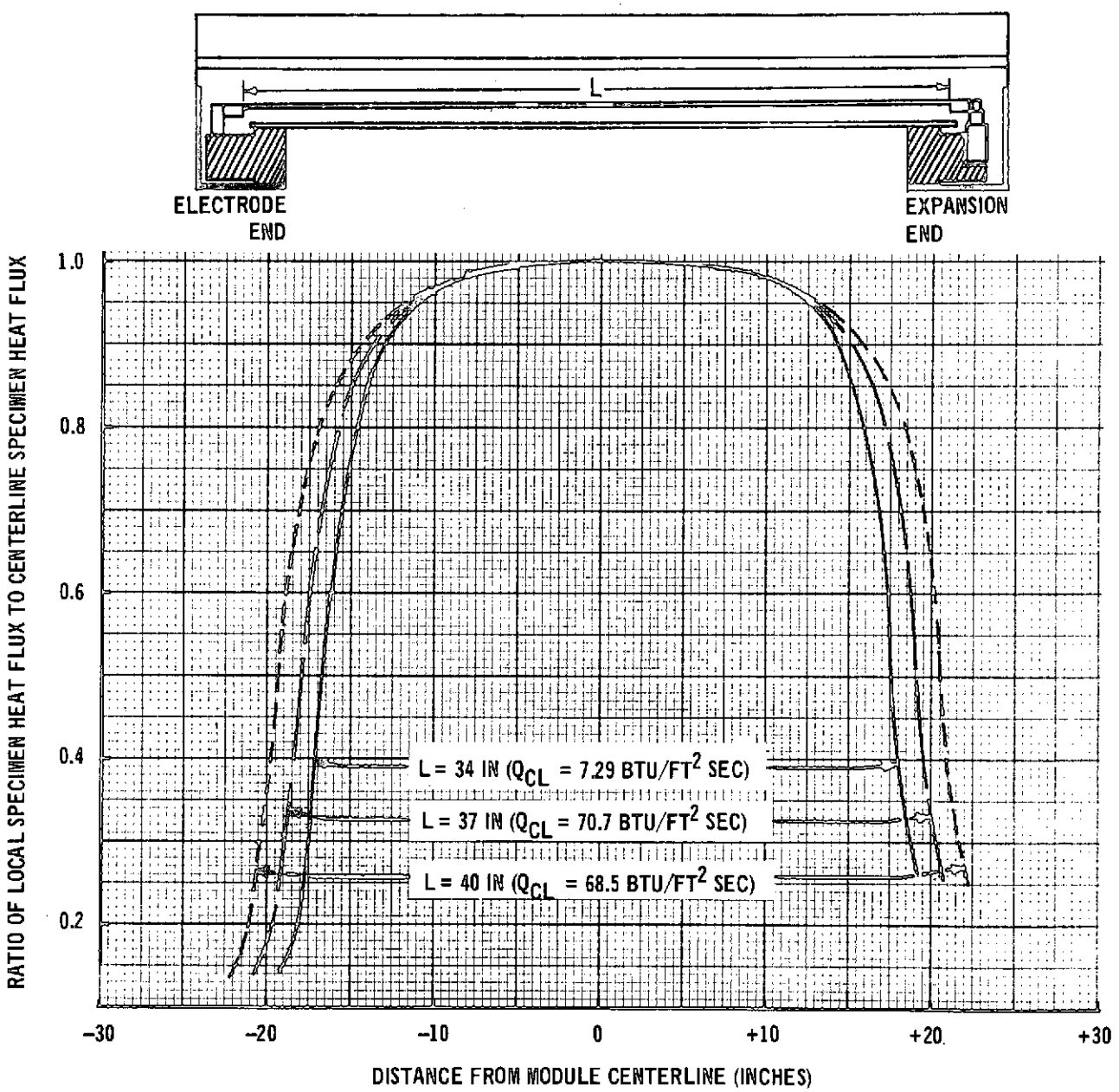

EFFECT OF HEATER ELEMENT LENGTH (L)
ON CALCULATED HEAT FLUX UNIFORMITY

FIGURE 7–18

- GOLD REFLECTORS (ρ= 0.83)
- POWER INPUT OF 24.7 BTU/SEC (25.8 KW)
- MODEL C, 100°F REFLECTORS

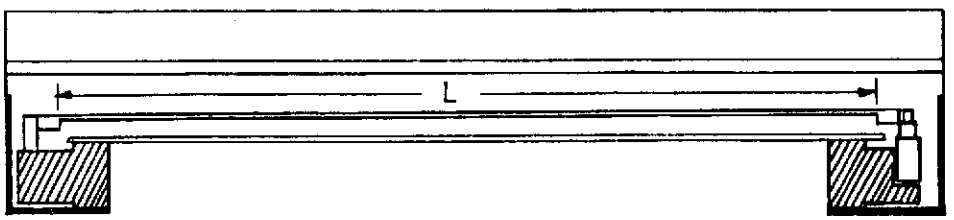

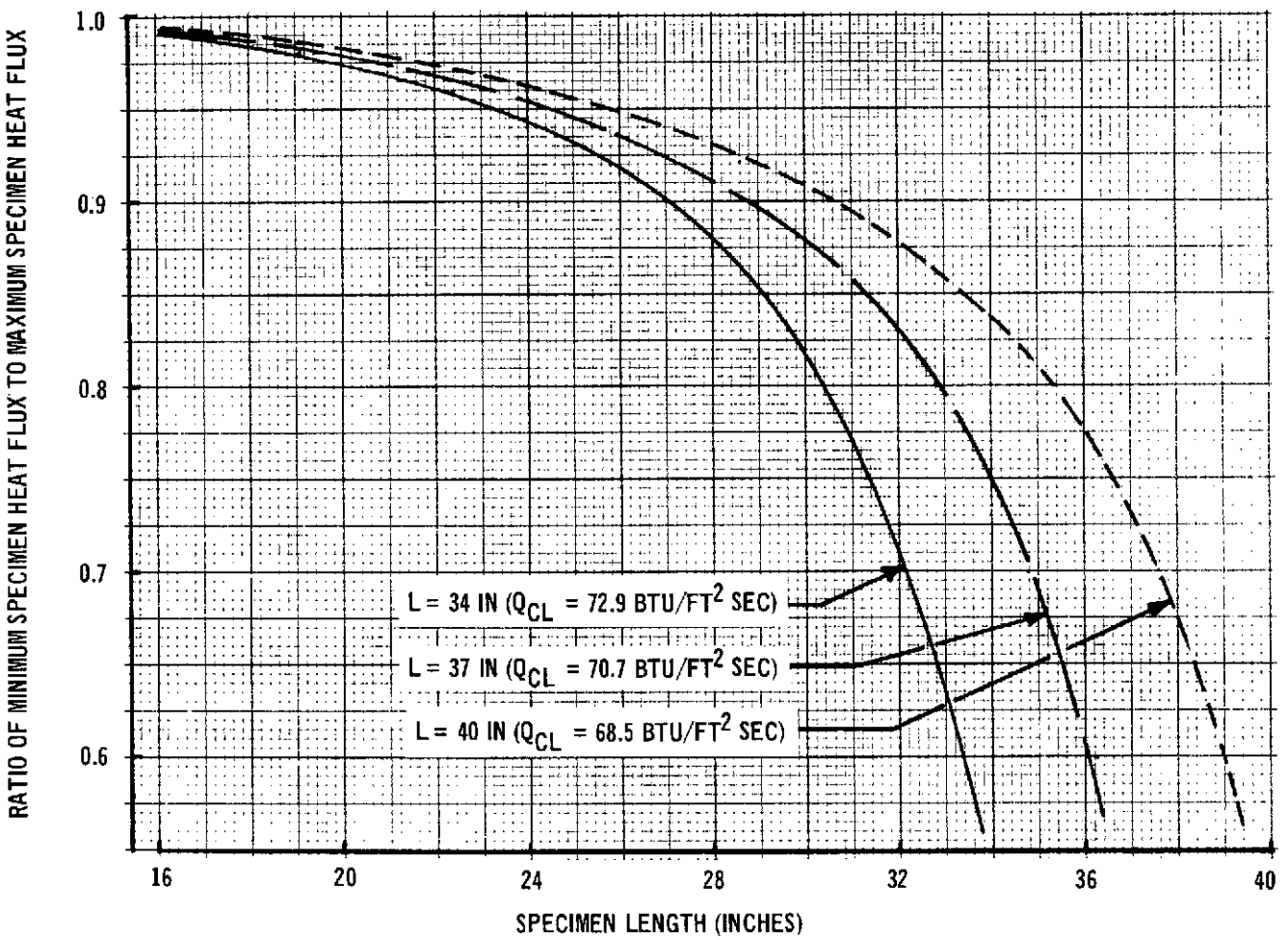

CALCULATED SPECIMEN HEAT FLUX UNIFORMITY FOR VARIOUS SPECIMEN AND MODULE LENGTHS

FIGURE 7–19

8.0 DESIGN OF FULL SCALE LEADING EDGE HEATING ARRAY

The preliminary design of the full scale heating array was performed utilizing the results from the analytical studies and the results from the heater module development. Configuration studies were performed and a standard module size was incorporated along with a design of a support structure which not only accommodates various sizes of leading edges but also provides cooling water and spray bar gas connections for each module. The array is a complete unit with guards and endcovers to prevent heating of the vacuum chamber which houses the unit. The quantity and type of auxiliary equipment were determined. Heater control systems and specimen temperature measurement systems studies were performed so as to be compatible with the instrumentation (or lack of instrumentation) on the full size test article. The array was designed so the unit can be expanded to test longer leading edges, test articles requiring oxidizing atmospheres, and even ablators.

The succeeding sections describe in detail the results of the preliminary design effort for the full scale heating array.

8.1 ARRAY CONFIGURATION STUDY. A study was conducted to determine the configuration that would best satisfy the leading edge heating array requirements. The first approach examined was the use of a minimum number of modules for testing the 8-inch radius leading edge. The modules which make up the array are listed below:

7 Zone I Heaters - Each 5 Inches Wide

1 Zone I Absorber - 5 Inches Wide

1 Zone II Heater - 8 Inches Wide

1 Zone II Absorber - 11 Inches Wide

The above array would provide the desired steady state temperature distribution on the 8-inch radius leading edge. It provides 38 inches of temperature control in Zone I and 29 inches of temperature control in Zone II.

The second approach studied was the use of one standard module size for testing the 8-inch radius leading edge. The modules which make up this array are as follows:

9 Heater Modules - Each 5 Inches Wide

5 Absorber Modules - Each 5 Inches Wide

This array provides the same temperature control as the first configuration but requires only two types of modules which can, therefore, be standardized.

A third configuration that was considered included sufficient modules to provide temperature control for all probable temperature distributions. It is possible that a leading edge temperature distribution would be desired which would require heater modules in all zones. This would require 14 heater modules 5 inches wide to cover 38 inches of Zone I and 29 inches in Zone II, regardless of the leading edge radius. In addition to these heater modules, a minimum of five absorbers would be required. This configuration results in the following number of modules:

14 Heater Modules - Each 5 Inches Wide

5 Absorber Modules - Each 5 Inches Wide

The major conclusions from this study are listed below:

(1) All modules should be standardized (5 inches wide) to provide interchangeability and versatility to the array and also to lower overall array costs.

(2) The maximum number of modules required to test a leading edge of any probable radius is 14.

(3) Both heater modules and absorber modules are required, and the number of each type of module is dependent on the area heated and on the temperature distribution desired.

(4) Nine heater modules and five absorber modules are required to provide the desired temperature distribution on the 8-inch radius leading edge.

8.1.1 Selected Modular Concept. The modular approach to the full size heater array offers the same advantages as do most standardized systems, namely, economy and versatility. Economy is attained by manufacturing larger numbers of standard parts and to a lesser extent by reducing spare parts inventory requirements. The modular concept gives the entire array more versatility by widening the spectrum of testing that can be accomplished. By simply changing the configuration of the two module support plates in the support structure, heaters can be arranged to test either airfoil shapes or flat surfaces.

8.1.2 Heater Module. The heater module consists of a standard width module of two serpentine heater elements with two passes each. Reflective surfaces surround the heater elements on all sides except one, which is directed at the test article. The cooling water tubes are arranged so as to nest with the adjacent modules to reduce cold lines between modules and to prevent the escape of radiated energy. The nesting idea also applies to the end reflectors so that complete arrays will nest end-to-end.

8.1.3 Absorber Module. A further reduction in array costs has been effected by designing an absorber module which is used when heat must be removed from a test article. In other words, a heat sink is required instead of a heater. The absorber module fills this requirement at a much lower cost than a heater module that has had its elements removed and that has had a high emissivity coating applied to its reflectors. For the proposed absorber module, the "guts" of the heater are eliminated, along with the cost of close tolerance machining operations. The absorber module is the same length and width as the heater module and incorporates the same interlocking feature. Figure 8-1 shows the absorber configuration.

8.2 ARRAY SUPPORT STRUCTURE. The array support structure is a U-shaped structure with the open side of the U-structure oriented upward. The structure supports the graphite heater modules, the specimen, and all necessary guard reflectors; and it incorporates the required gas and coolant manifolding.

The backbone of the basic support frame is a pair of U-shaped pipe manifolds located so as to line up with the individual module mounting flanges. The outer side of the U-shape contains all the coolant fittings while the inside features a universal support plate to which the heater modules support plates are fastened. The array is formed by bolting the individual modules to these plates around the periphery of a leading edge-shaped cutout. The basic support frame is completed with a steel channel structure which provides both a base and a means of support for the specimen, guard reflectors and other necessary ancillary equipment. Another pair of U-shaped pipe manifolds, made of smaller pipe than the coolant manifolds, is fastened to the channel structure to provide gaseous nitrogen to supply the gas cooling spray bars in the modules.

The leading edge test article is suspended by linkages from a roller mounted support frame thereby permitting the specimen to be rolled out the end of the array for easy servicing of either the specimen or the array.

Guard reflector assemblies are attached to the ends of the span by fastening plated liquid-cooled copper plates to a steel angle frame. These assemblies and the guard coolant supply manifolds are roller-mounted so that they may be rolled out of the way using the same track as the test article.

Figures 8-2 through 8-7 show the preliminary design of the heating array. A pictorial of the array is shown first to facilitate orientation of the remaining views of the array. Figure 8-3 is the span view of the array and shows the two end

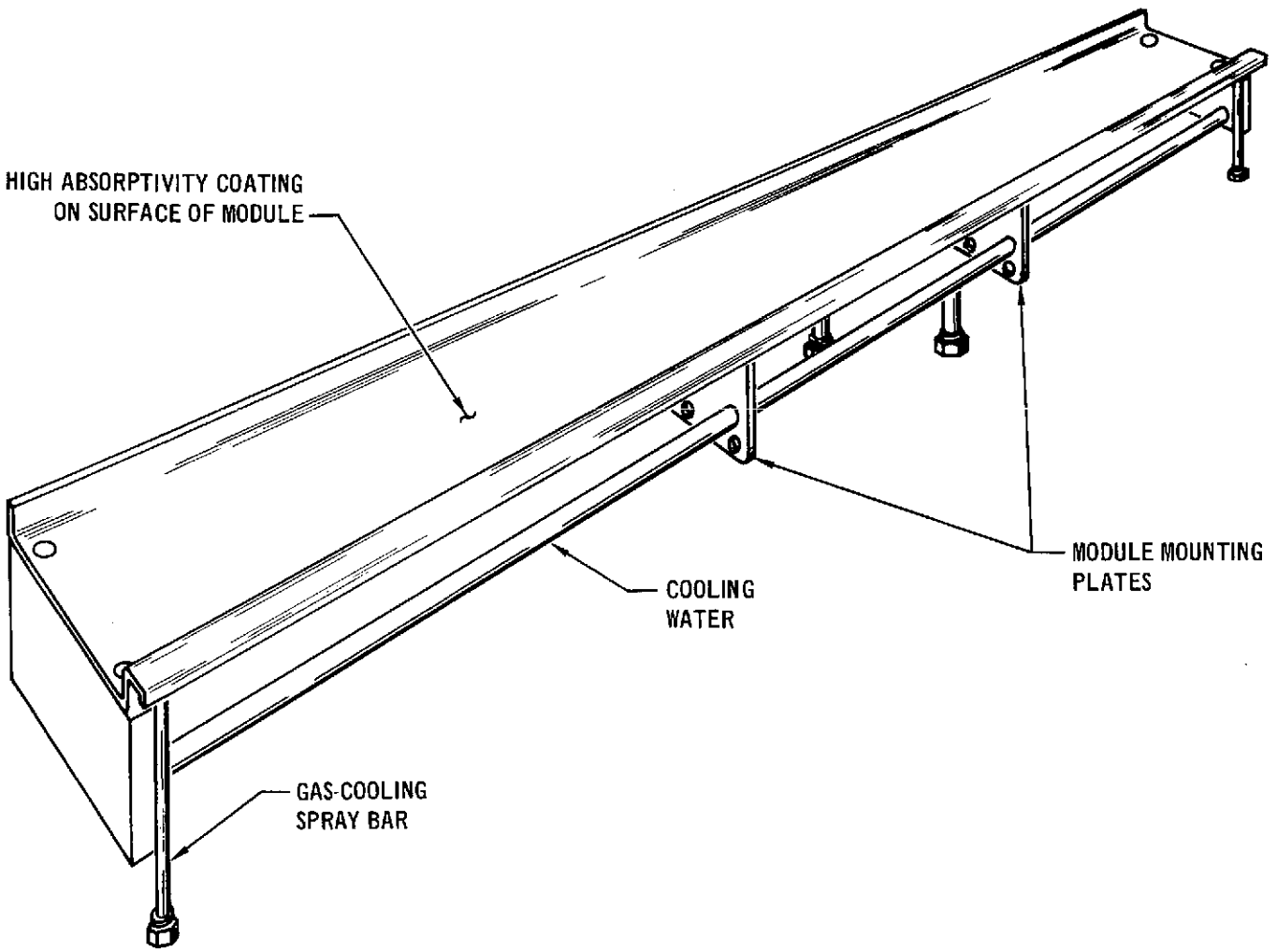

ABSORBER MODULE

(5 x 39 Inches)

457-3389

FIGURE 8-1

covers in place. Section B-B (Figure 8-4) of this figure, shows the mounting of individual modules, test article and edge guards as well as the support plates and manifolds. Figure 8-5 is an end view of the array and shows the end cover used to prevent unwanted dissipation of heat to the vacuum chamber walls. Another view of a module in the array is shown in Figure 8-6. Figure 8-7 shows the top view of the heater array.

8.3 WASTE HEAT REMOVAL. To prevent heating of the uncooled vacuum chamber walls, it is necessary to provide complete shielding of the radiation from the heater elements, the hot specimen and stray radiation emanating from any openings. The reflector system of the individual modules (heaters or absorbers) will prevent

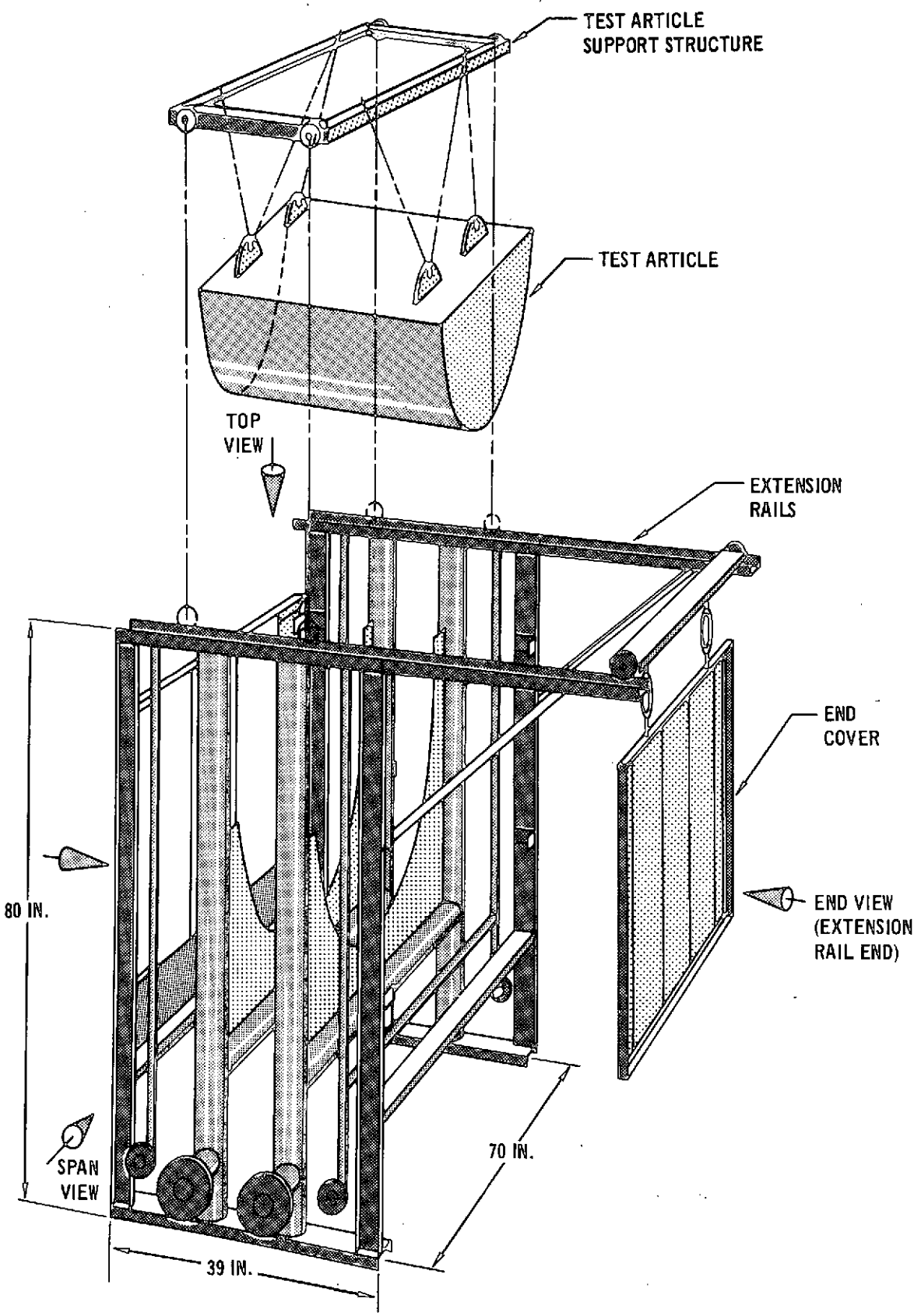

PICTORIAL OF THE HIGH TEMPERATURE LEADING EDGE HEATING ARRAY
(Heater Modules Not Shown)

457-3384

FIGURE 8-2

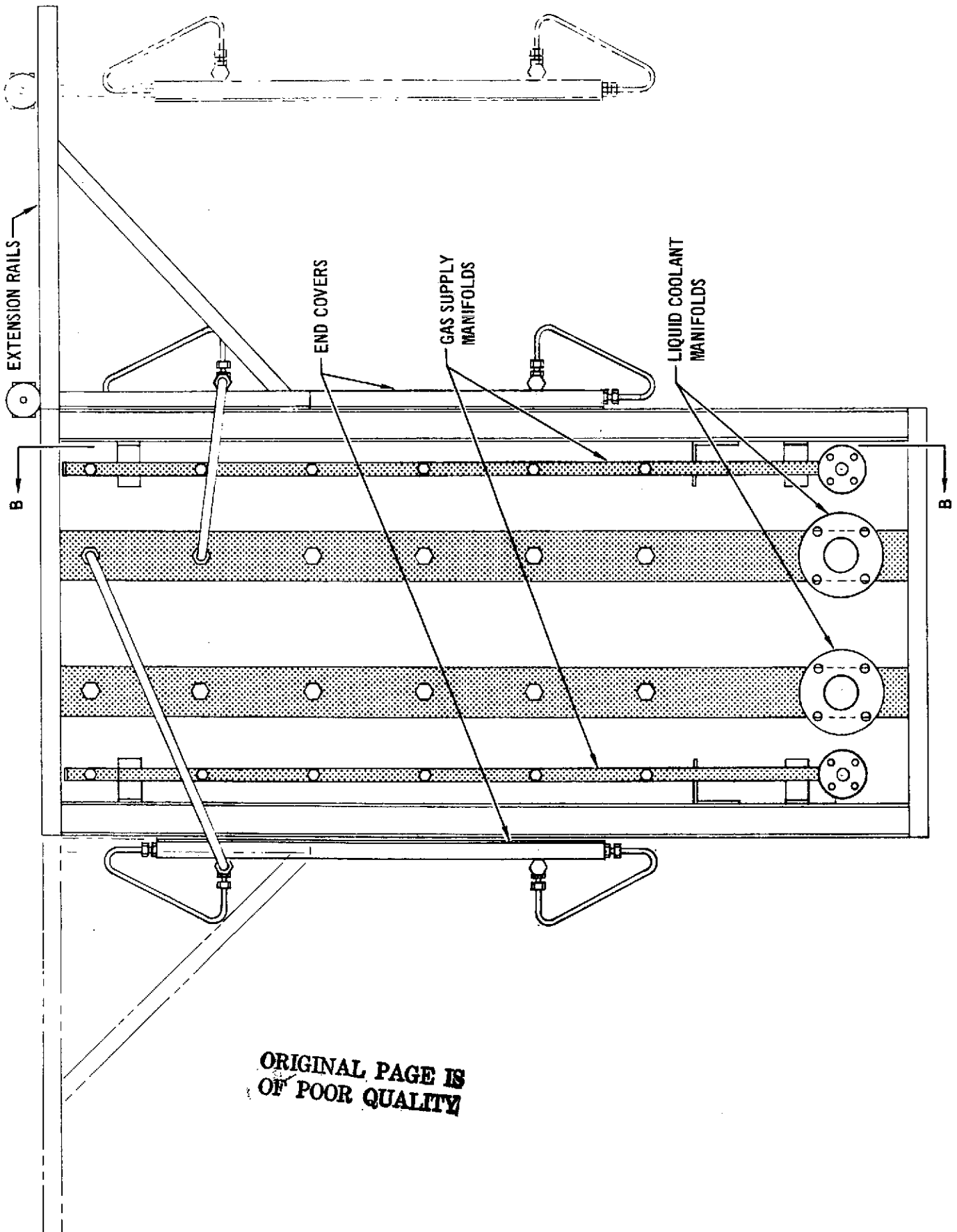

FIGURE 8–3

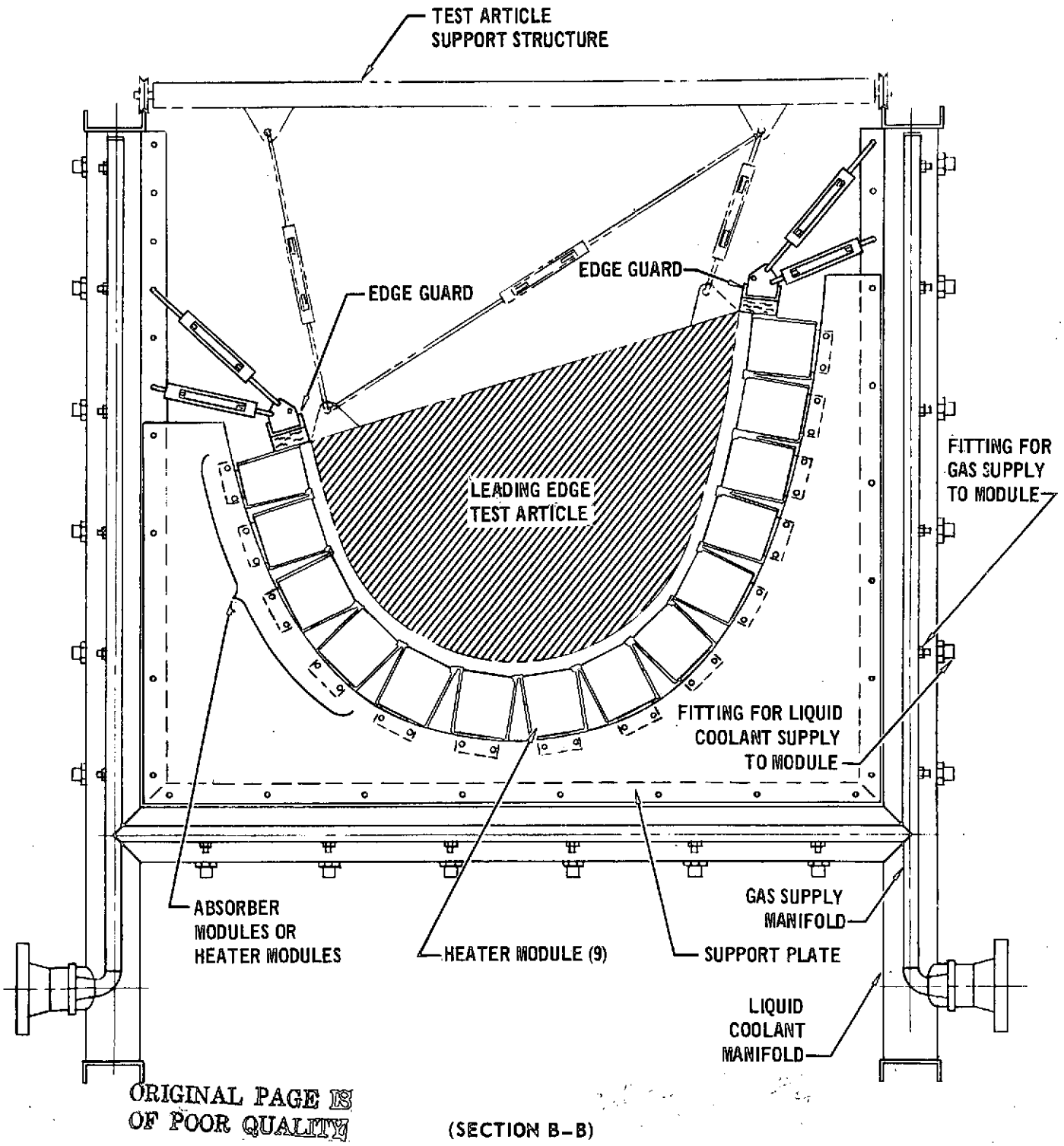

ORIGINAL PAGE IS
OF POOR QUALITY

(SECTION B–B)

END VIEW OF HEATING ARRAY

457–3385

FIGURE 8–4

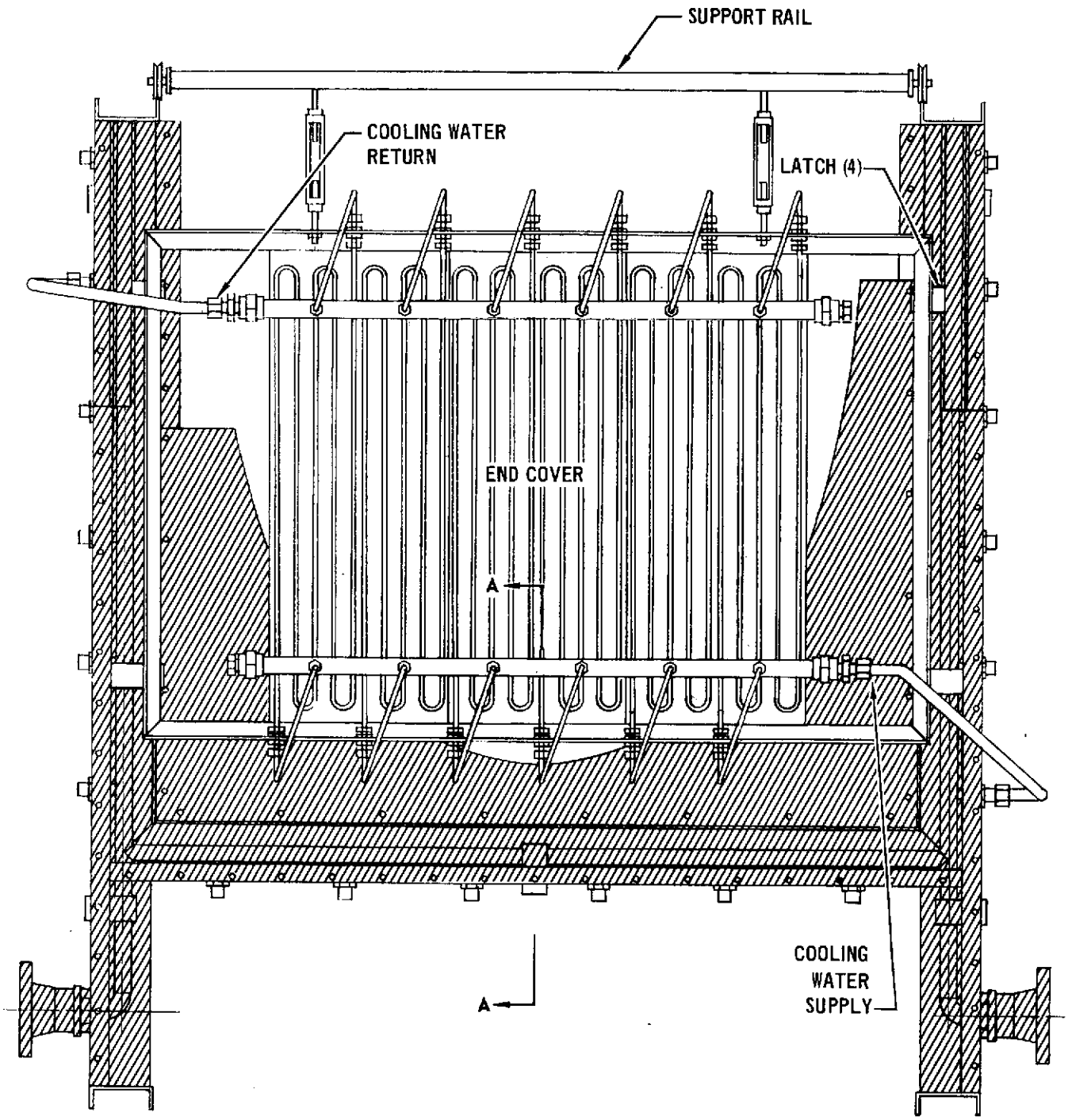

END COVER INSTALLED ON ARRAY
(View from Extension Rail End)

457-3386

FIGURE 8-5

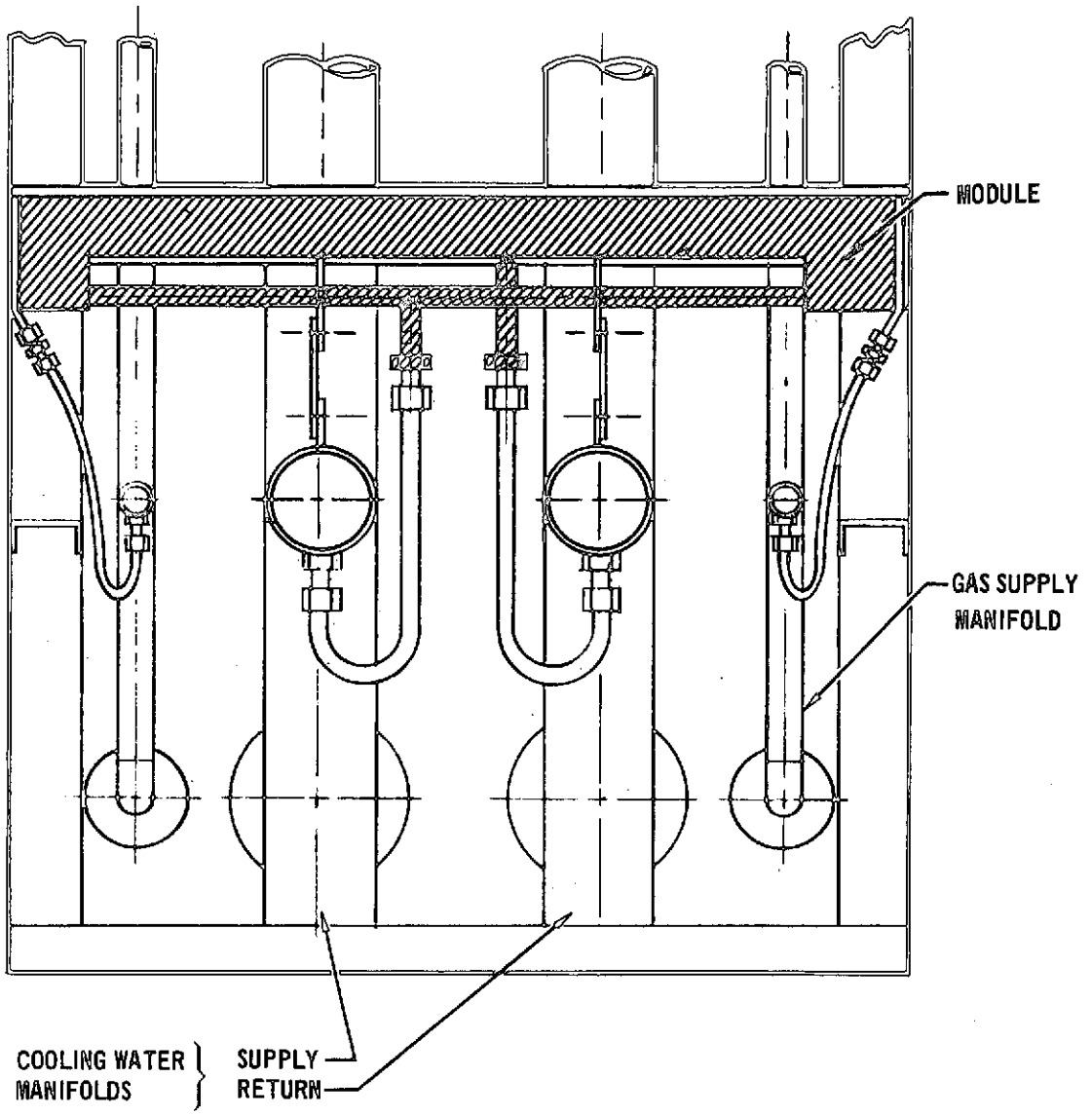

SECTION A-A

SPAN VIEW OF MODULE INSTALLED IN THE ARRAY

457-3387

FIGURE 8-6

any waste heat dissipation from within the modules themselves. The modules are designed so that when they are placed adjacent to one another, they will interlock and prevent escape of thermal radiation. The only other avenues for waste heat dissipation will be between the array and the test specimen both at the ends of the specimen and along the span at the rear of the specimen. Radiation out the ends is prevented by positioning rectangular liquid-cooled copper plates ("end covers", Figure 8-5 at each end of the array support structure. The inside surface

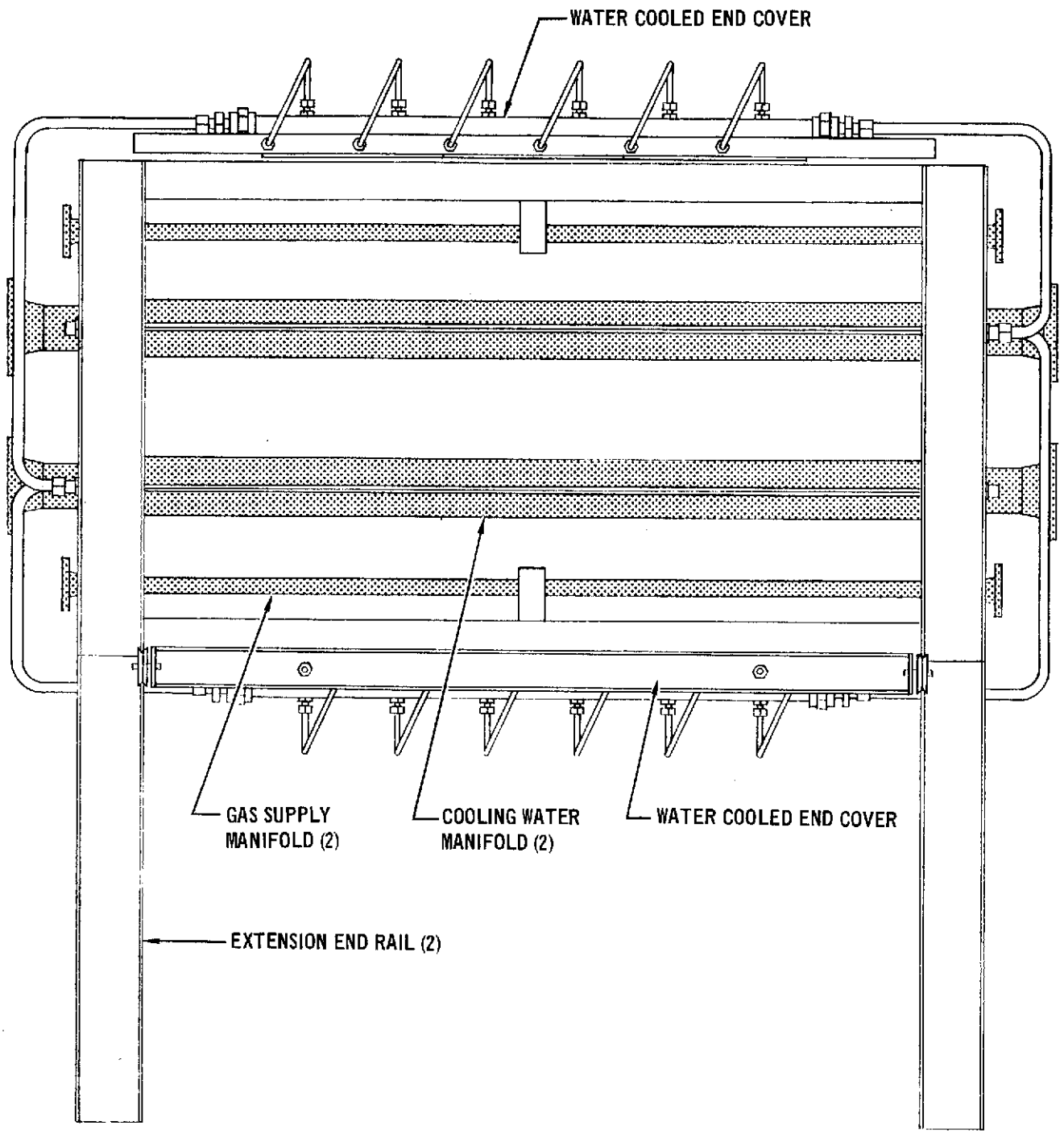

TOP VIEW OF HEATING ARRAY SUPPORT STRUCTURE

457-3388

FIGURE 8-7

of these plates will be plated to minimize heat transfer as well as to enhance the spanwise heat flux uniformity.

Radiation out of the gaps along the span aft of Areas II and IIa is dependent on details of the test specimen and supporting hardware and is most effectively controlled by using batts of Dynaflex insulation bonded onto liquid cooled copper plates. These "edge guards" will be mounted to the array support structure using a four-link system.

As described in detail above, the vacuum chamber walls will be shielded from both the heater array and the specimen using a series of reflectors and heat shields which, along with the electrodes and heater element supports, are all liquid cooled to remove the waste heat. The coolant flow rate through each module will be tailored such that the maximum total flow through the heater assembly is 250 gpm. This flow rate at maximum power (1 megawatt, heater capability) will result in a coolant temperature rise of 27°F which is compatible with the GFE cooling system. This compatibility, although it is of little importance with one heater assembly. is important when considering the future expansion to ensure a proper match between the overall heater assembly and the GFE cooling system.

8.4 TOTAL POWER REQUIREMENT ESTIMATE. Total power requirements to test the 8-inch radius carbon-carbon leading edge were estimated. The estimate assumed that nine heater modules with gold reflectors would be operated at sufficient power to achieve 3500°F on the test specimen analyzed in Section 4. It was also assumed that each module had to provide a maximum net power to the test specimen of 21 Btu/sec which is 50 percent greater than the maximum calculated net heat flux for any one module. For this, the worst case, 600 kilowatts would be required to test the 8-inch radius leading edge.

8.5 HEATING ARRAY CONTROL SYSTEM. A variety of ways exist to control the individual graphite heater modules making up the heater array. These may be divided into two general categories: surface temperature feedback and incident radiant flux feedback. For surfaces which have adiabatic back sides and are in radiation equilibrium with the surroundings, the two methods are equivalent. However, for surfaces behind which significant heat transfer occurs, the surface temperature is dependent upon the internal heat transfer as well as the imposed environmental conditions. The proper method is to devise a system which measures incident heat flux on the test article surface, compares it with a calculated value for the actual conditions and causes the test apparatus to operate in a manner which nulls out the difference.

Control systems that were investigated are:

- o Heat flux sensors in the test article
- o Heat flux sensors in test article guard
- o Heat flux sensors in bottom of heater module
- o Thermocouples on the test article
- o Radiometers in heater module

Heading the list of possible methods of controlling the individual modules in the array is a heat flux feedback system utilizing heat flux sensors installed in the leading edge test specimen. It is preferable to locate these sensors in the center of the leading edge. The nonstructural tee sealing strip between segments (Figure 8-8) is an excellent location for a set of heat flux sensors and does not require modification of either segment of the leading edge. The width of the leg of the tee would be locally thickened (Figure 8-9) to form a boss for the heat flux calorimeter. This approach also requires a slight modification of the leading edge attachment bolt, spacers and brackets. These sensors, when corrected for the specimen emissivity, will measure the incoming power to the test specimen from all sources including radiation, reradiation, and reflection. The output of the sensors will be compared with a control curve derived from actual trajectories and cause the heaters to supply a sufficient amount of power to cause the total power from all sources to be exactly as desired. The accuracy of this method of control is largely insensitive to reflector cleanliness, effects of reflected radiation, and to a large extent, changes in uniformity; the requirement for an optical system or auxiliary signal conditioning equipment is eliminated.

If installation of heat flux sensors in the leading edge test specimen is deemed undesirable for one reason or another, the next best control method is through the use of heat flux sensors mounted in the end guard reflectors that fill the gap between the end of the test specimen space and the array end reflectors. It is anticipated that these end guards will be wing leading edge shaped reflectors constructed of plated, water-cooled copper and fastened to the array end reflectors. These sensors will function in the control system exactly like the aforementioned sensors but will have to be corrected for the heat flux drop-off from the center to the end of the span and also for any uniformity changes that may occur as a function of power setting. It is also possible that the output of these sensors will be affected by the guard reflector induced emittance apparent enhancement of the elements directly under the reflectors which will, therefore, result in an output which is some function of the reflector cleanliness.

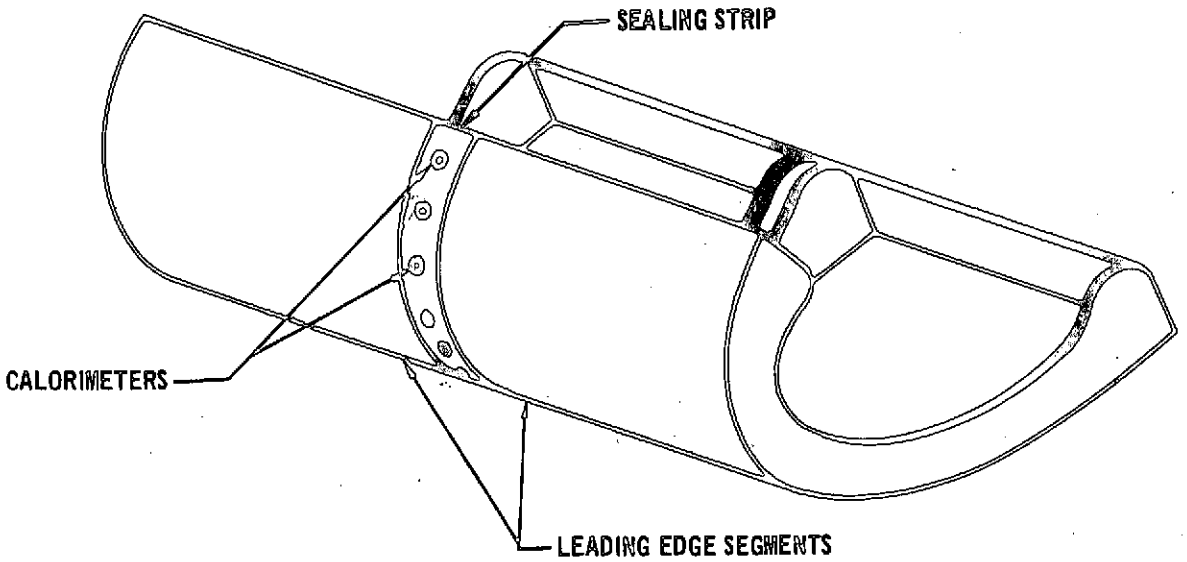

LOCATING HEAT FLUX SENSORS IN THE SEALING STRIP OF THE LEADING EDGE

FIGURE 8-8

One of the simplest systems for heat flux feedback control is comprised of a heat flux sensor installed in the bottom reflector of the individual heater module looking at the elements from approximately the same distance as a specimen mounted heat flux sensor. The most serious drawback of this method, aside from the need for correcting the output for specimen emissivity and the difference in radiation view factors is the fact that the presence of the module reflectors enhances the apparent emissivity of the graphite elements and causes the sensor to read high. This means that the effective "corrected calibration" of the sensor will change as contaminants deposit on the reflectors.

A straightforward method of control which eliminates the effects of emissivity, emittance enhancement, and reflector degradation is the use of thermocouples to directly measure the front surface temperature of the test specimen. Despite these advantages, this scheme is fraught with the typical thermocouple difficulties such as response, fragility, mounting effects, conduction down the wires, short circuits, and radiation characteristics. In addition to these normal thermocouple problems, the need to measure temperature in excess of 2700°F presents another set of complications. Thermocouple wire materials suitable for these temperatures are exceedingly susceptible to alloying with various contaminants such as silicon and carbon which change both the structural strength and ductility along with the

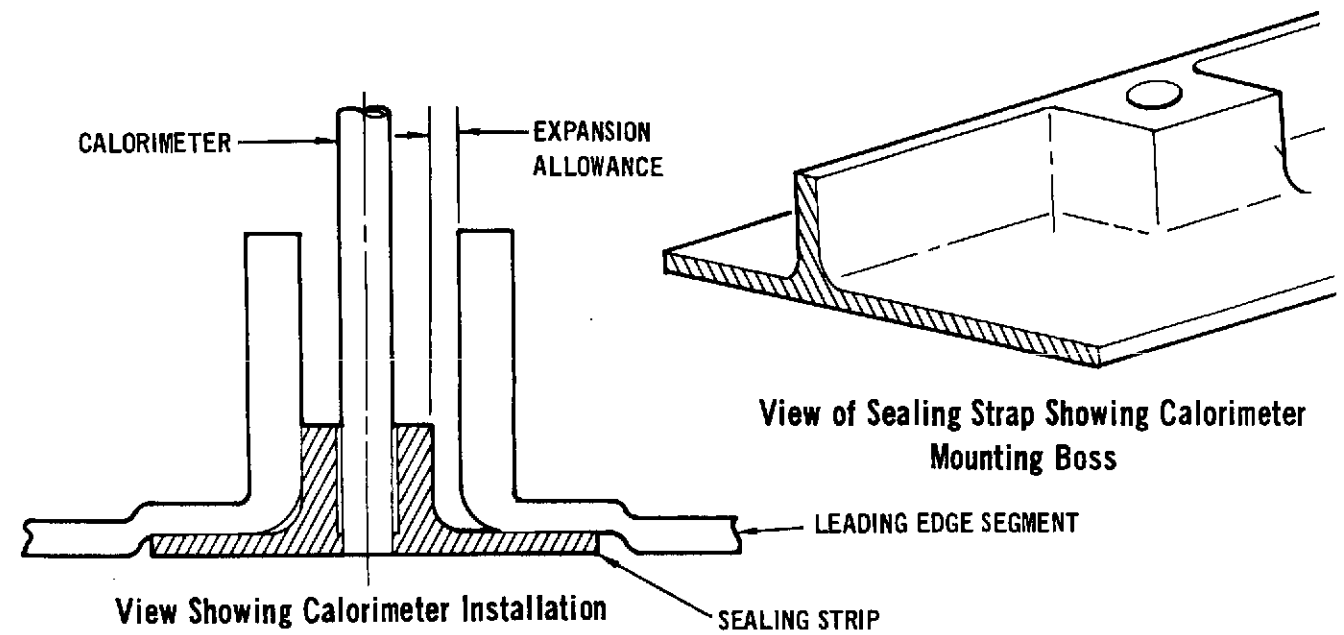

View Showing Calorimeter Installation

View of Sealing Strap Showing Calorimeter Mounting Boss

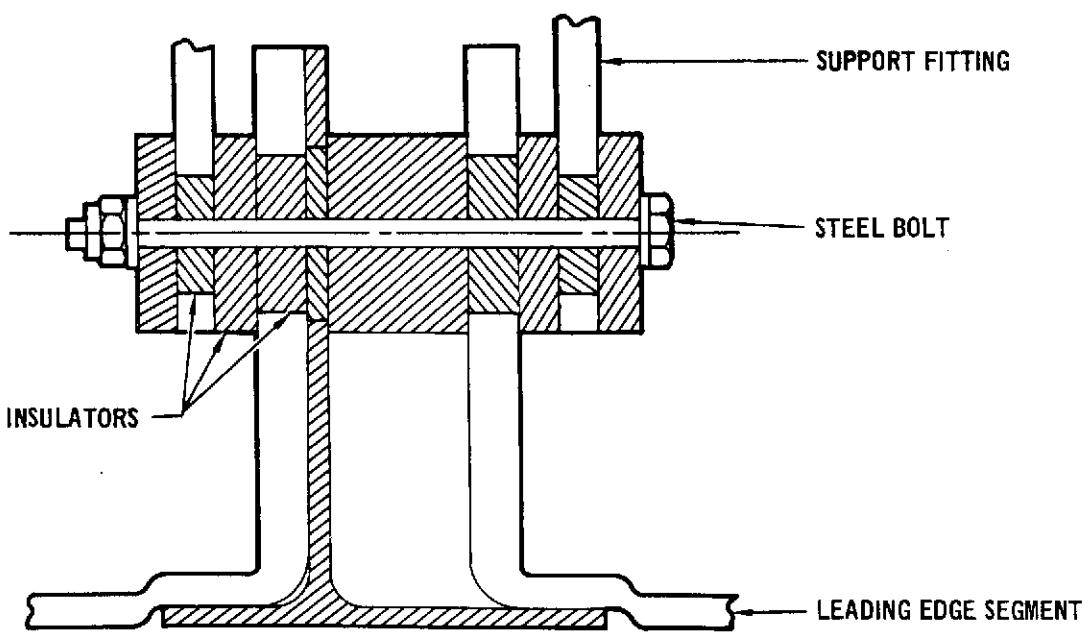

View Showing Support Fitting Modification

CALORIMETER INSTALLATION IN LEADING EDGE SEALING STRIP

FIGURE 8-9

thermoelectric potential. Electrical insulation at high temperature is also a problem along with mounting and shielding techniques. One further problem with thermcoouples is the noise generated by the chopped cycle power characteristics of ignitron power controllers.

Another technique in an attempt to measure the specimen surface temperature to feed back for control purposes involves the use of a narrow-angle radiometer mounted on the back reflector of each module and viewing the surface of the specimen through the gap between the elements. In spite of its simple concept, this method requires the development of an optical system, and suffers from effects of specimen emissivity, emissivity changes, and reflected radiation. These effects cause unknown errors in the output which should be fairly small at steady state but are quite large during transient heatup. In addition the sensor used put out a signal that requires additional conditioning to be suitable for feedback and also does not produce a signal below about 1400°F thereby requiring another control technique below this temperature.

Based on the above discussion, the use of heat flux sensors installed in the leading edge of the test specimen is recommended for supplying the control signal with an over-temperature interlock shut-off system based on one of the temperature measurement schemes. If, however, an alternate scheme is desired, a comparison of the desired scheme with the suggested method can be made using the fully instrumented prototype heater module and carbon-carbon test specimen.

8.6 TEMPERATURE MEASUREMENT. As described in Section 8.5, there are several methods for measuring the specimen surface temperature. This section is devoted to investigation of an electro-optical system which views the leading edge through apertures in the bottom of each module of the array. Hence, provisions for such a system must be incorporated into the final design of the array. The purpose of the investigation was to determine the feasibility and potential benefits of an optical system, to identify areas influencing performance, and to determine the most promising system.

The investigation was confined to radiometric temperature indicating systems which use an optical system, radiation detector, and signal processing electronics to provide an electrical output related to the radiant energy emanating from the specimen. An optical system based on the visual observation of the test specimen (e.g., disappearing-filament optical pyrometer) was used satisfactorily during prototype heater testing, but was discarded for the full-scale array because of the

difficulty of obtaining optical access from outside the vacuum chamber to the many points on the specimen, the slow sampling data rate, and the high per-test cost of labor.

The uses and advantages of a radiometric temperature indicating system and the influences of the measurement situation and radiometer design on system performance are discussed in succeeding sections. Practical considerations in the application of a radiometric system to the full-scale heater array are also discussed. Finally, the particular radiometric system showing most promise is identified.

8.6.1 Uses and Advantages of Radiometric Temperature Indication. An ideal radiometric temperature indicating system could perform three functions during the test of a leading edge. It could provide an overtemperature limit to shut down the heating array in the event of specimen overtemperature, provide specimen temperatures and be used as part of a heater control system. Because of necessary compromises, however, a practical radiometric system may not perform all three functions with equal facility. For instance, the output of an accurate radiometer, uncorrected for outside influences of the measurement situation, (as discussed in the next section) would not be sufficiently accurate for use in feedback control or as a data base, yet could be satisfactorily used for conservative overtemperature limit. Similarly, a radiometer output may be completed satisfactory as data after appropriate correction, yet may be unsuitable for feedback array control because the necessary corrections are too involved to be calculated in real time or because the output may not be conditioned properly to be used in a feedback loop.

An accurate radiometric temperature indicating system provides a number of advantages over other candidate means of determining the leading edge surface temperatures. First of all, the system is relatively independent mechanically of details of the test specimen internal construction, manner of support, or method of assembly. The specimen surface is neither contacted by extraneous materials nor is it altered in physical or thermal properties by attached instrumentation. Stress concentrations produced by instrumentation installations and undesirable damage to specimen coatings are avoided. Finally, a radiometer system may be expected to function more reliably at the highest specimen temperatures anticipated than a thermocouple system might.

Balanced against these advantages are some practical disadvantages of a radiometric system. First, because of the optical system, detector, and electronics required, the cost per instrumented point on the test specimen is considerably

greater than for thermocouples. Because of the system reuseability, however, this disadvantage decreases as more specimens are tested. Cost, radiometer size, and module interference problems also limit the number of instrumented points on the test specimen.

8.6.2 Functioning of the Radiometer. This section reviews briefly some elements of radiometer theory and the application of this theory to a test specimen, heater module, and radiometer.

Besides the use of radiometers mounted behind the module, back reflector viewing the specimen through gaps between the heater elements, two other sensor arrangements were considered and discarded. A sensor mounted in the module with a light pipe assembly extending out nearly to contact the specimen and a sensor suspended by water-cooled struts between the module heater elements and specimen. Clearance, construction difficulties, and fragility problems appeared to outweigh any advantages of the discarded arrangements.

Functioning of the Basic Radiometer. The output voltage V_o of a radiometer viewing a blackbody source at temperature T_b may be written as

$$V_o = G \int_{\lambda=0}^{\lambda=\infty} R_\lambda N_{b\lambda}(T_b)\, d\lambda \qquad (1)$$

where G is a geometrical factor including the relationship between the source and radiometer and the field of view characteristics of the radiometer. R_λ is the spectral response of the radiometer system at wavelength λ, and $N_{b\lambda}(T_b)$ is the spectral radiance of the blackbody source at wavelength (i.e., the energy emitted in a given direction per unit solid angle, per unit wavelength interval centered about λ, per unit projected source area in the appropriate direction). According to the Planck radiation law

$$N_{b\lambda}(T_b) = \frac{C_1}{\pi \lambda^5 \left[\exp(C_2/\lambda T_b) - 1\right]} \qquad (2)$$

where C_1 and C_2 are the first and second radiation constants. Design of a radiometer is controlled only by the geometrical factor G and the spectral response R_λ. Calibration of the radiometer involves experimentally determining values for these terms or for the complete equation (1) by measuring the output voltage of the

instrument while viewing a blackbody source of known temperature.

For example, consider a radial-gradient Garden foil heat flux sensor such as those used in the development tests reported in section 7.3. The response R of such a detector is essentially independent of wavelength, and the geometrical factor is proportional to the view factor $\mathcal{F}_{b-s}$ of the source to that of the sensor surface. Equation (1) can be simplfied in this case to

$$V_o = c\mathcal{F}_{b-s}R\int_0^\infty N_{b\lambda}(T_b)\,d\lambda \qquad c = \text{constant} \qquad (3)$$

substituting from equation (2) and integrating

$$V_o = c\mathcal{F}_{b-s}R(\sigma T_b^4) = c\mathcal{F}_{b-s}\dot{q}_b R \qquad \sigma = \text{Stefan-Boltzmann constant}$$

Rearranging, and calling 1/cR the sensor calibration factor $\mathcal{C}$ produces

$$\mathcal{C}V_o = \mathcal{F}_{b-s}\dot{q}_b \qquad (5)$$

This is the familiar equation used to analyze heat flux sensor data.

The wavelength dependence of the radiometer response R_λ forms one basis for a classification of radiometer types. If the responsivity of the instrument is essentially independent of wavelength over all wavelengths at which there is appreciable radiant energy, the unit may be called a total radiometer. If R_λ is, because of detector characteristics and/or filtering by the optical system, non-zero only over a nanon wavelength band, the instrument is called a brightness radiometer.

To provide accurate information from a radiometer, the instrument must maintain the same geometrical and response factors which were present at calibration. It is desirable to design the radiometer to be used with the full-scale array so that its geometrical scale factor, G, is independent of specimen to radiometer distance. This distance independence, together with the necessity for viewing the front surface of the specimen through gaps between module heater elements and for viewing a relatively small spot, not a large area, on the specimen, places an upper limit on the value of G and, hence, the maximum radiometer output voltage is a given situation. To achieve an adequate signal to noise ratio in the output voltage

and a reasonable lower limit on the specimen temperature, a sensitive and, probably, narrow wavelength band detector must be chosen.

The spectral response of a radiometer, R_λ, is determined chiefly by the transmission of optical elements in the instrument, by the characteristics of the detector, and by the electronics system which processes the detector output. Since R_λ is a function of the transmission of the optical path between the specimen and detector, contamination of the radiometer optics by products evolved from the heaters or specimen will change the instrument calibration. The radiometers for the full-scale array should be designed using a positive gas purge to sweep contaminants away from the radiometer optics. Similarly, evolved gases and particulates in the optical path between the radiometer and an ablating specimen will affect radiometer output in a manner which depends on R_λ and the spectral absorption produced.

It is desirable that R_λ be independent of the incident energy (i.e., that the detector have linear response) and of radiometer case temperature. By suitably restricting the range of energies over which the detector operates, linearity of response is not difficult to achieve. Radiometer case temperature variations may be compensated by electronic sensors thermally bonded to the detector or may be eliminated by temperature controlling the case with liquid cooling or electric heating.

Sources of radiation other than the desired test specimen can produce a radiometer output. In this case, the instrument output voltage is

$$V_o = G\int_0^\infty R_\lambda N_{b\lambda}(T_b)\,d\lambda + \int_0^\infty R_\lambda K_\lambda W_{E\lambda}\,d\lambda \qquad (6)$$

where $W_{E\lambda}$ is the radiant energy at the specified wavelength received by the detector from all sources of extraneous radiation and K_λ is a factor to take take into account the various transmission paths this radiation takes to the detector. Stray radiation may be off-axis radiation from the heater elements which is scattered into the detector within the radiometer; or, if the detector has significant sensitivity at appropriate infrared wavelengths, it may be radiation emitted by the detector surroundings within the unit. Scattered light can be reduced by careful design and construction of the optical system. Radiation from the detector surroundings is difficult to eliminate. Rather, the amount of radiation must be maintained at some constant value by keeping the temperature of the radiometer case constant so that the stray radiation term in equation (6) is compensated for in the calibration procedure.

Effects of Specimen Emittance. If the total normal emittance of the test specimen is not unity, other influences on the radiometer output appear. In the case of a freely radiating test specimen (no heater or absorber module present and no appreciable radiative interaction with other objects in the environment) the radiometer output would be

$$V_o = G\int_o^\infty R_\lambda \varepsilon_{s\lambda}(T_s) N_{b\lambda}(T_s)\, d\lambda \tag{7}$$

where $\varepsilon_{s\lambda}(T_s)$ is the normal spectral emittance of the test specimen at temperature T_s. In general, the emittance of an object is also a function of the angle at which the radiation is observed; it has been assumed, however, that the angular variation of emittance within the acceptance angle of the radiometer is negligible.

Knowing the calibration curve of radiometer output voltage versus temperature for a blackbody, an apparent temperature T_a can be obtained from the output of the same radiometer viewing a non-black specimen. The apparent temperature is related to the true specimen temperature by the equation

$$V_o = G\int_o^\infty R_\lambda N_{b\lambda}(T_a)\, d\lambda = G\int_o^\infty R_\lambda \varepsilon_{s\lambda}(T_s) N_{b\lambda}(T_s)\, d\lambda \tag{8}$$

In special cases, this equation can be simplified. For a total radiometer which responds equally to all wavelengths at which there is significant radiation, the equation becomes

$$T_s = \left[\varepsilon_s(T_s)\right]^{-1/4} T_a \tag{9}$$

where $\varepsilon_s(T_s)$ is the total normal emittance of the specimen at temperature T_s. For a brightness radiometer responding at essentially a single wavelength λ_{eff}, the true temperature is given by

$$\frac{1}{T_s} - \frac{1}{T_a} = \frac{\lambda_{eff}}{C_2} \ln\left[\varepsilon_{s\lambda_{eff}}(T_s)\right] \tag{10}$$

where C_2 is the second radiation constant 1.4388 cm.K. This latter equation with λ_{eff} = 665 nm is used to correct disappearing-filament optical pyrometer data to true temperature. Note that, in general, an iterative procedure is necessary to obtain true temperature from apparent temperature since the emittance is a function of the true specimen temperature.

In practical circumstances, the specimen emittance may not be accurately known or may vary unpredictably during the course of testing. If $\delta\varepsilon/\varepsilon$ is the fractional

uncertainty in specimen emittance, the fractional uncertainty in true specimen temperature for the two types of radiometers discussed above can be calculated from equations (9) and (10). For the total radiometer

$$\delta T_s / T_s = \tfrac{1}{4}\, \delta\varepsilon/\varepsilon \tag{11}$$

For the brightness radiometer

$$\delta T_s / T_s = \left(\frac{\lambda_{eff} T_s}{C_2}\right) \delta\varepsilon/\varepsilon \tag{12}$$

These relations assume that the specimen emittance is not significantly a function of temperature over the range δT_s. For a brightness radiometer with effective wavelength in the visible range and for temperatures expected in carbon-carbon leading edge testing $\frac{C_2}{\lambda_{eff} T_s}$ is of the order of 10. It can thus be seen that in this application a brightness radiometer is less affected by emittance uncertainties than is a total instrument. Figure 8-9 tabulates the uncertainty in true temperature indication produced in data from various types of radiometers by a 6% uncertainty in emittance for a specimen having an actual true temperature of 3000°F and a wavelength and temperature independent emittance of 0.85.

RADIOMETER TYPE	TEMPERATURE UNCERTAINTY PERCENT
NARROW BAND (0.65 μ m)	± 0.67
THERMOPILE (CaF_2 WINDOW)	± 2.0
THERMOPILE (PYREX WINDOW)	± 1.33
SILICON SOLAR CELL	± 0.67

EFFECT RADIOMETER TYPE ON TEMPERATURE UNCERTAINTY

Figure 8-9

As can be seen from equation (12), the effect of emittance uncertainty on brightness radiometer output decreases as the effective wavelength of the radiometer decreases. Shorter effective wavelength instruments are therefore advantageous from this standpoint (pyrometers operating in the near ultraviolet are marketed commercially) but the advantage is gained at the expense of decreased total amount of signal (as can be seen from equation (2) for a temperature of interest and a wavelength shorter than about 1300 nm) and of shorter temperature ranges for the instrument. Taking the logarithmic derivative of equation (2) and divided the

result by equation (2) yields the fractional change in radiance dN_λ/N_λ for a given fractional change in temperature $\frac{dT_b}{T_b}$ produces the relation

$$\frac{dN_\lambda}{N_\lambda} = \frac{C_2}{\lambda T_b}\left[\frac{1}{1-\exp(-C_2/\lambda T_b)}\right]\frac{dT_b}{T_b} \cong \left(\frac{C_2}{\lambda T_b}\right)\frac{dT_b}{T_b} \qquad (13)$$

At 665 nm. and 2800°F, $\frac{C_2}{\lambda T_b} \cong 13$ so the radiance varies as a very strong function of T_b ($N_\lambda \propto T_b^{13}$ Hence, for a given usable detector signal range, equivalent temperature range decreases as the effective wavelength decreases.

Because geometrical constraints place maximum available signal at a premium and because automatic range changing is complicated and expensive, the radiometer designed for incorporation in the full-scale heater array must trade insensitivity to emittance uncertainty for other parameters. The exact choice of effective wavelength will depend on results of a more detailed study and on data concerning the emittance uncertainties to be expected for actual leading edge test specimens.

Effects of Reflected Radiation. If the emittance of the test specimen is not unity, the presence of a graphite heater module radiating to the specimen causes a radiometer viewing the specimen to see an apparent radiance $N'_{s\lambda}$ which depends not only on the specimen temperature and radiative properties but also on the heater element temperature and module radiative properties. The radiometer output voltage can be expressed as

$$V_o = G\int_0^\infty R_\lambda N'_{s\lambda}\, d\lambda$$

where

$$N'_{s\lambda} = \varepsilon_{s\lambda}(T_s)N_{b\lambda}(T_s) + \left[\frac{\rho_{s\lambda}(T_s)\rho'_{H\lambda}(T_H)}{1-\rho_{s\lambda}(T_s)\rho'_{H\lambda}(T_H)}\right]\varepsilon_{s\lambda}(T_s)N_{b\lambda}(T_s) +$$

$$+\left[\frac{\rho_{s\lambda}(T_s)}{1-\rho_{s\lambda}(T_s)\rho'_{H\lambda}(T_H)}\right]\varepsilon'_{H\lambda}(T_H)N_{b\lambda}(T_H)$$

The second term in the apparent radiance describes the effect of the specimen "seeing itself" reflected by a heater module having an effective hemispherical reflectance $\rho'_{H\lambda}(T_H)$ (the specimen emittance and reflectance in this term should also properly be mispherical values). The third term in the apparent radiance represents heater radiation from a body having an apparent hemispherical

emittance $\epsilon'_{H\lambda}(T_H)$ and a temperature T_h reflected by the specimen. Because the second and third terms increase the apparent specimen radiance from the value appropriate to a freely radiating specimen, the temperature indication obtained by ignoring these terms and correcting for specimen emittance as usual will be higher than the true value.

In the case of a carbon-carbon leading edge specimen heated by graphite heater modules to a space shuttle flight heat flux versus time profile, the error in radiometer temperature indication produced by ignoring reflection will be greatest during the heat-up portion of the profile, less at steady state, and still less during cooldown. For many purposes, e.g., for overtemperature limit control, the conservative temperature indication obtained by ignoring reflection may be used without significant performance degradation. Such a conservative limit alarm is included in the radiometer system described in section 8.6.3. In the steady-state development tests reported in section 7.3, the effects of reflected radiation were also ignored in reducing the optical pyrometer data since a rough calculation indicated such effects produced less than a 3% change in temperatures and since the necessary radiative properties of the dummy test specimen were unavailable.

A calculation to determine the magnitude of the reflected radiation terms in the apparent specimen radiance as a function of time during a complete simulated space shuttle flight profile should be performed using the existing thermal models of the test specimen and heater modules and using improved radiative property data. This calculation would indicate the necessity of correcting for reflected radiation in full-scale array tests in order to obtain the desired temperature accuracy, and would provide approximate corrections to actual test data if other sources of such corrections were lacking.

Corrections to be applied to radiometer data from tests on uninstrumented test specimens might be experimentally obtained from comparison of radiometer indication with thermocouple-measured specimen surface temperatures during a preliminary calibration test of an instrumented specimen thermally similar to the uninstrumented articles.

If heat flux sensors are installed in the leading edge sealing strip, test data from these sensors may be used to calculate the reflected radiation corrections to radiometer data obtained in the same test. The output voltage of a heat flux

sensor V_{hf} can be written as

$$V_{Hf} = G_{Hf} R_{Hf} \int_0^\infty N'_{H\lambda}\, d\lambda$$

where

$$N'_{H\lambda} = \varepsilon'_{H\lambda}(T_H) N_{b\lambda}(T_H) + \left[\frac{\rho_{s\lambda}(T_s)\rho'_{H\lambda}(T_H)}{1-\rho_{s\lambda}(T_s)\rho'_{H\lambda}(T_H)}\right] \varepsilon'_{H\lambda} N_{b\lambda}(T_H) + \left[\frac{\rho'_{H\lambda}(T_H)}{1-\rho_{s\lambda}(T_s)\rho'_{H\lambda}(T_H)}\right] \varepsilon_{s\lambda}(T_s) N_{b\lambda}(T_s) \tag{15}$$

The output voltage of the heat flux sensor contains terms due to the radiating specimen and to heater-specimen reflections just as the radiometer output voltage does (note that these terms do not effect the accuracy of using the sensors for module/control, since

$$G_{Hf} \int_0^\infty N'_{H\lambda}\, d\lambda$$

is exactly the quantity which it is desired to control as a function of time during tests). If the necessary radiative properties are known, however, the heat flux sensor output and the radiometer output provide two equations in the two unknown temperatures T_s and T_h . Since, in both equations, the first term is dominant and the other terms are small corrections, a first approximation can be obtained for T_s from equation (14) and for T_h from equation (15) by ignoring reflection. Using these approximations, the reflected corrections can be computed and new estimates of T_s and T_h obtained. Further iterations can proceed until satisfactory values are calculated provided the values to which the process coverages are the correct ones. The convergence properties of this correction algorithm and the effect of inaccuracies in radiative properties on the corrections obtained should be investigated in further study.

The correction process, if it converges properly, could be implemented in an on-line computer to provide real-time specimen temperatures for control or for quick-look data. Post-test, off-line computation is of course also possible. In the case where a total radiometer is used and the emittances and reflectances may be assumed to be independent of temperature, direction, and wavelength, no iteration is necessary; and a simple analog computer to directly compute the correction can be constructed. Because of the various correction options and the dependance of option selection on the customer's particular needs and available equipment, it is recommended that no correction processing equipment be included in the radiometer system for the full-scale array and that only a direct radiometer output suitable for further processing or recording be provided.

8.6.3 Radiometric Temperature Indicating System Recommended for Full Scale Array. The system recommended for the full scale array provides over-temperature alarms and surface temperature measurement. The system configuration is based on the considerations discussed above, and estimated test requirements. The system, as presently envisioned, does not provide heater control from room temperature to 3500°F because of 4000:1 energy range and the high cost of automatic switching. The system consists of:

- One radiometer per module complete with mounting system.
- Signal processing electronics and over-temperature alarm circuit.
- A radiometer check source.

The radiometer design or selection should be based on optimization of all the variables affecting the output signal. The proper acceptance angle can minimize the effect of heater element radiation while maintaining an adequate signal level. The optic system should be arranged so that specimen to radiometer distance is not critical. The temperature range should be 1400°F to 3500°F for a reasonable single signal range. The effects of specimen emittance uncertainties and reflected radiation should be minimized by the detector characteristics.

Provision for liquid cooling of the radiometer case with near-constant temperature fluid would minimize thermal influences from changing sensor head temperatures. Gas purging of the radiometer optics would reduce contamination effects. The mount design should adequately align the detector optics without further adjustment so the detector "sees" the specimen surface through the gaps between the heater strips.

The signal processing electronics would accept the detector signal and provide a buffered low-impedance output signal suitable for acquistion by a digital data system. A presettable output limit trip circuit would provide an alarm and/or system shut down signal for over-temperature conditions.

The radiometer check source provides the radiometer with a target of known brightness so the radiometer output can be compared with a calibrated value. This source can be used with the radiometer mounted in the heater to check for possible optics contamination or derangement of other internal components of the radiometer. MDC experience with radiometric measurements indicates the check source is necessary for confident use of the radiometers. The functioning of the optical temperature alarm system is shown schematically in Figure 8-10.

This is a preliminary design and additional design, breadboard buildup and testing in conjunction with the prototype heater is necessary before the system can be used in the full scale heating array.

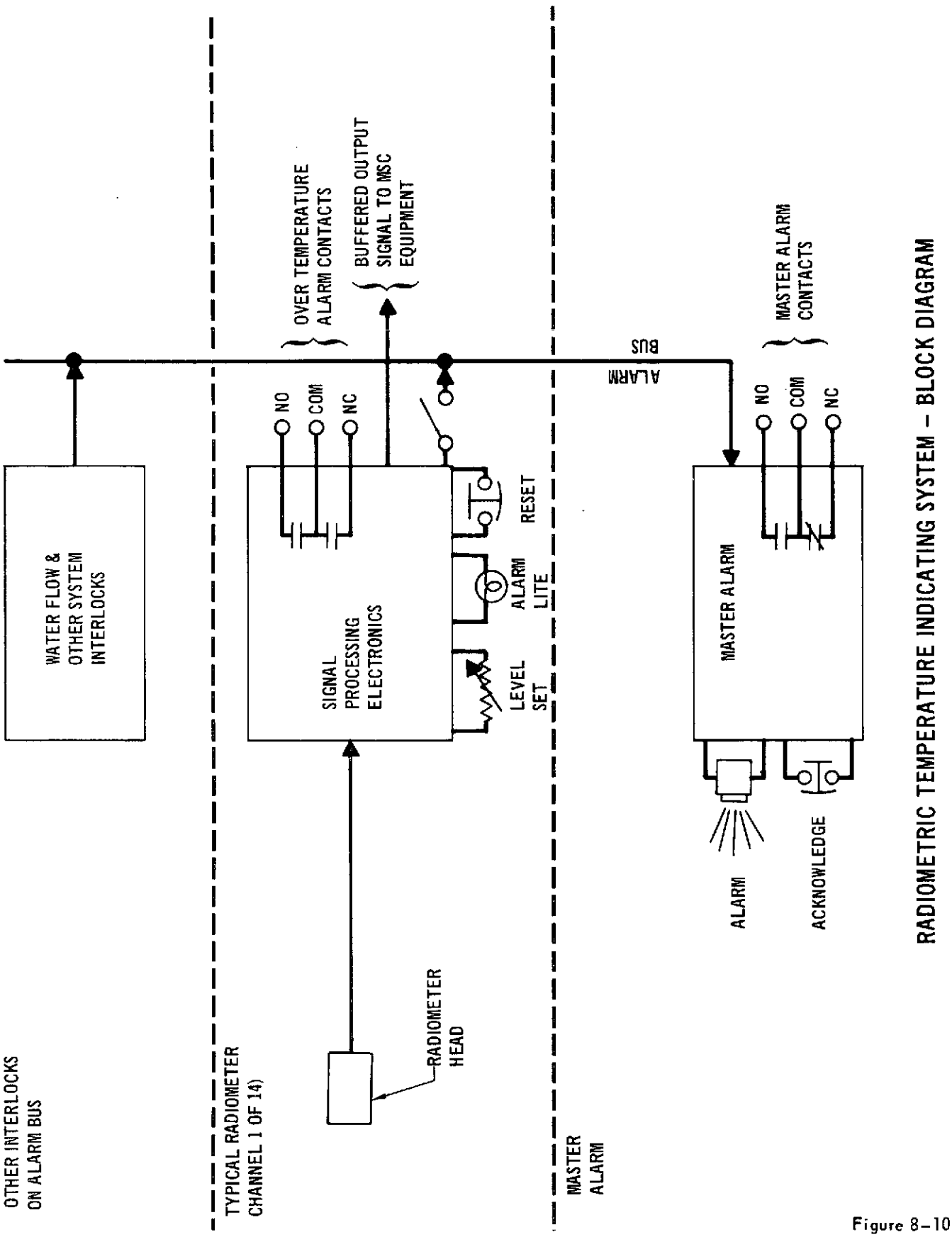

RADIOMETRIC TEMPERATURE INDICATING SYSTEM – BLOCK DIAGRAM

Figure 8-10

8.7 INTERFACES AND AUXILIARY EQUIPMENT. A study was made to determine the auxiliary equipment required to test a Shuttle leading edge specimen using the full-scale heater array. The equipment requirements are based on doing the testing at MSC. In some instances the required quantities depend on the test configuration, i.e., on the number of active heater modules being utilized. The tentative break-out of GFE and contractor supplied equipment, indicated in the following list, naturally requires concurrence by NASA-MSC. Figure 8-11 shows a schematic of the interface reflected in this list.

8.7.1 Electrical Equipment.

(1) Ignitron Power Controllers – Research Incorporated (RI) Model 8129, 440 VAC, 400 amps max. – 1 required per heater (MSC supplied)
(2) RI "Data-trak" Function Generators – 1 unit per heater (MSC supplied)
(3) RI "Data-trak" Temperature Controllers – 1 unit per heater (MSC supplied)
(4) Stepdown Transformers – 480/120 VAC, 100 KVA – 1 unit per heater (MSC supplied)
(5) Electrical cables from Ignitron power controllers to primary of stepdown transformers, 250 amps per channel (MSC supplied)
(6) Water-cooled wires from secondary of stepdown transformers to vacuum chamber feed-throughs, 1000 amps per wire, 2 wires per heater (MDAC-E supplied)
(7) Water-cooled wires from vacuum chamber feed-through to heater, 1000 amps per wire, 2 wires per heater (MDAC-E supplied)

8.7.2 Vacuum Equipment.

(1) Ten foot diameter vacuum chamber (MSC supplied)
(2) Chamber pumping system (MSC supplied)
(3) Chamber pressure readout equipment and controls (MSC supplied)
(4) Instrumentation feed-throughs (MSC supplied)
    a. Control feedback
    b. Temperature monitors
    c. Voltage monitors
    d. Coolant interlock controls
(5) Coolant feed-throughs, 250 gpm supply and drain (MSC supplied)
(6) Electrical feed-throughs 1000 amps max, 2 per heater (MSC supplied)
(7) Inert gas feed-throughs, 2 required – one for spray bar gas, one for chamber purge gas (MSC supplied)

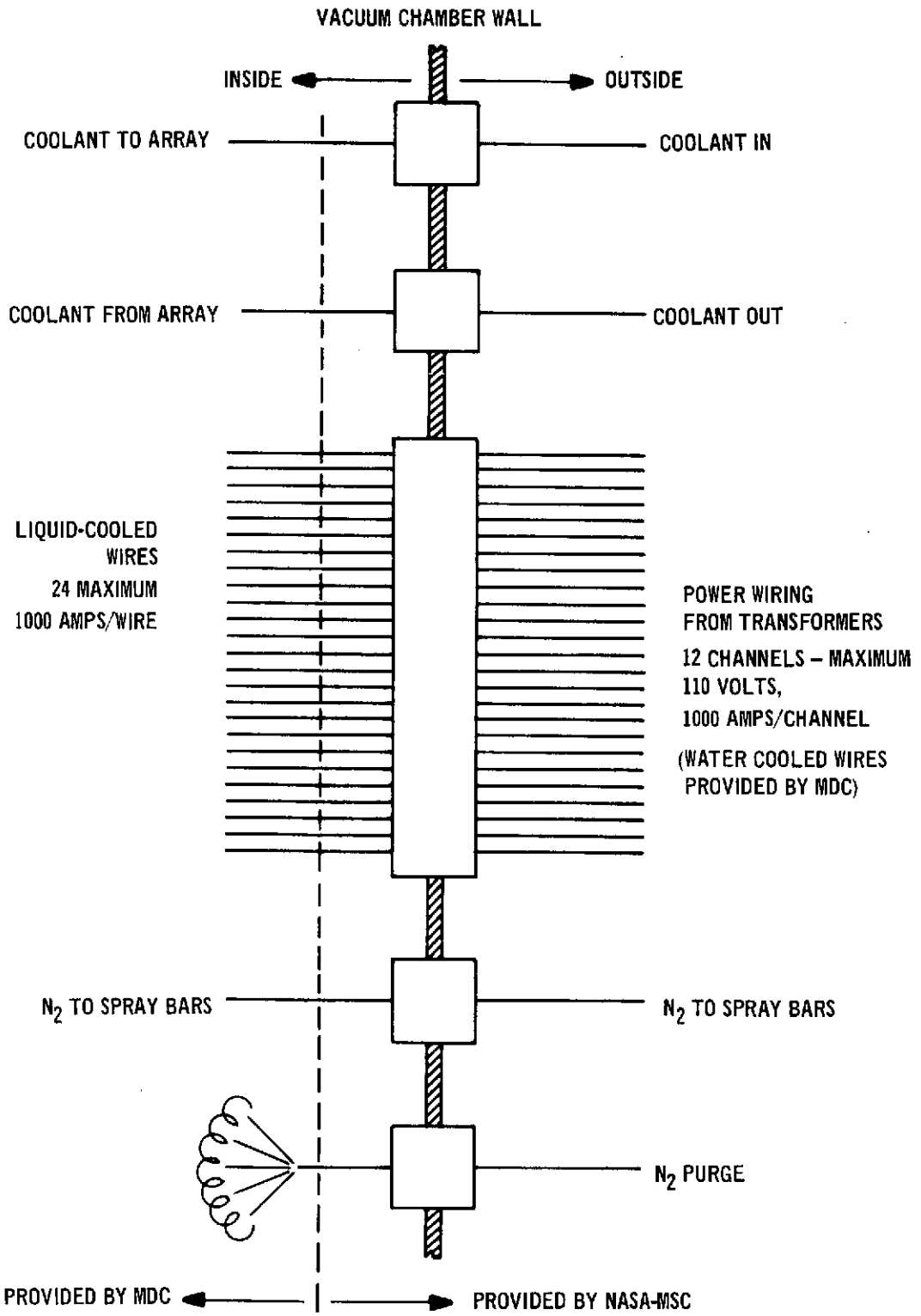

457-2427

INTERFACE SCHEMATIC FOR MSC INSTALLATION

Figure 8-11

8.7.3 Inert Gas System.

(1) Inert gas supply to vacuum chamber feed-throughs (MSC supplied)

(2) Throttling valve for chamber purge gas (MSC supplied)

(3) Throttling valve for spray bar gas (MSC supplied)

(4) Piping for specimen cooling spray bar gas from vacuum chamber feed-through to heater support structure gas manifolds (MDAC-E supplied)

8.7.4 Coolant System.

(1) Closed loop coolant system using glycol-water capable of heat dissipation of 4.2 Mw max. (Proposed system at MSC - less heat dissipation required for one heater array.) (MSC supplied)

(2) Piping to vacuum chamber feed-throughs, 250 gpm supply and drain (or return) (MSC supplied)

(3) Piping from vacuum chamber feed-throughs to heater support structure, 250 gpm supply and drain (or return) (MDAC-E supplied)

(4) Shutoff valves (2) (MSC supplied)

(5) Pressure gauges (optional) (MSC supplied)

(6) Flowmeter (optional) (MSC supplied)

8.7.5 Instrumentation.

(1) Heat flux calorimeters for feedback control, one per heater module (MDAC-E supplied)

(2) Radiometers for temperature indication, one per heater and absorber module (MDAC-E supplied)

(3) Coolant flow switches for power interlocks, one per heater and absorber module (MDAC-E supplied)

(4) Temperature monitoring thermocouples, as required (MSC supplied)

(5) Data acquisition system (MSC supplied)

Test article for acceptance test of full scale heating array is assumed to be supplied by NASA-MSC. This test article should be capable of surviving the maximum temperature for the heating duration required for the acceptance tests.

8.8 PROVISION FOR FUTURE EXPANSION. The individual heater modules and the complete heater array are designed so that leading edge test specimens having spans greater than 30 inches may be tested by placing additional arrays end to end. Such design consists chiefly of configuring the individual modules to achieve spanwise heat flux uniformity, and secondarily in mechanical arrangement of the modules to avoid interference between modules and to facilitate interconnection.

With the module design, three different concepts for spanwise stacking of individual modules may be implemented. Each concept represents an increase in the spanwise heat flux uniformity at the expense of increased complication in assembling and operating the stacked modules.

As shown in Figure 8-12, the first concept is to simply place the individual modules as close together as possible with the end reflectors touching. The module design will minimize the distance between heated portions of adjacent elements in this concept; but clearances for elimination of electrical discharge, thermal expansion, and cooling put a lower limit of about 2.9 inches on this distance. This first concept was evaluated during this program (Phase I).

The second concept is identical to the first except that the heater elements are replaced by elements in which the thick unheated portion of the element has been folded under the heated strip. These hot-end elements were developed by MDC to facilitate endwise stacking of modular heaters with minimum unheated area. MDC holds the patent (No. 3,573,429) covering the hot-end element. Hot-end elements reduce the distance between heated strips to about 1.80 inches at the expense of more costly and considerably more fragile elements.

The third concept resembles the second in using hot-end elements but reduces the distance between heated strips to the practical minimum of about 1.3 inches. The two standard end reflectors of adjacent modules are replaced by a single special siamese reflector connecting water manifolds of the two units.

8.8.1 Testing in an Oxidizing Atmosphere. As shown in Figure 8-13, the individual heater modules or the entire array can operate in an oxidizing environment by providing a coated columbium, carbon-carbon, or similar susceptor plate to cover each module. The interior of the module surrounding the elements can then be purged with an inert gas to protect the elements from oxidation. Maximum operating temperature is, of course, limited by the susceptor plate material and coating. Coated columbium, for instance, would limit operation to about 2500°F to 2700°F for multiple cycle tests.

Designs need to be investigated to improve sealing of reflector gaps and development of a clip-on susceptor plate.

8.8.2 Testing of Ablators. In addition to being suitable for testing thermal protection systems which have zero or low mass loss rates, the graphite heater is suitable for testing ablative materials. MDC graphite heaters have been used and are being used for testing silica phenolic (110 pcf) through a gamut of

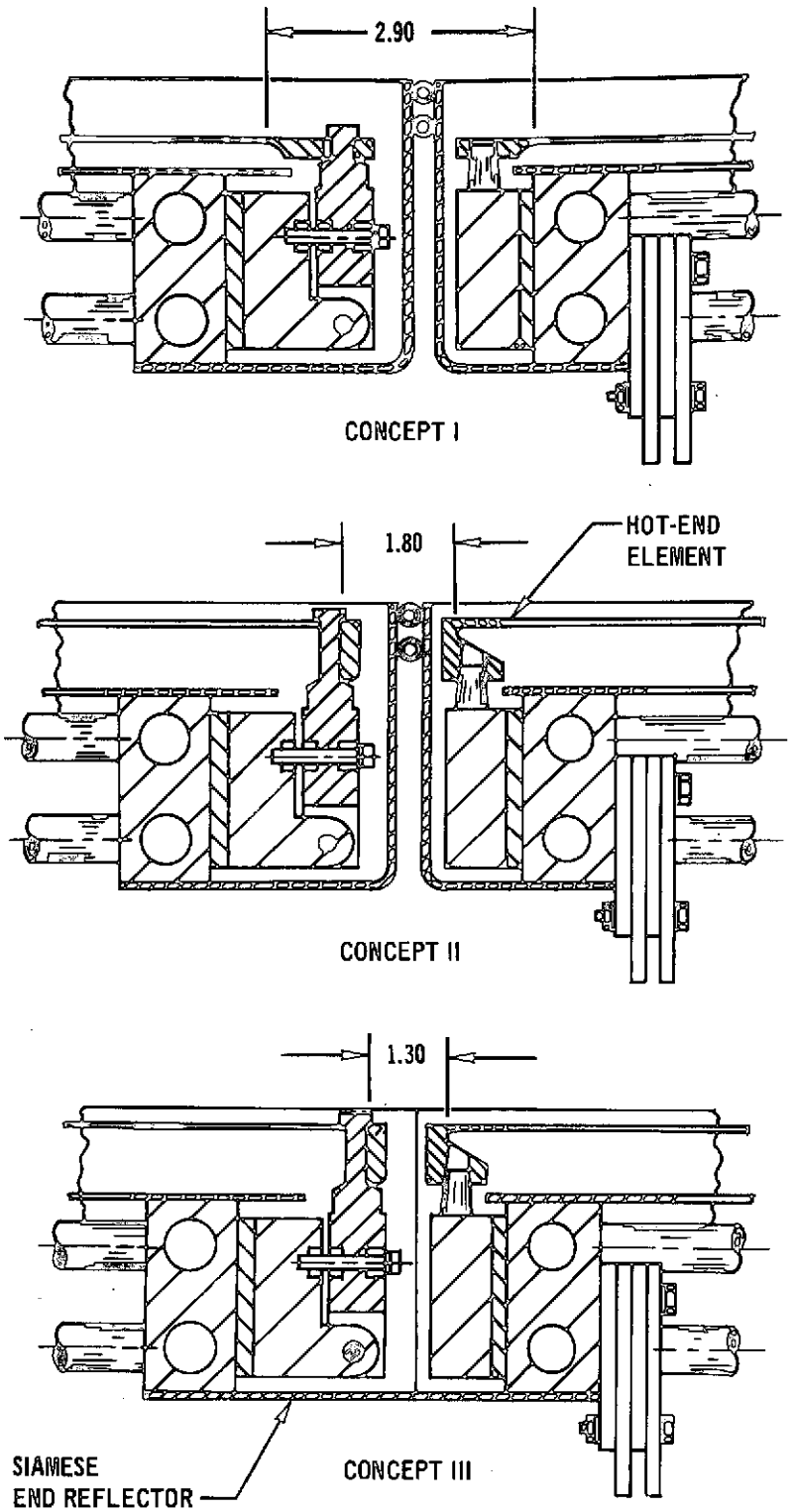

457-2421

CONCEPTS FOR MINIMIZING SPANWISE HEAT FLUX NON-UNIFORMITY WHEN TESTING TEST SPECIMENS LONGER THAN 30 INCHES

Figure 8–12

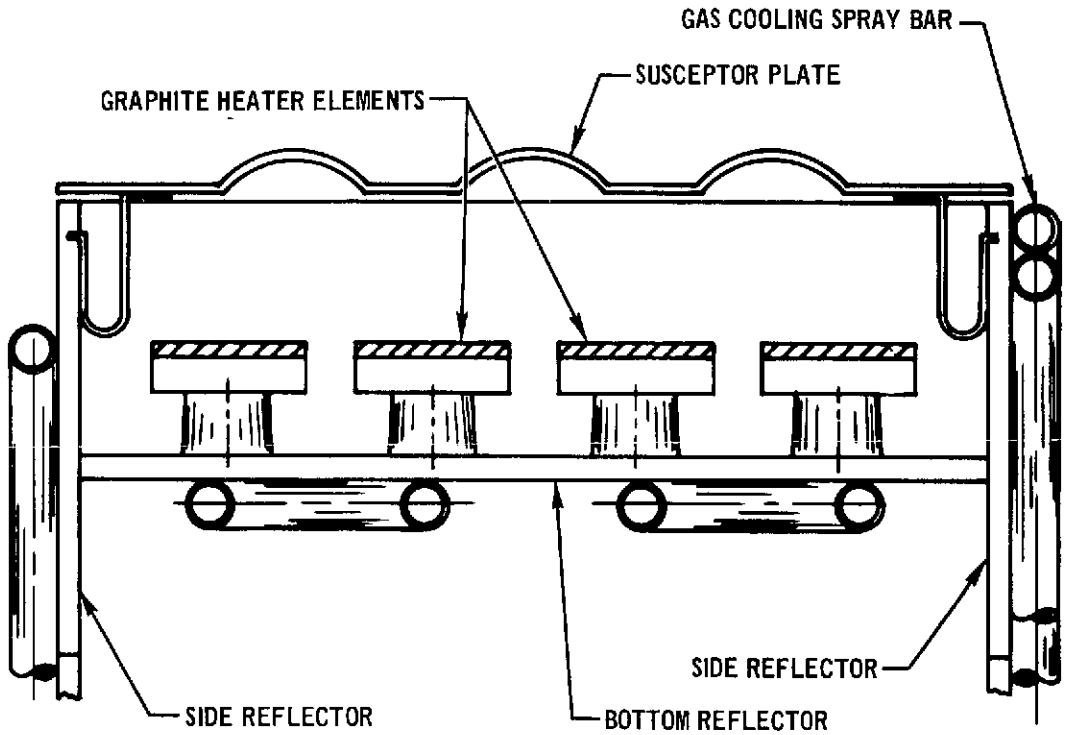

457-2420

TRANSVERSE SECTION OF HEATER MODULE SHOWING SUSCEPTOR PLATE FITTED FOR OXIDIZING ENVIRONMENT TESTS

Figure 8-13

densities down to 15 pcf silicone ablators including extensive testing of the Gemini heat shield material (DC 325). Heat flux versus time histories, as high as $225 \frac{Btu}{ft^2\ sec}$ have been programmed for ablative materials. Most of these programs were conducted without the use of a susceptor plate. During these tests, the pyrolysis by-products generated by the ablator coated the graphite heater element and deposited on the cool parts of the test chamber. Figures 8-14 and 8-15 show the post-test condition of the heater element, the charred ablator, and the test setup. The graphite heater elements, although coated, with ablation products, performed well throughout the test. This is in direct contrast with quartz lamps which fail shortly after the start of an ablator test because of contamination of the quartz envelope. Due to the single cycle testing for an ablator specimen, graphite elements have been replaced after each test run. When the susceptor plate is used, the graphite elements are protected and their life increases to more than 100 mission simulations.

The heating array is suitable for testing ablative leading edges but design and experimental studies are necessary to insure cleanliness of the reflectors for high heat flux testing. Gas spray bars in the bottom of the reflectors, or the use of a susceptor plate will probably be necessary.

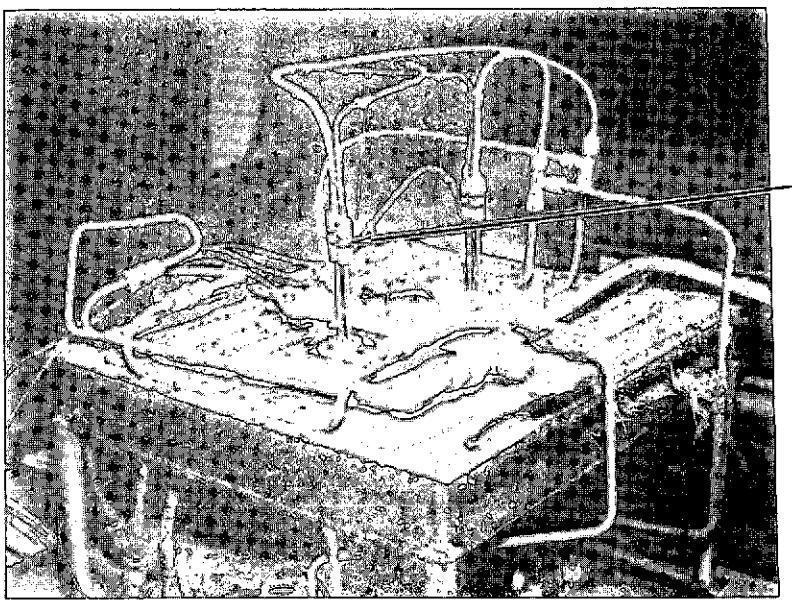

DEPOSITION OF ABLATION PRODUCTS ON
COLD PLATES OF GRAPHITE HEATER TEST SETUP

Figure 8–14

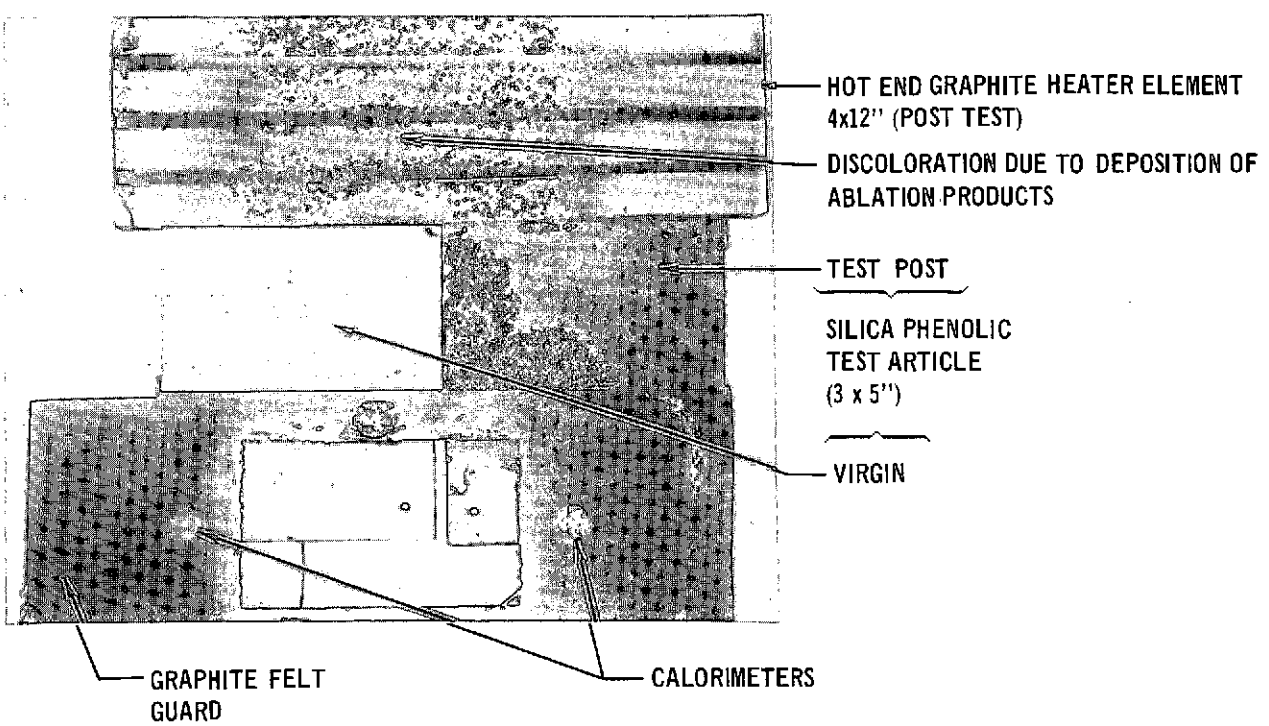

TESTING OF A SILICA PHENOLIC ABLATOR WITH THE GRAPHITE HEATER

Figure 8–15

NOTE: (PAGE 102 IS BLANK)

9.0 ESTIMATES FOR PHASE II

Rough Order of Magnitude (ROM) cost information for accomplishing Phase II were submitted to NASA-MSC for planning purposes as specified in Reference 1. Four ROM's submitted represented alternatives to meet NASA's objectives. Briefly, estimates were prepared for the following packages:

A. Those items necessary to provide the desired temperature distribution on the 8-inch radius leading edge test article. These items also satisfy the requirements for testing 6 to 15 inch radius leading edges. The major items were:

- o nine heater modules
- o five absorber modules
- o one support structure consisting of cooling water manifolds, gas manifolds, module support plates, edge guards, test article end guards, end covers, specimen support, heat flux sensors, water cooled power cables, etc.
- o spare parts
- o engineering effort consisting of array final design, module operational testing and performance mapping, design final report, acceptance test plan, supervising acceptance tests, acceptance test report, and operational and maintenance manuals.

B. Same as (A) plus five additional heater modules. This allows heating the entire exterior surface of the leading edge wetted circumference of 65 inches. These heater modules can be substituted for the absorber modules to provide greater versatility in desired heat distribution.

C. Those items necessary to optically measure the surface temperatures around the leading edge.

D. Installation of the heater array in MDC's St. Louis facilities and three weeks of testing.

This information was transmitted to Farris R. Tabor of NASA, MSC Houston via Letter 982-09-E016-3484 dated 10 November 1972.

10.0 CONCLUSIONS AND RECOMMENDATIONS

The principal analysis and design considerations for the design of a high temperature leading edge heating array have been explored. The array uses graphite heater modules and absorber modules to achieve the desired temperature distribution around the leading edge. Many new design innovations were incorporated into a prototype heater module which was designed, fabricated and tested at entry pressures to determine its performance and heat flux uniformity. Design studies and performance testing showed that a significant increase in heater performance can be achieved by using gold coated reflectors. Operation of the heater module was demonstrated using thermocouple and heat flux sensors as feedback to an Ignitron control system. Preliminary design of the full scale heating array incorporated flexibility for testing 6 to 15 inch radius leading edges of arbitrary length by nesting heating arrays. The utilities for the individual modules are supplied through the array support structure which supports the modules, the test article, and the end covers that prevent stray radiation from heating the vacuum chamber which houses the array.

Because of the flexible design of the array using heater and absorber modules, the array can be used to test a variety of Thermal Protection Systems (TPS) ranging from a 6-inch radius leading edge to a flat panel. Some of the types of material/systems that can be tested are:

- o RPP type carbon-carbon
- o Ablators
- o Metallics including heat pipe TPS
- o Ceramic Reusable Surface Insulations
- o Antenna Materials
- o Orbital Thermal Control Coatings

The basic module can also be adapted with a susceptor plate for testing hardware requiring an oxidizing environment. This type testing is limited by the temperature capabilities of the susceptor plate material. Coated columbium has been successfully used as a susceptor plate for repeated tests to 2500°F. The heating array also provides an economical means for thermally testing Shuttle Antennas located in the main body heat protection or in curved regions such as the "chine," etc.

This Phase I program was a short (5 months) development program, and additional work is recommended before finalizing the array design and fabricating the full scale array. The areas requiring additional effort are as follows:

- Continue performance and uniformity testing of the prototype module for several levels of thermal conductance through the test article.
- Fabricate another set of reflectors for the prototype module incorporating gold coatings, additional view ports for radiometers and susceptor plate mounts for testing in an oxidizing atmosphere.
- Perform analytical and experimental investigations to determine the amount of spray bar gas required to cool various types of leading edges during the latter stages of entry simulation.
- Further explore methods of mounting the control thermocouple or heat flux sensor, etc, preferably in the test article, for controlling the array during time-profiled entry heating.
- Investigate temperature measurements of the test article at high temperatures.

References

1. NASA Contract NAS9-13091, Design and Fabrication of a High Temperature Leading Edge Heating Array.

Appendix A

Drawings

The Engineering drawings and layout drawings listed below for the various components of the leading edge heating array were furnished to NASA-MSC.

List of Drawings

Drawing No.	Title
T-055352	High Temperature Leading Edge Heating Array
T-055351	Leading Edge Heating Array Absorber Module
T-055327	Shuttle Leading Edge Prototype Graphite Heater